

NAVAL UNDERWATER SYSTEMS CENTER NEW LONDON CT NEW LO--ETC F/G 12/1  
SPECTRAL ANALYSIS VIA QUADRATIC FREQUENCY-SMOOTHING OF FOURIER--ETC(U)  
JUN 81 A H NUTTALL  
NUSC-TR-6459 NL

UNCLASSIFIED

NIL

1 OF 1  
ALP A  
12503

END  
DATE  
FILMED  
10-81  
DTIC

NUSC Technical Report 6459 ✓  
1 June 1981

**LEVEL**

12

# Spectral Analysis via Quadratic Frequency-Smoothing of Fourier- Transformed, Overlapped, Weighted Data Segments

Albert H. Nuttall  
Surface Ship Sonar Department

DTIC

SEP 4 1981

H



**Naval Underwater Systems Center**  
Newport, Rhode Island / New London, Connecticut

Approved for public release, distribution unlimited

81 9 04 030

AD A103821

DTIC FILE COPY

### **Preface**

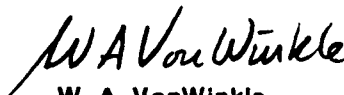
This research was conducted under NUSC Project No. A75205, Subproject No. ZR0000101, "Applications of Statistical Communication Theory to Acoustic Signal Processing," Principal Investigator Dr. Albert H. Nuttall (Code 3302), Program Manager CAPT. David F. Parrish, Naval Material Command (MAT 08L).

The Technical Reviewer for this report is Dr. G. Clifford Carter (Code 313).

### **Acknowledgment**

The author would like to acknowledge Dr. G. Clifford Carter of NUSC for the mutual formulation of the generalized spectral analysis technique analyzed here.

**REVIEWED AND APPROVED: 1 June 1981**



**W. A. VonWinkle**  
**Associate Technical Director**  
**for Technology**

The author of this report is located at the Naval Underwater  
Systems Center, New London Laboratory,  
New London, Connecticut 06320

14 NUSC- REPORT DOCUMENTATION PAGE		READ INSTRUCTIONS BEFORE COMPLETING FORM
REPORT NUMBER TR-6459	2. GOVT ACCESSION NO. AD-A10382-1	3. RECIPIENT'S CATALOG NUMBER
4. TITLE (and Subtitle) SPECTRAL ANALYSIS VIA QUADRATIC FREQUENCY- SMOOTHING OF FOURIER-TRANSFORMED, OVERLAPPED, WEIGHTED DATA SEGMENTS.		5. TYPE OF REPORT & PERIOD COVERED
AUTHOR(s) Albert H. Nuttall		6. PERFORMING ORG. REPORT NUMBER
9. PERFORMING ORGANIZATION NAME AND ADDRESS Naval Underwater Systems Center New London Laboratory New London, CT 06320		8. CONTRACT OR GRANT NUMBER(s)
11. CONTROLLING OFFICE NAME AND ADDRESS Naval Material Command Code MAT 08L Washington, DC 20362		10. PROGRAM ELEMENT, PROJECT, TASK AREA & WORK UNIT NUMBERS A75205
12. MONITORING AGENCY NAME & ADDRESS (if different from Controlling Office) (12) 194		11. REPORT DATE 1 Jun 81
		13. NUMBER OF PAGES 84
		15. SECURITY CLASS. (of this report) UNCLASSIFIED
		15a. DECLASSIFICATION/DOWNGRADING SCHEDULE
16. DISTRIBUTION STATEMENT (of this Report)  Approved for public release; distribution unlimited.		
(16) ZR000001 (17) ZR00000101		
18. DISTRIBUTION STATEMENT (of the abstract entered in block 20, if different from Report)		
18. SUPPLEMENTARY NOTES		
19. KEY WORDS (Continue on reverse side if necessary and identify by block number)		
Correlation	Lag Window	Reshaping
Effective Weighting	Normalized Quality	Resolution
Effective Window	Ratio	Spectral Analysis
Frequency Smoothing	Overlapping	Stability
Lag Weighting	Quality Ratio	Temporal Weighting
20. ABSTRACT (Continue on reverse side if necessary and identify by block number)		
<p>A generalized framework for spectral analysis is presented, which includes as special cases the Blackman-Tukey technique and the weighted overlapped segment-averaging FFT technique. The general method is analyzed in terms of the mean and variance of the spectral estimate, thereby revealing the fundamental dependence of its performance on the temporal weighting, lag weighting, amount of overlap, number of pieces, available data record length, and frequency resolution. To enable a fair tradeoff study and comparison between many different special cases of the technique, it is demanded that the spectral analysis</p>		

19. Key Words (Cont'd)

Temporal Window

Variance of Spectral Estimate

Weighted Data

20. Abstract (Cont'd)

technique achieve a specified frequency resolution with the given data record length. This necessitates a detailed investigation of the windowing capabilities of the temporal and lag weightings, their interaction, and the definition of an overall effective weighting and window. The possibility of using lag-resampling to achieve desirable effective windows is considered and found to be reasonable for a wide variety of windows with good side lobe behavior and decay rates.

Results for the variance of the spectral estimate for rectangular temporal weighting indicate that if the length of the temporal weighting is selected to be somewhat larger than the length of the lag weighting, the variance is at a near minimum. Furthermore, in this situation, the possibly deleterious side lobes of the temporal weighting can be compensated by proper choice of lag weighting, resulting in low side lobes and good decay of the overall effective spectral window. For Hanning temporal weighting, the lengths of the temporal and lag weighting should be approximately equal for minimum variance of the spectral estimate.

Accession For	
NTIS GRA&I	<input checked="checked" type="checkbox"/>
DTIC TAB	<input type="checkbox"/>
Unannounced	<input type="checkbox"/>
Justification	
By	
Distribution	
Availability Codes	
Dist Special	
A	

## Table of Contents

	Page
List of Illustrations .....	ii
List of Tables .....	ii
List of Symbols .....	iii
Introduction .....	1
Ultimate Stability Attainable From a Given Record Length .....	3
Description of Spectral Analysis Technique .....	6
Average Value of Spectral Estimate .....	13
Constraint on Temporal and Lag Weighting Lengths .....	16
Normalization of Weightings .....	23
Examples of Effective Windows .....	25
Lag Reshaping for Desired Effective Windows .....	36
Variance of Spectral Estimate .....	41
Quality Ratio .....	43
Special Cases of Generalized Spectral Analysis Technique .....	44
General Results on Stability .....	51
Summary .....	58
Appendix A - Comparison of Two Bandwidth Measures .....	A-1
Appendix B - Some Lag Weighting and Lag Windowing Considerations For Discrete-Time Processing .....	B-1
Appendix C - Correlation $\phi_1(\tau)$ of a General Class of Temporal Weightings .....	C-1
Appendix D - Derivation of Variance of Spectral Estimate .....	D-1
Appendix E - Computational Considerations for Non-Overlapping Segments .....	E-1
Appendix F - Computational Considerations for Overlapping With Hanning Temporal Weighting .....	F-1
References .....	R-1

### List of Illustrations

Figure		Page
1	Power Transfer Function of Narrowband Linear Filter .....	3
2	Temporal Weighting $w_1(t)$ .....	6
3	Lag Weighting $w_2(\tau)$ .....	8
4	Correlation $\phi_1(\tau)$ of Temporal Weighting $w_1(t)$ .....	14
5	Interrelationship of Lengths $L_1$ and $L_2$ for Fixed Shapes of the Temporal and Lag Weightings .....	17
6	Allowed Lengths of Various Temporal and Lag Weighting Pairs ..	20-22
7	Examples of Effective Windows for Rectangular Temporal Weighting .....	26-27
8	Effective Window for Hanning Temporal Weighting and Hanning Lag Weighting .....	28
9	Effective Window for Discrete-Time Rectangular Temporal Weighting and Hanning Frequency-Smoothing .....	31
10	Effective Window for Discrete-Time Rectangular Temporal Weighting and Rectangular Frequency-Smoothing with $N_2 = 5$ .....	33
11	Effective Window for Discrete-Time Rectangular Temporal Weighting and Rectangular Frequency-Smoothing with $N_2 = 11$ .....	34
12	Effective Window for Discrete-Time Hanning Temporal Weighting .....	35
13	Some Attainable Effective Windows via Lag Reshaping for Rectangular Temporal Weighting and $L_2 = L_1$ .....	37-38
14	$B_e L_2$ vs $B_e L_1$ Plot for Lag Reshaping to Desired Weighting $w_d(\tau)$ ..	40
15	Normalized Quality-Ratio for Rectangular Temporal Weighting and No Overlap .....	49
16	Normalized Quality-Ratio for Overlapped Rectangular Temporal Weighting and Lag Reshaping to C1 .....	53
17	Overall Weighting of $x^2(t)$ for $q = .5$ , $P = 2$ , Rectangular $w_1(t)$ .....	54
18	Normalized Quality-Ratio for Hanning Temporal Weighting and Hanning Lag Weighting; $B_e T = 100$ .....	56
19	Normalized Quality-Ratio for Hanning Temporal Weighting and Hanning Lag Weighting; $q \approx 3/8$ .....	57

### List of Tables

1	Shape Factor for Lag Weighting $w_2(\tau)$ .....	18
2	Shape Factor for Correlation $\phi_1(\tau)$ of Temporal Weighting $w_1(t)$ ..	19
A-1	Bandwidths for Various Weightings .....	A-2

## List of Symbols

$T$	available record length in seconds
$B_e$	effective frequency resolution in hertz (eq. 1)
$t$	time
$x(t)$	data record
$f$	frequency
$G(f)$	true (unknown) spectrum of $x(t)$
$W_o(f)$	spectral window
$H(f)$	filter voltage transfer function
$\hat{P}$	estimate of power (eq. 2)
$g(t)$	gate function (eq. 3)
$Q$	quality ratio (eq. 4)
$Av(\hat{P})$	average value of random variable $\hat{P}$
$Var(\hat{P})$	variance of random variable $\hat{P}$
overbar	ensemble average
$\tau$	lag (delay) variable
$R_z(\tau)$	correlation of random process $z(t)$
$\phi_g(\tau)$	correlation of function $g(t)$ (eq. 9)
$w_1(t)$	temporal weighting (figure 2 and eq. 13)
$W_1(f)$	temporal window (Fourier transform of $w_1(t)$ )
$L_1$	duration of $w_1(t)$ ; length of $\phi_1(\tau)$ (figures 2 and 4)
$S$	time shift of temporal weightings (eq. 13)
$P$	number of data pieces in first-stage spectral estimate (eqs. 13 and 14)
$y_p(t)$	$p$ -th weighted data segment (eq. 13)
$\hat{G}_1(f)$	first-stage spectral estimate (eq. 14)
$\hat{R}_1(\tau)$	first-stage correlation estimate (eq. 16)
$W_2(f)$	lag window (eq. 18)
$w_2(\tau)$	lag weighting (eq. 20)
$L_2$	length of $w_2(\tau)$ (figure 3 and eq. 21)
$\hat{G}_2(f)$	second-stage spectral estimate (eq. 18)
$\hat{R}_2(\tau)$	second-stage correlation estimate (eq. 19)
$\Delta_t$	time spacing in discrete samples of $x(t)$ (eq. 24) = time spacing of impulsive temporal weighting $w_1(t)$
$N_1$	number of impulses in discrete $w_1(t)$ (eq. 24)
$w_{1m}$	$m$ -th sample weight in discrete $w_1(t)$ (eq. 24)
$y_{pm}$	$m$ -th weighted sample of $p$ -th data piece (eq. 26)



## List of Symbols (Cont'd)

$\hat{R}_{1k}$	first-stage correlation estimate (eq. 28)
$\hat{R}_k^{(p)}$	k-th correlation estimate of p-th data piece (eq. 29)
$\Delta_F$	frequency increment used for calculation of spectral estimates (eq. 32)
$N$	size of FFT (power of 2) (eq. 33)
$\hat{R}_{2k}$	second-stage correlation estimate (eq. 36)
$\Delta_f$	frequency spacing in discrete samples of $\hat{G}_1(f)$ (eq. 38) = frequency spacing of impulsive lag window $W_2(f)$
$N_2$	number of impulses in discrete $W_2(f)$ (eq. 38)
$W_{2n}$	n-th sample weight in discrete $W_2(f)$ (eq. 38)
$\phi_1(\tau)$	correlation of temporal weighting $w_1(t)$ (eq. 44)
$w_e(\tau)$	effective weighting of generalized spectral analysis technique (eq. 48)
$W_e(f)$	effective window of generalized spectral analysis technique (eq. 51)
$L_m$	minimum of $L_1, L_2$ (eqs. 54 and 55)
$c\{g\}$	shape factor of function $g$ (eq. 57)
$C5, C3, C1$	three weighting functions (eq. 60)
$B_d$	desired effective frequency resolution
$w_d(\tau)$	desired effective weighting (eq. 98)
$W_d(f)$	desired effective window (eq. 100)
$\gamma(x, y)$	window convolution function (eq. 105)
$Q_P(u)$	periodic function (eq. 106)
$\phi_3(\tau, \mu)$	third-order correlation of $w_1(t)$ (eq. 108)
$NQR$	normalized quality ratio (eq. 110)
$\phi_2(\tau)$	correlation of $w_1^2(t)$ (eq. 113)
$q = q\{w_1\}$	shift-fraction (eq. 139)
$P_{\max}$	maximum value of $P$ (eq. 141)

## **Spectral Analysis via Quadratic Frequency-Smoothing of Fourier-Transformed, Overlapped, Weighted Data Segments**

### **Introduction**

Spectral analysis techniques have received a great deal of attention in the past (references 1-12), ranging from the original autocorrelation approach of Blackman-Tukey (reference 2) to the more recent weighted, overlapped, segment-averaging FFT approach (references 7-12). These two apparently disparate approaches are shown here to be limiting special cases of a generalized framework for spectral analysis; thus consideration of this general technique elucidates the fundamental behavior and performance of a rather wide variety of spectral approaches and their tradeoffs. This generalized framework has already been presented in references 13-15, where a brief summary of some of the main features has been mentioned. Additionally, some of the analytical results to be presented here were alluded to there; however, none of the detailed derivations or quantitative results in this report were given at that time.

There are two fundamental parameters that critically affect the performance of any spectral estimation technique. They are the available record length,  $T$ , of the stationary random process under investigation, and the effective frequency resolution,  $B_e$ , of the technique under consideration. We would like to be able to attain fine resolution (small  $B_e$ ) with short data lengths and storage (small  $T$ ); however, stable results (small fluctuations) are achievable only if the product  $TB_e$  is much larger than unity. The problems we address are how to make optimum use of a given *limited* amount of data in order to realize a specified desired resolution with maximum stability, and to determine what tradeoffs are available regarding windowing and weighting at different stages of the spectral analysis procedure. It is assumed that the reader is familiar with the tradeoffs presented in reference 9 for the weighted, overlapped, segment-averaging FFT procedure.

The generalized framework for spectral analysis that is presented here is capable of a wide variety of forms in addition to the Blackman-Tukey and FFT approaches mentioned above. In order to compare these various forms with each other on a reasonable basis, it is required that each analysis technique realize the same effective resolution bandwidth,  $B_e$ , and that they all utilize the same data record length  $T$ . Without these reasonable constraints, valid conclusions about relative performances of different techniques are tentative at best. This insistence upon equal effective frequency resolution necessitates a rather detailed investigation of the effects of the weightings and windows employed in the generalized framework and their allowed durations. The desirability of an overall effective window for spectral analysis with low side lobes and good decay is achievable only through careful choice of the combined weightings. The constraint upon the effective frequency resolution naturally also shows up in the analysis of the variance of the spectral estimation technique, as well as in its average value, leading to some numerical analysis complications; nevertheless, it is believed to be the proper basis of comparison and is maintained throughout.

The two major statistical parts of this report deal with the mean and the variance of the spectral estimate. The result for the average value leads to the definition of the effective window of the generalized spectral analysis technique, in terms of the temporal and lag windows. The variance result incorporates, additionally, the amount of overlap, the number of data pieces, and the ambiguity functions of the temporal and lag windows; the complexity of the latter results debilitates easy interpretation and it has been found necessary to resort to numerical evaluation of the variance, for practical cases of interest.

### Ultimate Stability Attainable From a Given Record Length

Suppose a stationary (complex) data record  $x(t)$  of length  $T$  seconds is available, and that we wish to estimate its power density spectrum\*  $G(f)$  with an effective frequency resolution of  $B_e$  Hz, where  $W_o(f)$  is the narrowband window through which the power density spectrum is to be observed. These two frequency-domain quantities are related according to†

$$B_e = \frac{\left[ \int df W_o(f) \right]^2}{\int df W_o^2(f)} \quad (1)$$

This bandwidth measure,  $B_e$ , is called the statistical bandwidth of  $W_o(f)$  in reference 5, page 265. The relation of effective bandwidth  $B_e$  to half-power bandwidth  $B_h$  is considered in appendix A; it is shown that for good windows, the ratio of the two bandwidths is relatively independent of the exact window shape. Thus it is possible to translate results to other bandwidth measures without significantly affecting the essential quantitative aspects.

If we take the original data record and pass it through a narrowband linear (complex) filter with power transfer function equal to the window,  $|H(f)|^2 = W_o(f)$ , and which is centered at a frequency,  $f_o$ , of interest, we will have lost no relevant information about the process in the frequency band of interest, because we have filtered out information of no use. We can now estimate the power in the narrowband filter output process and use it as a measure of the spectrum of the input process in the neighborhood of frequency  $f_o$ . See figure 1.

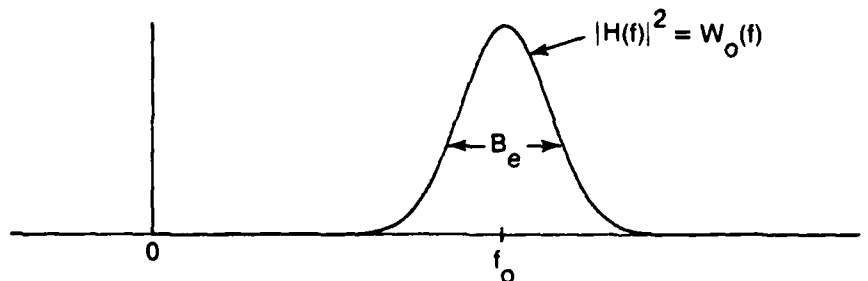


Figure 1. Power Transfer Function of Narrowband Linear Filter

Let  $z(t)$  be the complex output process from the narrowband filter when excited by the available  $T$  seconds of data  $x(t)$ . If we ignore a starting transient (i.e., assuming  $T \gg 1/B_e$ ), the filter output power estimate in the band of width  $B_e$  is

$$\hat{P} = \frac{1}{T} \int_T dt |z(t)|^2 = \int dt g(t) |z(t)|^2 \quad (2)$$

\*For brevity, we use the term spectrum rather than autospectrum in this report.

†Integrals without limits are over the range of the nonzero integrands.

where gate function

$$g(t) \equiv \begin{cases} 1/T & \text{for } t \in T \\ 0 & \text{otherwise} \end{cases}. \quad (3)$$

The measure of stability we adopt for this estimator, and for the others to follow, is the quality ratio defined as

$$Q \equiv \frac{\text{Var}(\hat{P})}{\text{Av}^2(\hat{P})} = \frac{\overline{\hat{P}^2} - \overline{\hat{P}}^2}{\overline{\hat{P}}^2}, \quad (4)$$

where  $\text{Av}(\hat{P})$  and  $\text{Var}(\hat{P})$  denote the average value and variance of  $\hat{P}$ , respectively, and an overbar denotes an ensemble average. We have average value

$$\begin{aligned} \text{Av}(\hat{P}) &= \int dt \, g(t) \overline{|z(t)|^2} = \overline{|z(t)|^2} = R_z(0) = \int df \, G(f) |H(f)|^2 \\ &\equiv G(f_0) \int df \, |H(f)|^2, \end{aligned} \quad (5)$$

assuming that filter-input spectrum  $G(f)$  does not vary quickly with respect to  $B_c$ , in the neighborhood of  $f_0$ .  $R_z(\tau)$  is the correlation\* of filter output process  $z(t)$ .

Also, we have mean square value

$$\overline{\hat{P}^2} = \iint dt \, du \, g(t) g(u) \overline{|z(t)|^2 |z(u)|^2}. \quad (6)$$

Now in the interval  $T$ , filter output  $z(t)$  will be approximately a stationary zero-mean, complex, analytic Gaussian process for small  $B_c$ ; filter  $H(f)$  has filtered out zero and all negative frequencies. Then fourth-order moment

$$\overline{z(t) z^*(t) z(u) z^*(u)} \equiv R_z^2(0) + |R_z(t - u)|^2. \quad (7)$$

There follows from (4) and (6),

$$\text{Var}(\hat{P}) = \iint dt \, du \, g(t) g(u) |R_z(t - u)|^2 = \int d\tau \, \phi_g(\tau) |R_z(\tau)|^2, \quad (8)$$

where gate-correlation† of function  $g(t)$  is

$$\phi_g(\tau) \equiv \int dt \, g(t) g(t - \tau). \quad (9)$$

\*For brevity, we use the term correlation instead of autocorrelation in this report.

†For stationary processes, we let  $R$  denote the ensemble-average correlation, whereas for aperiodic nonrandom functions, we let  $\phi$  denote the integral correlation; see (5) and (9).

Since the gate-correlation  $\phi_g(\tau)$  extends over  $\pm T$ , while process correlation  $R_z(\tau)$  extends only over approximately  $\pm 3/B_e$ , we have, via Parseval's theorem and for  $TB_e \gg 1$ ,

$$\begin{aligned} \text{Var}(\hat{P}) &\equiv \phi_g(0) \int d\tau |R_z(\tau)|^2 = \frac{1}{T} \int df G_z^2(f) \\ &= \frac{1}{T} \int df |H(f)|^4 G^2(f) \approx \frac{1}{T} G^2(f_0) \int df |H(f)|^4. \end{aligned} \quad (10)$$

The quality-ratio measure of stability is then, from (4), (5), (10), and (1),

$$Q = \frac{1}{T} \frac{\int df |H(f)|^4}{\left[ \int df |H(f)|^2 \right]^2} = \frac{1}{T} \frac{\int df w_o^2(f)}{\left[ \int df w_o(f) \right]^2} = \frac{1}{TB_e}. \quad (11)$$

This is the limiting (smallest) value of  $Q$  for specified frequency resolution  $B_e$  and available record length  $T$  when  $TB_e \gg 1$ . No other spectral procedures can improve on it; they can merely approximate it. As such, (11) is the benchmark against which other procedures can be compared, under the condition that  $T$  and  $B_e$  are equal to those values for the various procedures under consideration.

The normalized quality ratio is defined as  $Q \cdot TB_e$ . Thus the normalized quality ratio can never be smaller than unity, which value can only be approached for large  $TB_e$  through proper processing techniques.

### Description of Spectral Analysis Technique

We begin by defining a temporal weighting function  $w_1(t)$  of finite duration  $L_1$ ; that is,

$$w_1(t) \neq 0 \text{ only for } |t| < L_1/2 \quad (12)$$

As shown in figure 2, temporal weighting  $w_1(t)$  is real, even, and peaked at the origin. Although this presentation is couched in terms of continuous functions, we shall show shortly that it includes discrete digital processing as a special case.

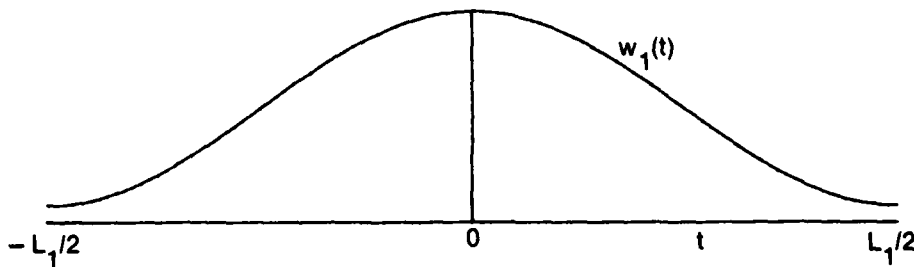


Figure 2. Temporal Weighting  $w_1(t)$

The available data record is  $x(t)$  for  $0 < t < T$ ; this (complex) random process is presumed second-order stationary in that observation interval. We shift the temporal weighting by  $L_1/2 + pS$  and multiply it by  $x(t)$  to generate the  $p$ -th piece of weighted data:

$$y_p(t) \equiv x(t) w_1\left(t - \frac{L_1}{2} - pS\right) \text{ for } 0 \leq p \leq P - 1 \quad (13)$$

Here  $p$  is an integer; if shift  $S < L_1$ , then  $y_p(t)$  and  $y_{p+1}(t)$  will overlap on the  $t$ -axis.

The first-stage power density spectral estimate at frequency  $f$  is obtained by averaging the magnitude-squared value of the Fourier transform of data piece  $y_p(t)$ , over a total of  $P$  pieces:

$$\hat{G}_1(f) = \frac{1}{P} \sum_{p=0}^{P-1} \left| \int dt \exp(-i2\pi ft) y_p(t) \right|^2 \text{ for any } f \quad (14)$$

This procedure is the same as that considered in reference 7 and in reference 9, eqs. (2) and (3). Since  $x(t)$  is available only for  $0 < t < T$ , we prevent the weighting in (13) from extending beyond that interval; mathematically this means that we must have

$$L_1 + (P - 1) S \leq T \quad (15)$$

An alternative interpretation of (14) is very illuminating. We define the inverse Fourier transform of (14) as the first-stage (auto)correlation estimate; there follows immediately at delay  $\tau$ ,

$$\begin{aligned}\hat{R}_1(\tau) &= \int df \exp(i2\pi f\tau) \hat{G}_1(f) \\ &= \frac{1}{P} \sum_{p=0}^{P-1} \int dt y_p(t) y_p^*(t - \tau) \quad \text{for all } \tau, \quad (16)\end{aligned}$$

where we have allowed random processes  $x(t)$  and  $y_p(t)$  to be complex. This is recognized as the average of the sample correlations that can be formed at delay  $\tau$ , from each of the  $P$  pieces of weighted data in (13). Since temporal weighting  $w_1(t)$  is zero for  $|t| > L_1/2$  according to (12), we see from (13) and (16) that

$$\hat{R}_1(\tau) = 0 \quad \text{for } |\tau| > L_1. \quad (17)$$

The parameter,  $\tau$ , is called the lag domain variable, because of the way it appears as a delayed time in (16). Equation (16) (and those to follow) is true for all  $\tau$ . Both sides of (16) are zero over most of the range of  $\tau$ ; nevertheless, it is mathematically convenient to employ the equality of both sides of (16) for all  $\tau$  in various transformations below.

The second-stage power density spectral estimate is defined as a frequency-smoothed version of the first-stage result:

$$\hat{G}_2(f) = \hat{G}_1(f) \otimes W_2(f) = \int du \hat{G}_1(u) W_2(f - u), \quad (18)$$

where  $\otimes$  denotes convolution. This is termed quadratic smoothing since it is done in terms of power quantities rather than voltages. Equation (18) is the desired output from the generalized spectral analysis technique considered here.  $W_2(f)$  is called the lag window, for reasons to be given below. The equivalent statement to (18) in the lag domain is obtained by Fourier transforming (18); the second-stage correlation is

$$\hat{R}_2(\tau) = \int df \exp(i2\pi f\tau) \hat{G}_2(f) = \hat{R}_1(\tau) w_2(\tau), \quad (19)$$

where we used (18) and (16) and defined the Fourier transform pair

$$\begin{aligned}w_2(\tau) &= \int df \exp(i2\pi f\tau) W_2(f), \\ W_2(f) &= \int d\tau \exp(-i2\pi f\tau) w_2(\tau).\end{aligned} \quad (20)$$

$w_2(\tau)$  and  $W_2(f)$  are both real, even, and peaked at their origins. Since  $w_2(\tau)$  appears multiplicatively in (19), it is called the lag weighting; its transform  $W_2(f)$  is the lag window. The convention adopted throughout this report is that multiplication by a function in the  $t$  or  $\tau$  domains is called a weighting; the counterpart to this operation in the Fourier transform domain (frequency  $f$  domain) is convolution and is called windowing.



We shall let lag weighting  $w_2(\tau)$  be of duration  $2L_2$ ; that is,

$$w_2(\tau) = 0 \quad \text{for } |\tau| > L_2 \quad . \quad (21)$$

A typical plot is shown in figure 3; the reason for the apparent notational discrepancy between the lengths in figures 2 and 3 will become clear when the lag-domain counterpart of temporal weighting  $w_1(t)$  is encountered later.

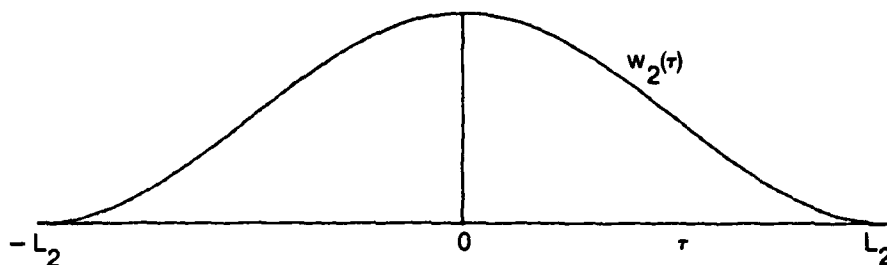


Figure 3. Lag Weighting  $w_2(\tau)$

We have already observed that  $\hat{R}_1(\tau)$  is zero for  $|\tau| > L_1$  in (17). Therefore, it follows from (19) and (21) that

$$\hat{R}_2(\tau) = 0 \quad \text{for } |\tau| > \min \{L_1, L_2\} \quad . \quad (22)$$

However, although we must have temporal length  $L_1 < T$  (from (15) for  $P = 1$ ), there is no restriction on  $L_2$ . We could have  $L_2$  larger than  $L_1$  and  $T$ ; this would simply mean that we would be lag-weighting some zero estimates of  $\hat{R}_1(\tau)$  in (19) for the larger values of  $|\tau|$ . Also there are no constraints such as realizeability on the lag weighting or window.

For example, the special case of no quadratic frequency-smoothing corresponds to

$$w_2(f) = \delta(f), \quad w_2(\tau) = 1, \quad L_2 = \infty \quad \text{for no smoothing,} \quad (23)$$

for which (18) yields  $\hat{G}_2(f) = \hat{G}_1(f)$ . Thus we have our standard first-stage spectral estimate (14) as a limiting case of the generalized spectral analysis technique. On the other hand, if lag window  $W_2(f)$  were broad (small  $L_2$ ), there would be a significant amount of smoothing taking place in the band about  $u = f$  in (18) where window  $W_2$  is non zero.

There is no inherent limitation on the relative sizes of  $L_1$  and  $L_2$  as yet:  $L_2$  can be chosen as large as desired, while  $L_1$  is subject to the upper bound  $T$ . However, when we specify the overall effective frequency resolution of the generalized technique, a relation between  $L_1$  and  $L_2$  will ensue.

Another important special case of the generalized spectral analysis technique is afforded by  $P=1$ ,  $w_1(t)=1$  for  $|t| < L_1/2$ , and  $L_1 = T$ . Then (16) and (13) indicate that  $\hat{R}_1(\tau)$  is simply the sample correlation of the available data  $x(t)$  of length  $T$ , while  $\hat{R}_2(\tau)$  in (19) is a weighted version of  $\hat{R}_1(\tau)$  for  $|\tau| < L_2$ . But this is precisely the Blackman-Tukey approach described in reference 2; the choice of lag weighting  $w_2(\tau)$  and its length is fully discussed there. For example, if  $w_2(\tau) = (T-|\tau|)^{-1}$  for  $|\tau| < L_2 < T$ , then  $\hat{R}_2(\tau)$  is an unbiased estimator for  $|\tau| < L_2$ ; see reference 2, page 11.

For  $P>1$  and general temporal weighting  $w_1(t)$ , lag weighting  $w_2(\tau)$ , and overlap, a wide variety of processors is possible via the generalized framework set up above. How should the two weightings be traded off against each other? Can the deleterious effects of a poor or preselected temporal weighting be undone by proper choice of lag weighting? Recall that none of these techniques can hope to better the quality-ratio result (11), but hopefully, some can do as well, with less computational effort and storage.

A related procedure to the one presented here has been given in references 16 and 17. However, neither incorporate overlapping, and the fundamental tradeoffs between the temporal and lag weightings were not studied. Furthermore, the only frequency-smoothing case considered was a rectangular boxcar, which severely limits the potential of the technique; some advantages of the generalized technique considered here will become apparent at a later stage. For the time being, we observe that side lobe control will be realized by a mixture of temporal weighting and lag weighting (frequency smoothing), while stability will be achieved by a combination of segment averaging and frequency smoothing (lag weighting).

### Discrete-Time Processing

All the functions above have been tacitly assumed no worse than discontinuous; see figures 2 and 3 for example. However, there is nothing in the above mathematics which precludes impulsive behavior. For example, suppose the temporal weighting is a sum of  $N_1$  equispaced impulses:

$$w_1(t) = \Delta_t \sum_m w_{1m} \delta(t - m\Delta_t) \quad , \quad (24)$$

where  $\{w_{1m}\}$  is a finite length, real sequence, symmetric about  $m=0$ ; this corresponds to discrete sampling of waveform  $x(t)$  at time spacing  $\Delta_t$ . The  $p$ -th piece of weighted data is, from (13),

$$\begin{aligned} y_p(t) &= x(t) \Delta_t \sum_m w_{1m} \delta\left(t - \frac{L_1}{2} - pS - m\Delta_t\right) \\ &= \Delta_t \sum_m y_{pm} \delta\left(t - \frac{L_1}{2} - pS - m\Delta_t\right) \quad , \end{aligned} \quad (25)$$

where weighted sample

$$y_{pm} \equiv w_{1m} x\left(\frac{L_1}{2} + pS + m\Delta_t\right) \quad . \quad (26)$$

The first-stage correlation estimate, (16), becomes

$$\hat{R}_1(\tau) = \Delta_t \sum_k \hat{R}_{1k} \delta(\tau - k\Delta_t) , \quad (27)$$

where the area of each impulse is given by

$$\hat{R}_{1k} = \frac{1}{P} \sum_{p=0}^{P-1} \hat{R}_k^{(p)} \quad (28)$$

and

$$\hat{R}_k^{(p)} = \Delta_t \sum_m y_{p,m} y_{p,m-k}^* . \quad (29)$$

The last quantity is the sample correlation of the  $p$ -th set of samples, and  $\hat{R}_{1k}$  is their average over the total of  $P$  pieces.

The first-stage spectral estimate is the Fourier transform of (27) as usual:

$$\hat{G}_1(f) = \Delta_t \sum_k \hat{R}_{1k} \exp(-i2\pi f k \Delta_t) , \quad (30)$$

which is finite for all  $f$  and is of period  $1/\Delta_t$  in  $f$ . An alternative expression is available by substitution of (25) in (14):

$$\hat{G}_1(f) = \frac{1}{P} \sum_{p=0}^{P-1} \left| \Delta_t \sum_m y_{pm} \exp(-i2\pi f m \Delta_t) \right|^2 . \quad (31)$$

These two expressions hold for arbitrary  $f$ ; either one can be used to obtain the first-stage spectral estimate. If we restrict our calculations of interest to multiples of some frequency increment  $\Delta_F$ , (31), for example, specializes to

$$\hat{G}_1(q\Delta_F) = \frac{1}{P} \sum_{p=0}^{P-1} \left| \Delta_t \sum_m y_{pm} \exp(-i2\pi m q \Delta_t \Delta_F) \right|^2 , \quad (32)$$

where  $q$  is an integer. At this point, there needn't be any relation between  $\Delta_t$  and  $\Delta_F$ ; we can calculate the spectral estimate at any frequencies we please. However, a favorite choice for computational purposes is to choose frequency increment

$$\Delta_F = \frac{1}{N\Delta_t} , \quad N = \text{power of } 2 , \quad (33)$$

to get the special digital processing result

$$\hat{G}_1\left(\frac{q}{N\Delta_t}\right) = \frac{1}{P} \sum_{p=0}^{P-1} \left| \Delta_t \sum_m y_{pm} \exp(-i2\pi m q / N) \right|^2 , \quad (34)$$

which is recognized as the familiar power average of N-point FFTs of weighted data sequences. All the impulsive functions in (24)-(27) have dropped out of first-stage spectral estimates (30)-(34).

The temporal window associated with impulsive weighting (24) is its Fourier transform

$$w_1(f) = \Delta_t \sum_m w_{1m} \exp(-i2\pi f m \Delta_t) \quad . \quad (35)$$

Having picked an impulsive temporal weighting  $w_1(t)$ , we are still free to select the lag weighting or lag window as we please. For example, for any lag weighting function  $w_2(\tau)$ , (19) and (27) yield second-stage correlation estimate

$$\hat{R}_2(\tau) = \Delta_t \sum_k w_2(k\Delta_t) \hat{R}_{1k} \delta(\tau - k\Delta_t) \equiv \Delta_t \sum_k \hat{R}_{2k} \delta(\tau - k\Delta_t) \quad . \quad (36)$$

The corresponding second-stage spectral estimate is the Fourier transform

$$\hat{G}_2(f) = \Delta_t \sum_k w_2(k\Delta_t) \hat{R}_{1k} \exp(-i2\pi f k \Delta_t) = \Delta_t \sum_k \hat{R}_{2k} \exp(-i2\pi f k \Delta_t) \quad , \quad (37)$$

which is everywhere finite and has period  $1/\Delta_t$  in  $f$ . Evaluation of (37) can therefore be confined to  $|f| < (2\Delta_t)^{-1}$ .

These results apply for general lag weighting. A specific choice is the lag window with  $N_2$  equispaced nonzero impulses:

$$w_2(f) = \Delta_f \sum_n w_{2n} \delta(f - n\Delta_f) \quad . \quad (38)$$

Frequency spacing  $\Delta_f$  need not be related to time spacing  $\Delta_t$  in (24), nor to frequency increment  $\Delta_F$  used in the frequency and FFT calculations above in (32)-(34). Also there are no relations between the real symmetric sets of numbers  $\{w_{1m}\}$  in (24) and  $\{w_{2n}\}$  in (38). Substitution of (38) in (18) yields for the second-stage spectral estimate

$$\hat{G}_2(f) = \Delta_f \sum_n w_{2n} \hat{G}_1(f - n\Delta_f) \quad , \quad (39)$$

which is a local average (of the first-stage estimates) in the band about the frequency,  $f$ , of interest. Equation (39) is a discrete, quadratic, frequency-smoothing operation. In fact, (39) holds for lag window (38) and *any* temporal weighting  $w_1(t)$ ; it is not limited to the discrete-time form (24).

If we limit our calculations of  $\hat{G}_2(f)$  to multiples of frequency increment  $\Delta_F$  as in (32), then (39) yields

$$\hat{G}_2(q\Delta_F) = \Delta_f \sum_n w_{2n} \hat{G}_1(q\Delta_F - n\Delta_f) \quad ; \quad (40)$$

we can use (30) for  $\hat{G}_1$  on the right-hand side. Finally, if we take frequency increment (33) and frequency spacing  $\Delta_f = (M\Delta_t)^{-1}$ , where integer  $M$  is a submultiple of  $N$ , and  $M\Delta_t$  is of the order of  $2L_1$ , the FFT results of (34) can be employed in (40). More will be said later on the choice of frequency spacing  $\Delta_f$ .

The variety of forms available at different stages of the data processing illustrates a great deal of flexibility in exactly how the available data  $x(t)$  is processed. For example, one might first evaluate  $\hat{G}_1$  via FFT procedure (34). Then, since (30) can be expressed as

$$\hat{G}_1\left(\frac{q}{N\Delta_t}\right) = \Delta_t \sum_k \hat{R}_{1k} \exp(-i2\pi kq/N) \quad , \quad (41)$$

it follows that the complete nonzero portion of correlation sequence  $\{\hat{R}_{1k}\}$  is recoverable from the set of numbers  $\{\hat{G}_1(-\frac{q}{N\Delta_t})\}_{0}^{N-1}$  if  $N \geq 2N_1 - 1$ , where  $N_1$  is the number of nonzero weights  $\{w_{1k}\}$  in (24) (see reference 18). On the other hand, for  $N < 2N_1 - 1$ , the inverse FFT of  $\{\hat{G}_1(-\frac{q}{N\Delta_t})\}_{0}^{N-1}$  would yield  $\hat{R}_{1k}$  only for  $|k| \leq N - N_1$  (reference 18, eq. (15)); thus the central values of  $\hat{R}_{1k}$  are recoverable from  $\hat{G}_1$ . Then second-stage correlation estimate

$$\hat{R}_{2k} = w_2(k\Delta_t) \hat{R}_{1k} \quad (42)$$

follows from (36), and the final spectral estimate follows from (37). The lag weighting samples in (42) are arbitrary; thus this is a very general procedure for obtaining estimate  $\hat{G}_2(f)$  at any  $f$ .

The relations in this subsection hold for arbitrary values of  $\tau$ ,  $f$ , and  $q$ . However, the functions of  $\tau$  are impulsive, and are zero outside limited ranges, while the functions of  $f$  and  $q$  are periodic. These properties should be utilized in any computer processing technique employing these forms. Some further useful properties and interrelationships of the sampled lag weightings and lag windows are presented in appendix B.

### Average Value of Spectral Estimate

We now return to the general situation for both the temporal and the lag weightings; that is, we do not presume discrete sampling in time or discrete smoothing in frequency. From (16) and (13), the mean value of the first-stage correlation estimate is

$$\begin{aligned} \text{Av}\{\hat{R}_1(\tau)\} &= \frac{1}{P} \sum_{p=0}^{P-1} \int dt \overline{x(t)x^*(t-\tau)} w_1\left(t - \frac{L_1}{2} - pS\right) \\ &\bullet w_1\left(t - \tau - \frac{L_1}{2} - pS\right) = \overline{x(t)x^*(t-\tau)} \phi_1(\tau) = R(\tau) \phi_1(\tau) \end{aligned} \quad (43)$$

where  $R(\tau)$  is the true correlation of stationary process  $x(t)$ , and where

$$\phi_1(\tau) = \int dt w_1(t) w_1(t - \tau) \quad (44)$$

will be called the correlation of real temporal weighting  $w_1(t)$ ; see the footnote to (9). We have not presumed process  $x(t)$  Gaussian; relation (43) holds for any stationary process  $x(t)$ .

Since the first-stage spectral estimate  $\hat{G}_1(f)$  is a linear operation (Fourier transform) of  $\hat{R}_1(\tau)$ , the mean value of  $\hat{G}_1(f)$  is the Fourier transform of (43); that is,

$$\begin{aligned} \text{Av}\{\hat{G}_1(f)\} &= \int d\tau \exp(-i2\pi f\tau) R(\tau) \phi_1(\tau) \\ &= G(f) \otimes W_1^2(f) = \int du G_1(u) W_1^2(f - u) \end{aligned} \quad (45)$$

where  $G(f)$  is the true spectrum of  $x(t)$ , i.e., Fourier transform of  $R(\tau)$ , and we have Fourier transformed (44) by interchanging integrals and using temporal window

$$W_1(f) = \int dt \exp(-i2\pi ft) w_1(t) \quad (46)$$

The convolution result in (45) is a familiar one for the standard FFT processing of weighted, overlapped data segments; see reference 9, eq. (5), for example. Window  $W_1(f)$  is real and even about  $f=0$ , since weighting  $w_1(t)$  is real and even about  $t=0$ .

The mean value of the second-stage correlation estimate follows immediately from (19) and (43):

$$\text{Av}\{\hat{R}_2(\tau)\} = R(\tau) \phi_1(\tau) w_2(\tau) = R(\tau) w_e(\tau) \quad (47)$$

where

$$w_e(\tau) \equiv \phi_1(\tau) w_2(\tau) \quad (48)$$

is called the effective (overall) weighting of the generalized spectral analysis technique. It incorporates the temporal weighting  $w_1(t)$  through its correlation  $\phi_1(\tau)$  defined in (44), and it involves lag weighting  $w_2(\tau)$  directly. Reference to (44) and to figure 2, for a typical temporal weighting, shows that  $\phi_1(\tau)$  is as depicted in figure 4;  $\phi_1(\tau)$  extends over  $(-L_1, L_1)$  and is zero for  $|\tau| > L_1$ . Since the effective weighting  $w_e(\tau)$  in (48) involves  $\phi_1(\tau)$  and  $w_2(\tau)$ , we now see the reason for the particular choices of  $L_1$  and  $L_2$  in figures 2-4. Specifically,  $\pm L_1$  and  $\pm L_2$  measure the non-zero extent, in the  $\tau$ -domain, of the functions that are relevant to the effective weighting. Although  $L_1$  measures the nonzero extent of temporal weighting  $w_1(t)$  in the time domain in figure 2, and the nonzero extents of  $\phi_1(\tau)$  and  $w_2(\tau)$  are  $2L_1$  and  $2L_2$  in figures 4 and 3, respectively, we will nevertheless refer to  $L_1$  and  $L_2$  as the "lengths" of  $\phi_1(\tau)$  and  $w_2(\tau)$ , respectively, in the  $\tau$ -domain, for convenience.

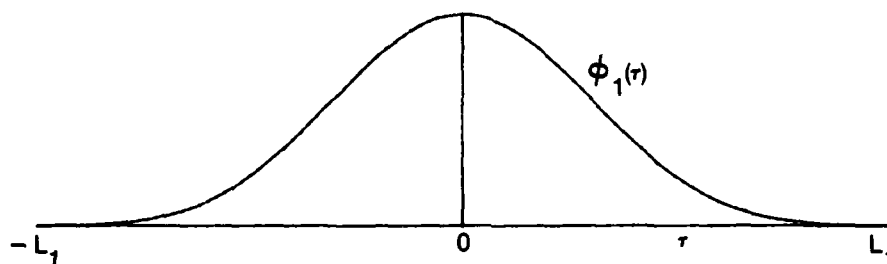


Figure 4. Correlation  $\phi_1(\tau)$  of Temporal Weighting  $w_1(t)$

In appendix C,  $\phi_1(\tau)$  is evaluated for the class of temporal weightings\*

$$w_1(t) = \sum_k \alpha_k \exp(i2\pi kt/L_1) \quad \text{for } |t| < L_1/2, \quad (49)$$

which includes a wide variety of weightings such as rectangular, Hamming, Hanning, Blackman, Harris, and the recent optimal weightings of Nuttall, reference 19. Specializations to real symmetric  $\{\alpha_k\}$  and to a limited number of nonzero coefficients are also made in appendix C.

Finally, since second-stage spectral estimate  $\hat{G}_2(f)$  is a Fourier transform of  $\hat{R}_2(\tau)$ , its mean value follows from (47) and (48) as

$$\text{Av}\{\hat{G}_2(f)\} = G(f) \odot W_e(f), \quad (50)$$

where

$$W_e(f) = \int d\tau \exp(-i2\pi f\tau) w_e(\tau) = W_1^2(f) \odot W_2(f) \quad (51)$$

\*For brevity, here and later, we omit the "0 otherwise" statement that applies for  $|t| > L_1/2$ , as was done in (3).

is the effective (overall) window of the generalized spectral analysis technique of interest here. The result in (51) follows by Fourier transformation of the product in (48) and use of (44) (just as done in (45)). Relation (50) is a simple and informative one for the average spectral estimate; it enables ready determination of the amount of spreading caused by particular choices of temporal and lag windows. It holds for any stationary process  $x(t)$  with spectrum  $G(f)$ ; thus  $x(t)$  needn't be a Gaussian process for (50) to hold true.

As a special case of (50), consider lag weighting  $w_2(\tau)$  to be 1 for all  $\tau$ . Then  $W_2(f) = \delta(f)$  and (50) reduces to the result in (45) as expected, since we are employing no lag weighting at all in this case.

As another special case, let temporal weighting  $w_1(t)$  be 1 for all  $|t| < L_1/2$  and let  $L_1 = T$ ,  $L_2 \ll T$ . This corresponds to Blackman-Tukey processing. Then  $W_1^2(f)$  is proportional to  $\text{sinc}^2(Tf)$ , which is much narrower in  $f$  than  $W_2(f)$ , meaning that  $W_e(f) \approx W_2(f)$ , the lag window alone.

Interpretation of the response of the effective window,  $W_e(f)$ , via convolution (51) can sometimes be deceiving, and it may be helpful and necessary to resort to (48). For example, suppose  $w_2(\tau)$  is 1 for  $|\tau| < L_2$  and 0 otherwise, where  $L_2 \geq L_1$ . Then (51) says that we have to convolve  $\text{sinc}(L_2 f)$ , which has -6.63 dB side lobes, with  $W_1^2(f)$ . Our first impression would be that  $W_e(f)$  is bound to have bad side lobes regardless of the temporal window. But recourse to (48) and figure 4 immediately reveals that  $w_e(\tau) = \phi_1(\tau)$  for all  $\tau$ , and that  $W_2(f)$  is totally irrelevant, provided that  $L_2 \geq L_1$ . The scaling of  $\phi_1(\tau)$  by a constant in (48), over the range of nonzero  $\phi_1(\tau)$ , obviously has no effect on the relative side lobes of  $W_e(f)$ . Furthermore, the actual calculation of the effective window via (51) is often tedious, whereas a Fourier transformation of the product in (48) is a reasonable approach, even if only by an FFT.



### Constraint on Temporal and Lag Weighting Lengths

The effective window  $W_e(f)$  was presented in (51). Its "width" is given approximately by the sum of the widths of the temporal and lag windows. As discussed earlier, we wish to constrain the effective bandwidth  $B_e$  of  $W_e(f)$ , so as to be able to fairly compare the performance of different spectral analysis techniques. The effective bandwidth is given by (1) and can be developed as

$$B_e = \frac{\left[ \int df w_e(f) \right]^2}{\int df w_e^2(f)} = \frac{w_e^2(0)}{\int d\tau w_e^2(\tau)} = \frac{\phi_1^2(0) w_2^2(0)}{\int d\tau \phi_1^2(\tau) w_2^2(\tau)}$$

$$= \left( \int d\tau \left[ \frac{\phi_1(\tau)}{\phi_1(0)} \right]^2 \left[ \frac{w_2(\tau)}{w_2(0)} \right]^2 \right)^{-1}, \quad (52)$$

where we have used Parseval's theorem, the Fourier transform relationship in (51), and (48). Since  $B_e$  is to be considered fixed, (52) forces a relationship between lengths  $L_1$  and  $L_2$  of  $\phi_1(\tau)$  and  $w_2(\tau)$ .

For example, consider rectangular temporal and lag weightings (this is not a practical case and is presented only for illustration purposes):

$$w_1(t) = 1 \quad \text{for } |t| < L_1/2,$$

$$\phi_1(\tau) = L_1 - |\tau| \quad \text{for } |\tau| < L_1,$$

$$w_2(\tau) = 1 \quad \text{for } |\tau| < L_2. \quad (53)$$

Then (52) yields

$$B_e^{-1} = 2 \int_0^{L_m} d\tau \left( 1 - \frac{\tau}{L_1} \right)^2, \quad (54)$$

where

$$L_m = \min(L_1, L_2). \quad (55)$$

Given a value of  $B_e$ , (54) can be considered as an equation for  $L_2$  in terms of  $L_1$ , or vice versa. Here we have fixed the *shapes* of the weightings and are varying the lengths so as to realize the specified frequency resolution  $B_e$ .

Generally, the qualitative character of the interrelationship between lengths is as depicted in figure 5, for fixed weighting shapes. The larger one of the lengths is made, the smaller the other length can get and still satisfy the specified bandwidth of the effective window. For a specified pair of shapes for  $w_1(t)$  and  $w_2(\tau)$ , a plot like figure 5 can be used in two different ways. If we pick a value for  $B_e L_1$ , this determines  $B_e L_2$  and hence  $L_2/L_1$ . On the other hand, choice of a value for the ratio of lengths,  $L_2/L_1$ , puts a line through the origin of slope  $L_2/L_1$ , and thereby determines  $B_e L_1$  and  $B_e L_2$  where the line intersects the curve. We note therefore that knowledge of one of the following three quantities determines the other two:  $L_2/L_1$ ,  $B_e L_1$ ,  $B_e L_2$ .

The limiting parameter values on figure 5 are determined as follows: as  $L_1 \rightarrow \infty$ , then  $L_2 \rightarrow L_2(\min)$ , where now (from (52))

$$B_e^{-1} = \int d\tau \left[ \frac{w_2(\tau)}{w_2(0)} \right]^2 = 2L_2(\min) c\{w_2\} . \quad (56)$$

Here,  $c\{ \}$  is a "shape factor" defined for any limited-duration function  $g$  as

$$c\{g\} = \frac{1}{2L_g} \int d\tau \left[ \frac{g(\tau)}{g(0)} \right]^2 , \quad (57)$$

where it is assumed that

$$g(\tau) = 0 \quad \text{for} \quad |\tau| > L_g ; \quad (58)$$

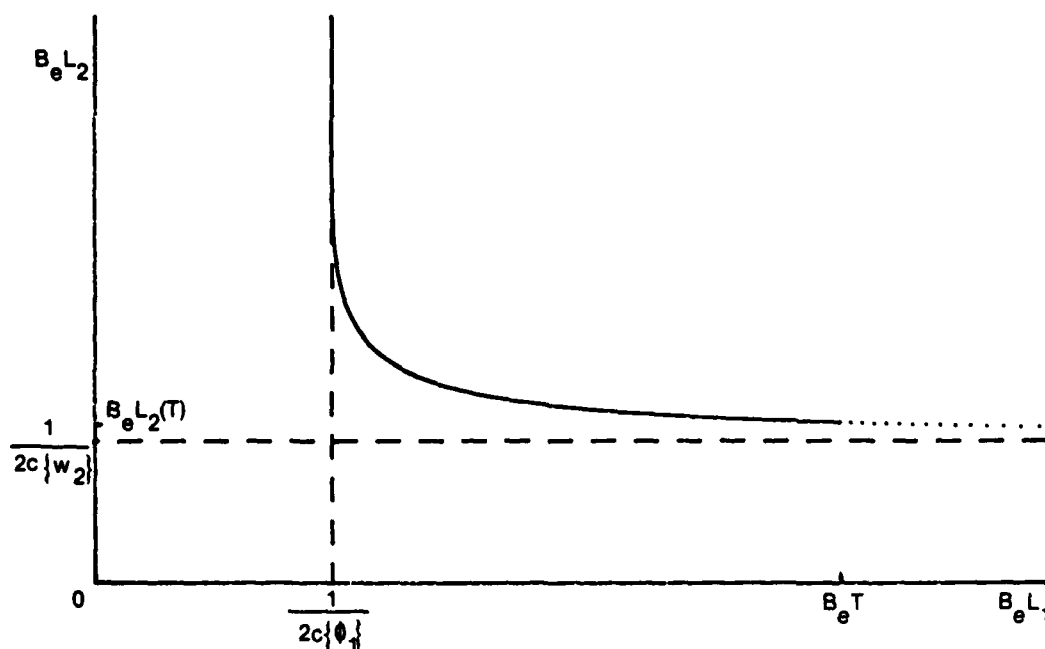


Figure 5. Interrelationship of Lengths  $L_1$  and  $L_2$  for Fixed Shapes of the Temporal and Lag Weightings

that is,  $2L_g$  is the nonzero extent of  $g(\tau)$ . Shape factor  $c\{g\}$  is independent of the magnitude of  $g(\tau)$  and of its length on the  $\tau$ -scale. Thus (56) yields  $B_e L_2(\min) = (2 c\{w_2\})^{-1}$ , which is entered on the ordinate in figure 5. However, since  $L_1$  is limited by  $T$ , the dotted portion of the curve on the far right is not attainable.

Conversely, if instead,  $L_2 \rightarrow \infty$ , then  $L_1 \rightarrow L_1(\min)$ , where now (from (52))

$$B_e^{-1} = \int d\tau \left[ \frac{\phi_1(\tau)}{\phi_1(0)} \right]^2 = 2L_1(\min) c\{\phi_1\} ; \quad (59)$$

that is,  $B_e L_1(\min) = (2 c\{\phi_1\})^{-1}$ . This value is attainable; it corresponds to no lag weighting. The ratio,  $L_2/L_1$ , of weighting lengths can take values in the range  $L_2(T)/T$  to  $\infty$ ; for  $B_e T \gg 1$ , this constitutes the range from almost zero to infinity.

Since the shape factors  $c\{w_2\}$  and  $c\{\phi_1\}$  are important limits on the weighting lengths, tables of their numerical values for a number of useful weight functions are given below. The weightings listed under C5, C3, C1 are those given in reference 19, figures 10, 11, 12, respectively; the notation means

- C5: continuous fifth derivative of weighting  
 C3: continuous third derivative of weighting  
 C1: continuous first derivative of weighting
- (60)

For the class of lag weightings given by

$$w_2(\tau) = \sum_{k \geq 0} a_k \cos(\pi k \tau / L_2) \quad \text{for } |\tau| < L_2 , \quad (61)$$

the shape factor is

$$c\{w_2\} = \frac{1}{2L_2} \int d\tau \left[ \frac{w_2(\tau)}{w_2(0)} \right]^2 = \frac{a_0^2 + \frac{1}{2} (a_1^2 + a_2^2 + \dots)}{(a_0 + a_1 + a_2 + \dots)^2} . \quad (62)$$

This is evaluated for several weightings in table 1.

**Table 1. Shape Factor for Lag Weighting  $w_2(\tau)$**

$w_2(\tau)$	$c\{w_2(\tau)\}$
Rectangular	1.000
Hanning	.3750
Hamming	.3964
Blackman	.3046
C5	.2256
C3	.2442
C1	.2558

For the class of temporal weightings given by

$$w_1(t) = \sum_{k \geq 0} a_k \cos(2\pi kt/L_1) \quad \text{for } |t| < L_1/2, \quad (63)$$

the correlation  $\phi_1(\tau)$  is evaluated in general in appendix C. The shape factor of  $\phi_1(\tau)$ ,

$$c\{\phi_1\} = \frac{1}{2L_1} \int d\tau \left[ \frac{\phi_1(\tau)}{\phi_1(0)} \right]^2, \quad (64)$$

can then be evaluated numerically and is given in table 2.

**Table 2. Shape Factor for Correlation  $\phi_1(\tau)$  of Temporal Weighting  $w_1(t)$**

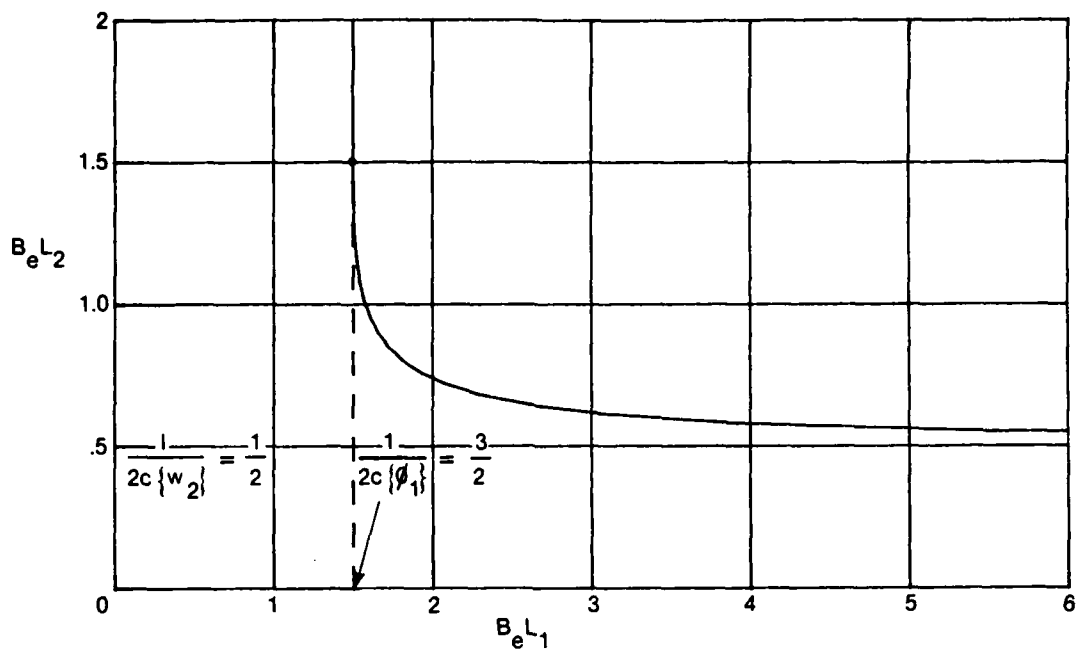
$w_1(t)$	$c\{\phi_1\}$
Rectangular	.3333 = 1/3
Hanning	.2405 = $(8\pi^2 + 35)/(48\pi^2)$
Hamming	.2628
Blackman	.2073
C5	.1545
C3	.1678
C1	.1763

Plots of the relationship between  $L_1$  and  $L_2$  dictated by (52) are given in figure 6 for various combinations of temporal and lag weightings. For a rectangular lag weighting, the curve will actually reach  $B_e L_1 = (2c\{\phi_1\})^{-1}$  when  $L_2 = L_1$ ; then the curve goes vertically up from this point for  $L_2 \geq L_1$  (see figure 6A). The procedure for the evaluation of figure 6 is as described under figure 5; namely, pick a value for  $L_2/L_1$ , compute  $B_e L_1$  via (52), and then compute  $B_e L_2 = B_e L_1 * (L_2/L_1)$ .

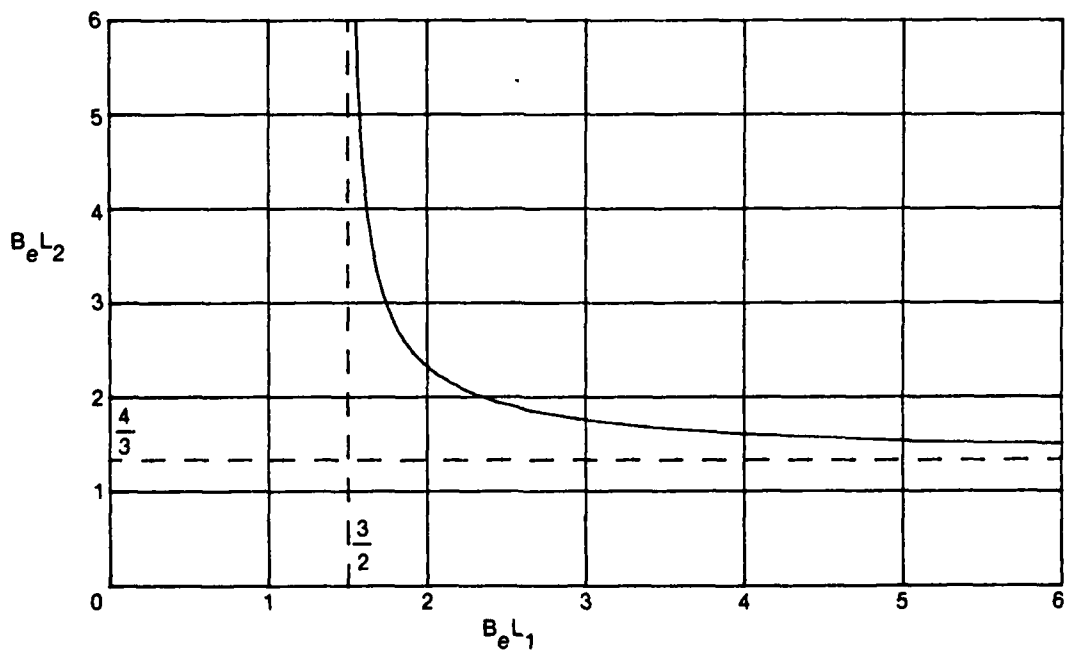
If the maximum segment length,  $L_1$ , is specified (as for example, when the maximum FFT size and the time-sampling spacing  $\Delta_t$  are fixed), under what condition can a desired effective frequency resolution,  $B_d$ , be met? The answer to this question is available from figure 5; namely, we see that

$$B_e L_1 \geq (2c\{\phi_1\})^{-1}, \quad \text{or} \quad B_e \geq \frac{1}{2c\{\phi_1\}L_1}. \quad (65)$$

Thus if desired resolution  $B_d$  is greater than or equal to the right-most term of (65), there exists a choice for lag length  $L_2$  that will yield the desired frequency resolution. The shape factor in (65) depends only on the temporal weighting  $w_1(t)$ .

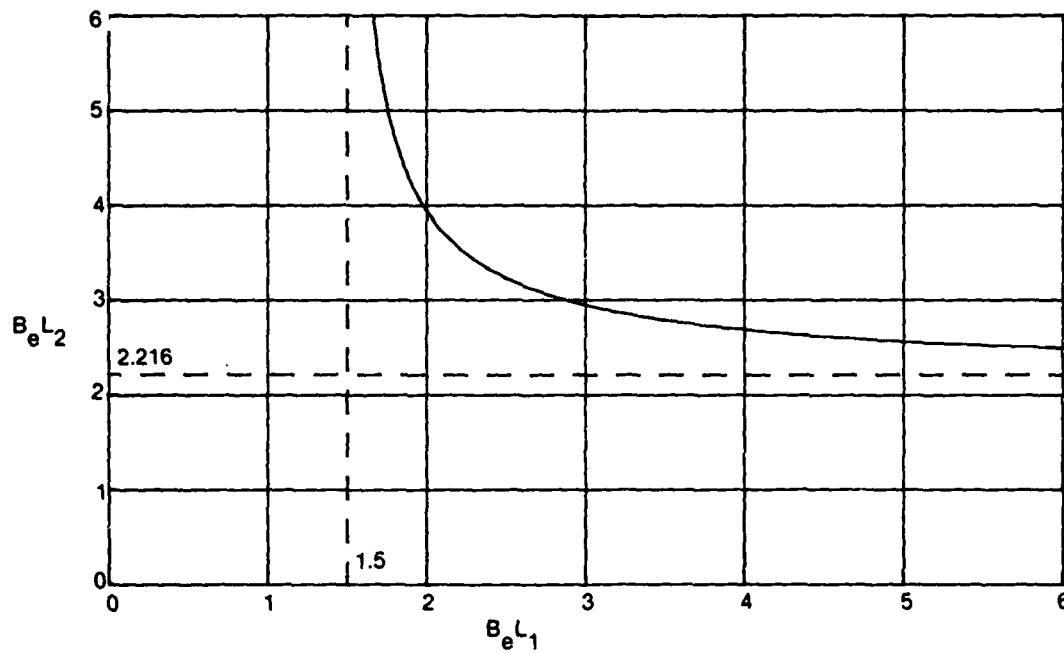


6A. Rectangular Temporal Weighting, Rectangular Lag Weighting

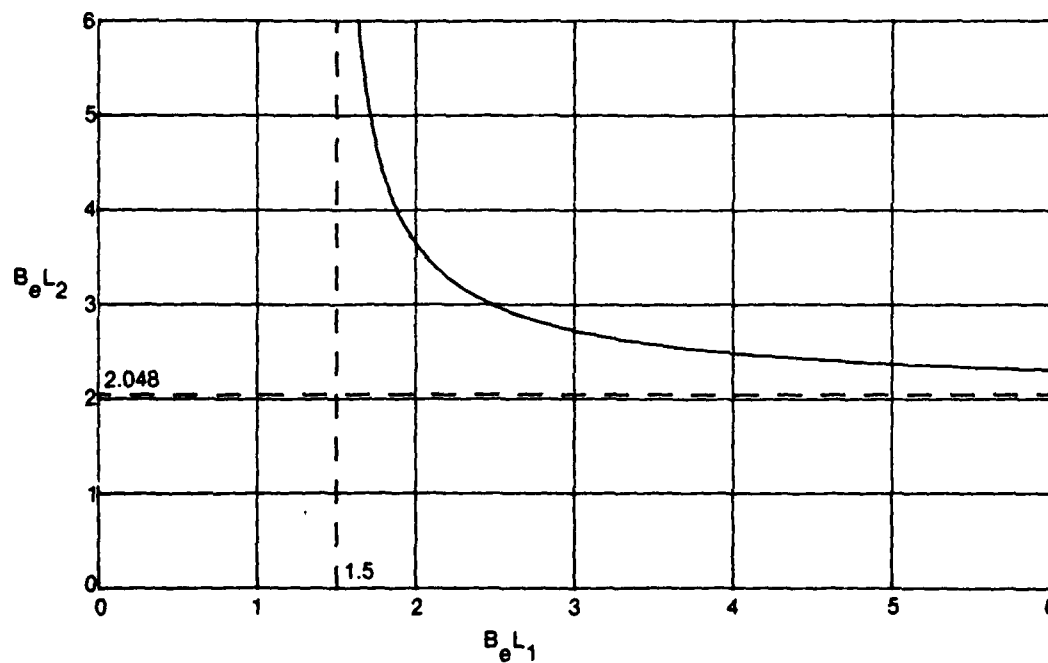


6B. Rectangular Temporal Weighting, Hanning Lag Weighting

Figure 6. Allowed Lengths of Various Temporal and Lag Weighting Pairs

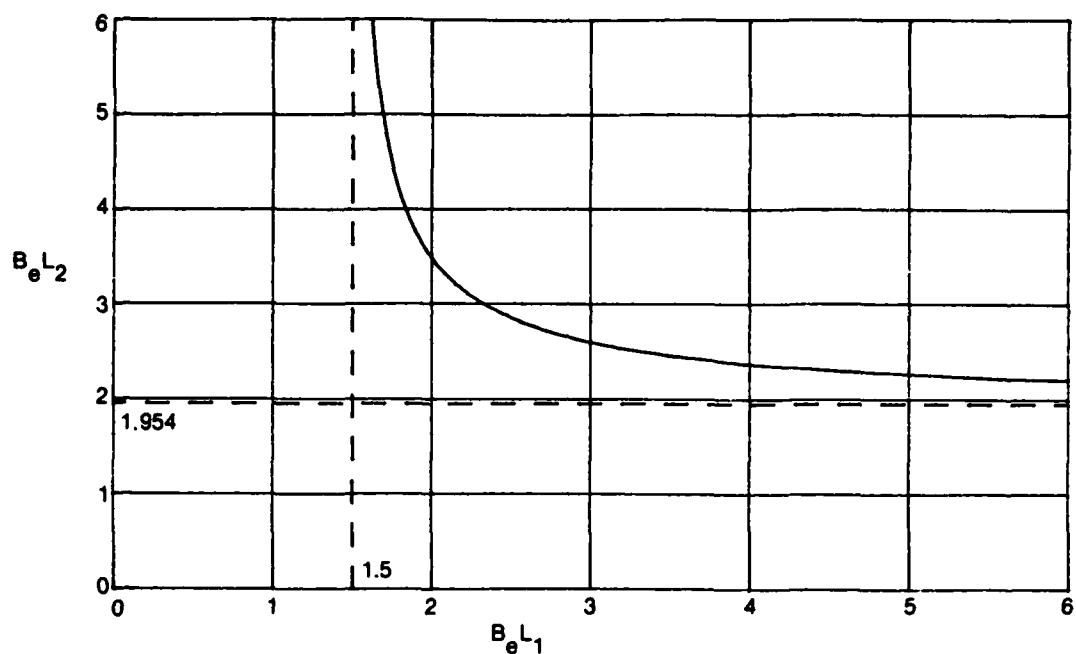


6C. Rectangular Temporal Weighting, C5 Lag Weighting

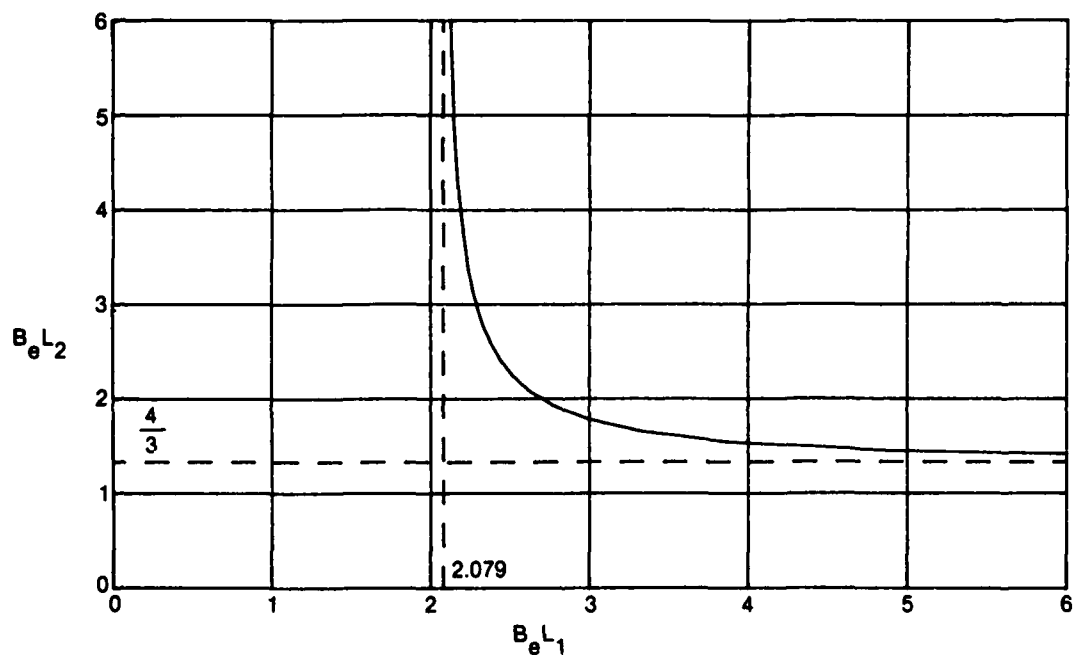


6D. Rectangular Temporal Weighting, C3 Lag Weighting

Figure 6. Allowed Lengths of Various Temporal and Lag Weighting Pairs (Cont'd)



6E. Rectangular Temporal Weighting, C1 Lag Weighting



6F. Hanning Temporal Weighting, Hanning Lag Weighting

Figure 6. Allowed Lengths of Various Temporal and Lag Weighting Pairs (Cont'd)

### Normalization of Weightings

The average of the first-stage correlation estimate was given in (43). For  $\tau = 0$ , it yields

$$\text{Av}\{\hat{R}_1(0)\} = R(0) \phi_1(0) \quad . \quad (66)$$

Since  $R(0)$  is the true power in the process  $x(t)$  under investigation, it is convenient to normalize according to

$$1 = \phi_1(0) = \int dt w_1^2(t) \quad . \quad (67)$$

Then  $\hat{R}_1(0)$  is an unbiased estimator of  $R(0)$ .

Additionally, from (47) and (48), we have, for the second-stage correlation estimate,

$$\text{Av}\{\hat{R}_2(0)\} = R(0) \phi_1(0) w_2(0) \quad . \quad (68)$$

Therefore, in addition to (67), we also set lag weighting value

$$w_2(0) = 1 \quad , \quad (69)$$

making  $\hat{R}_2(0)$  an unbiased estimator of  $R(0)$ . There follows, for the effective weighting,

$$w_e(0) = 1 \quad . \quad (70)$$

Since there is no significant loss of generality, the normalizations in (67), (69), and (70) will be used in the rest of this report.

### Discrete-Time Processing

For the impulsive temporal weighting introduced in (24)-(29), the normalization (67) must be modified somewhat, since the integral of  $w_1^2(t)$  in (24) would be infinite. We resort to (28) and require that the origin value of the sample correlation satisfy the unbiased requirement that

$$\text{Av}\{\hat{R}_{10}\} = R(0) \quad . \quad (71)$$

Reference to (28), (29), (26), and (43) yields

$$\text{Av}\{\hat{R}_{10}\} = \text{Av}\{\hat{R}_0^{(p)}\} = \Delta_t \sum_m \overline{|y_{pm}|^2} = \Delta_t \sum_m w_{1m}^2 R(0) \quad ; \quad (72)$$



therefore the normalization is

$$\Delta_t \sum_m w_{1m}^2 = 1 \quad . \quad (73)$$

This is the discrete analog to the integral constraint in (67).

The correlation  $\phi_1(\tau)$  of temporal weighting  $w_1(t)$  in (24) is given by (44) as usual and is expressible as

$$\phi_1(\tau) = \Delta_t \sum_k \phi_{1k} \delta(\tau - k\Delta_t) \quad , \quad (74)$$

where

$$\phi_{1k} \equiv \Delta_t \sum_m w_{1,m} w_{1,m-k} \quad . \quad (75)$$

Thus we see that (73) is tantamount to  $\phi_{10} = 1$ , which replaces the constraint  $\phi_1(0) = 1$  in (67) for the continuous temporal weighting case.

If we also require that second-stage correlation estimate (42) satisfy the unbiased requirement

$$\text{Av}\{\hat{R}_{20}\} = R(0) \quad , \quad (76)$$

then, as before, we require

$$w_2(0) = 1 \quad . \quad (77)$$

Finally, the effective weighting becomes, upon use of (74),

$$w_e(\tau) = \phi_1(\tau) w_2(\tau) = \Delta_t \sum_k \phi_{1k} w_2(k\Delta_t) \delta(\tau - k\Delta_t) \quad . \quad (78)$$

The normalizations adopted above make the area of the impulse at  $\tau = 0$  equal to

$$\Delta_t \phi_{10} w_2(0) = \Delta_t \quad . \quad (79)$$

### Examples of Effective Windows

We consider first a rectangular temporal weighting  $w_1(t)$ , for which the correlation is triangular,

$$\phi_1(\tau) = 1 - |\tau|/L_1 \quad \text{for } |\tau| < L_1, \quad (80)$$

and the class of lag weightings as given earlier by (61):

$$w_2(\tau) = \sum_{k \geq 0} a_k \cos(\pi k \tau / L_2) \quad \text{for } |\tau| < L_2. \quad (81)$$

Then constraint (52) yields

$$B_e L_2 = \left( 2 \int_0^1 dx \left[ \sum_{k \geq 0} a_k \cos(\pi k x) \right]^2 \left[ 1 - \frac{L_2 x}{L_1} \right]^2 \right)^{-1} \quad \text{for } L_2 \leq L_1. \quad (82)$$

The effective weighting,  $w_e(\tau)$ , is given by the product of (80) and (81); its Fourier transform is the effective window

$$w_e(f) = \frac{2L_2}{\pi^2} \sum_{k \geq 0} a_k \left\{ \left( 1 - \frac{L_2}{L_1} \right) 2\pi v \sin(2\pi v) \frac{(-1)^k}{4v^2 - k^2} \right. \\ \left. + \frac{L_2}{L_1} \left[ 1 - (-1)^k \cos(2\pi v) \right] \frac{4v^2 + k^2}{(4v^2 - k^2)^2} \right\} \quad \text{for } L_2 \leq L_1, \quad (83)$$

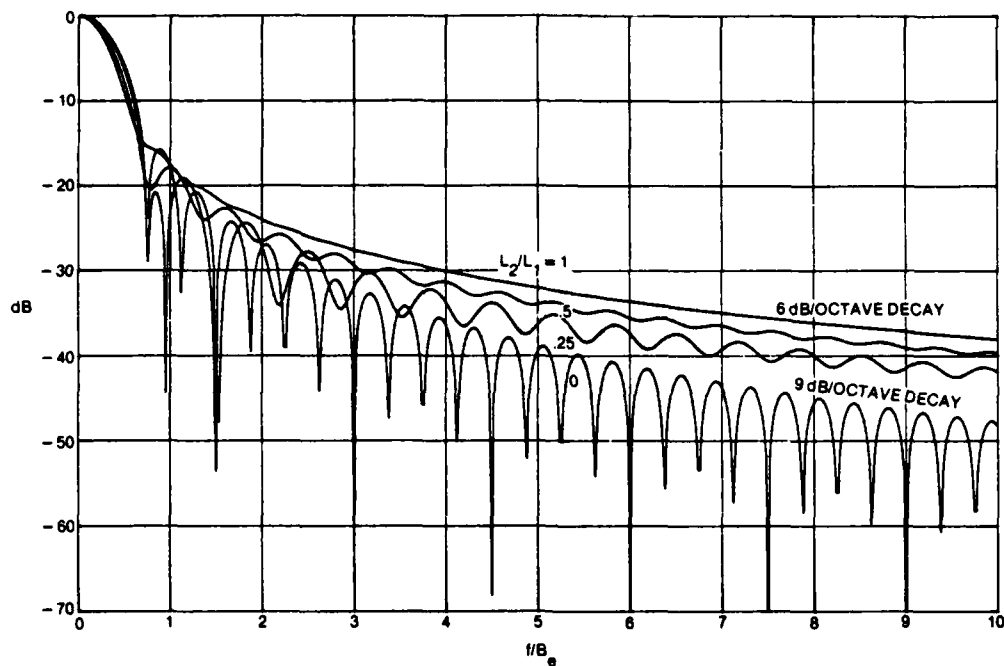
where

$$v \equiv B_e L_2 u, \quad u \equiv f/B_e. \quad (84)$$

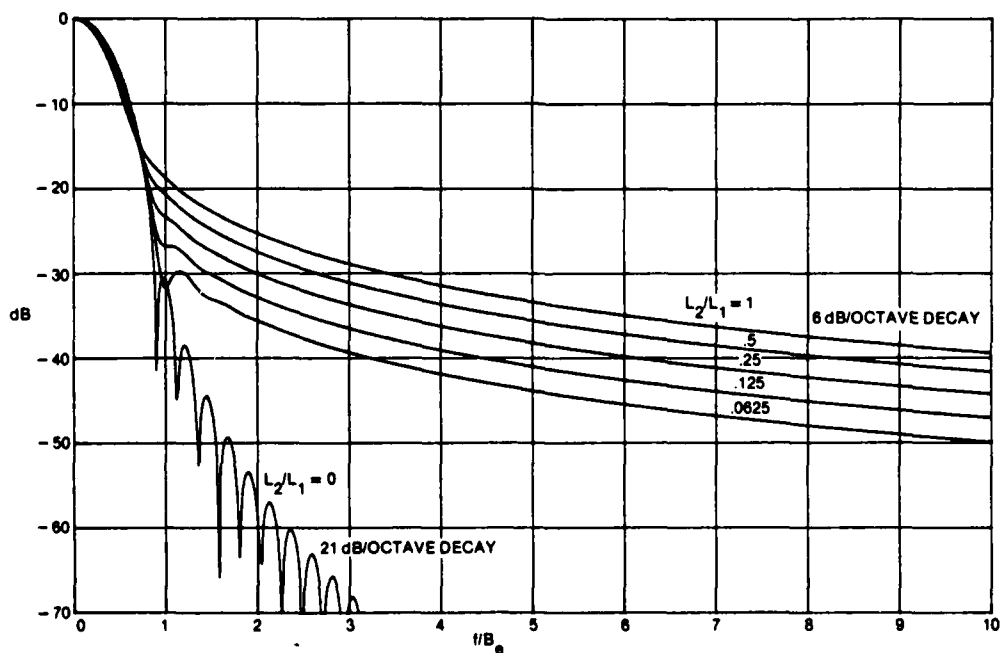
Although (82) and (83) could be extended to the case where  $L_2 > L_1$ , that range is not of practical interest, as will become apparent later.

The numerical procedure for evaluation of the effective window is to first select the shape of the lag window by specifying coefficients  $\{a_k\}$ . Then we choose a value for  $L_2/L_1$  and compute  $B_e L_2$  from (82). We can then employ (83) and (84) to determine  $W_e(f)$ . Four examples are given in figure 7, where we have plotted

$$\text{dB} \equiv 10 \log \frac{W_e(f)}{W_e(0)} \quad \text{vs} \quad \frac{f}{B_e}. \quad (85)$$

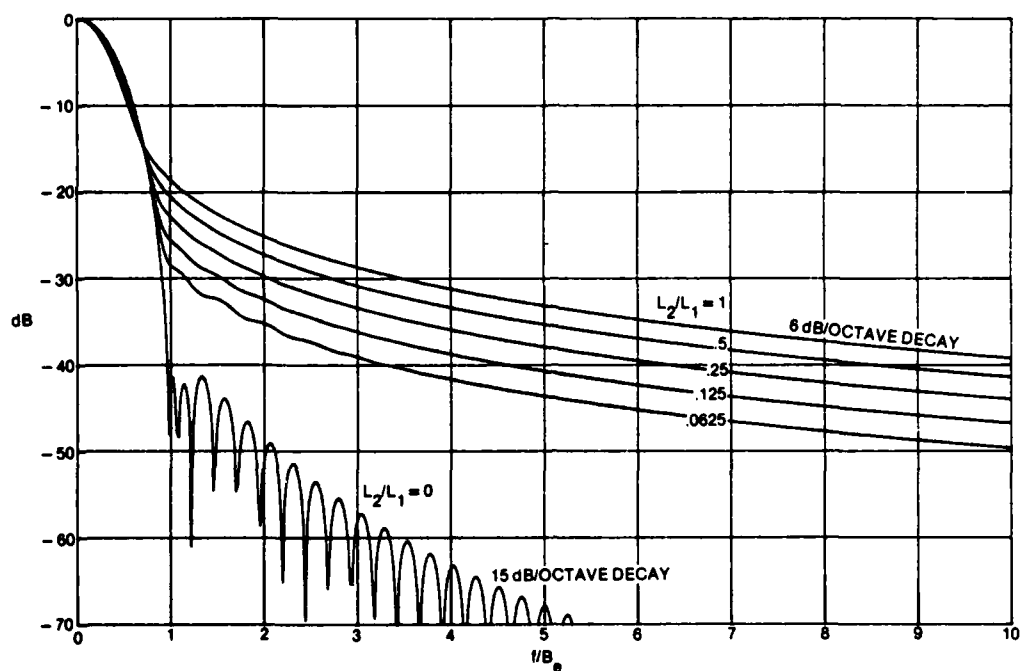


7A. Effective Window for Rectangular Temporal Weighting and Hanning Lag Weighting

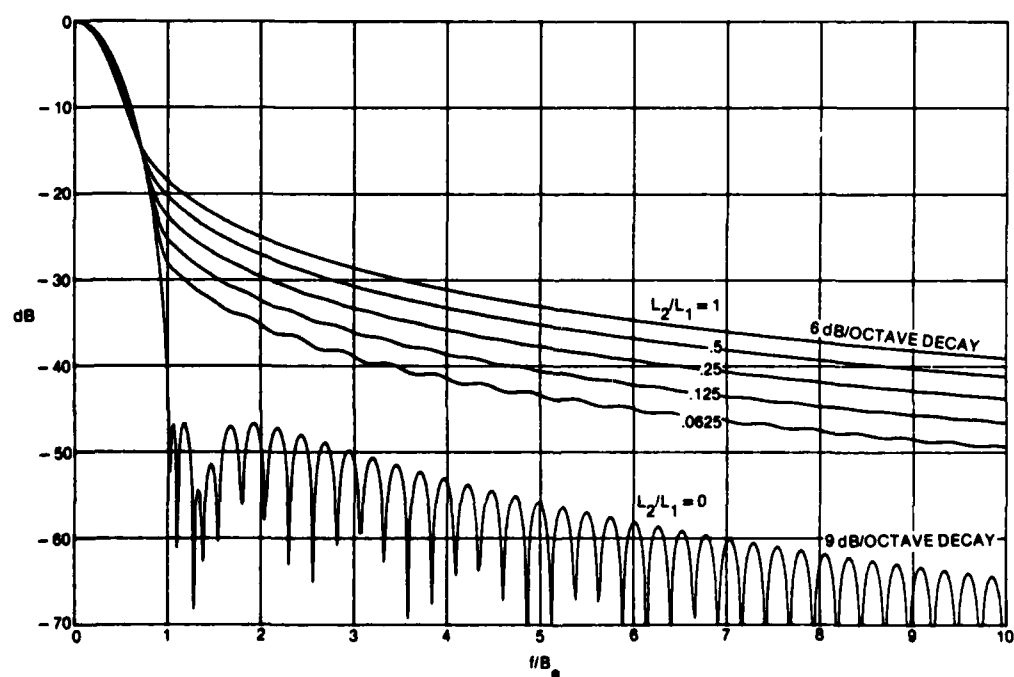


7B. Effective Window for Rectangular Temporal Weighting and C5 Lag Weighting

Figure 7. Examples of Effective Windows for Rectangular Temporal Weighting



7C. Effective Window for Rectangular Temporal Weighting and C3 Lag Weighting



7D. Effective Window for Rectangular Temporal Weighting and C1 Lag Weighting

Figure 7. Examples of Effective Windows for Rectangular Temporal Weighting (Cont'd)

The curve corresponding to  $L_2/L_1 = 0$  (i.e.,  $L_1 = \infty$ ) is that for the lag window alone.

The overriding impression of the plots in figure 7 is that the effective window has poor side lobe behavior and decay unless  $L_2/L_1$  is chosen very small. That is, the poor side lobe behavior of temporal window  $W_1^2(f)$  enters the convolution (51) for  $W_e(f)$ , and is difficult to suppress, even by choice of good lag windows. It would be desirable to realize the bottom-most figures in each of these plots, since these latter curves have good side lobes and decay; a procedure for accomplishing this goal is presented in the next section.

The situation is significantly improved when the temporal weighting is tapered. An example for Hanning temporal and lag weightings is given in figure 8. The bottom-most curve has an eventual 18 dB/octave decay because  $\phi_1(\tau)$  has a discontinuous fifth derivative at  $\tau = 0$ , which is not compensated by  $w_2(\tau)$ . ( $\phi_1(\tau)$  also has a discontinuous fifth derivative at  $\tau = \pm L_1$ , but this is converted to a discontinuous seventh derivative for  $w_e(\tau)$  by means of  $w_2(\tau)$  when  $L_2 = L_1$ .)

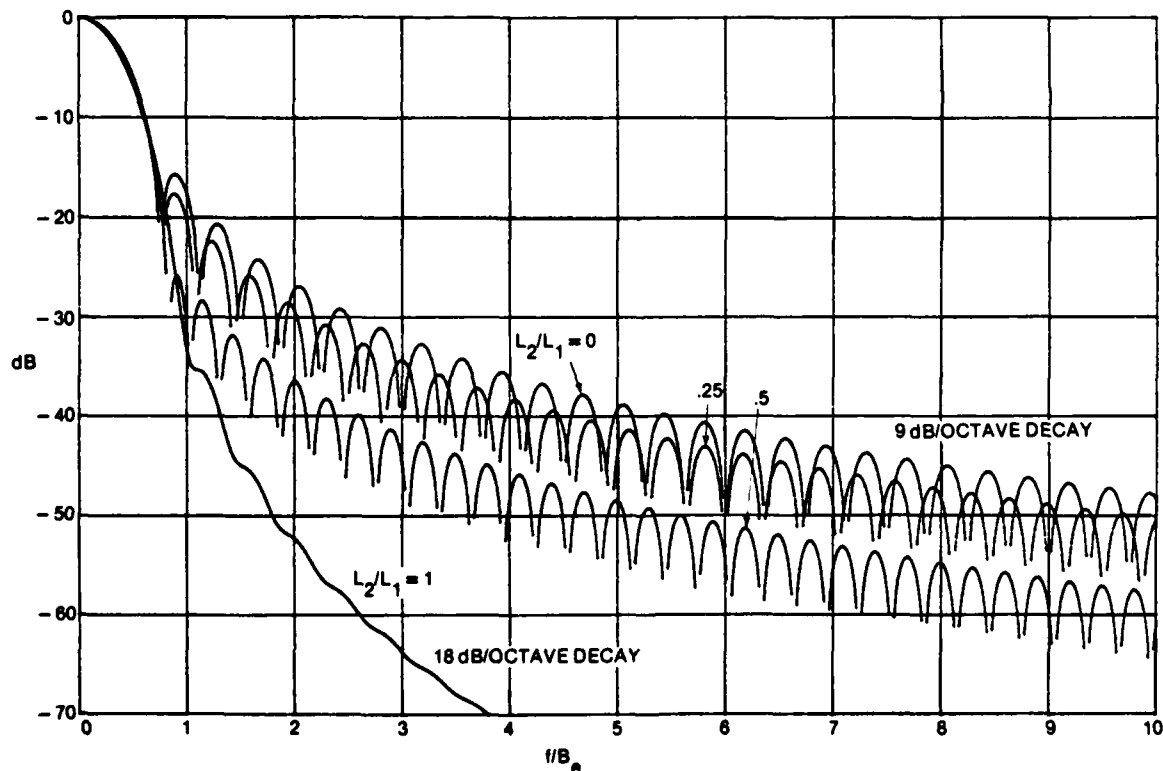


Figure 8. Effective Window for Hanning Temporal Weighting and Hanning Lag Weighting

### Discrete-Time Processing

The temporal weighting  $w_1(t)$  is given by (24), and its correlation  $\phi_1(\tau)$  by (74), where coefficients  $\{\phi_{1k}\}$  are given by (75). The Fourier transform of (24) leads to temporal window

$$W_1(f) = \Delta_t \sum_m w_{1m} \exp(-i2\pi f m \Delta_t) \quad , \quad (86)$$

which has period  $1/\Delta_t$  in  $f$ , and is real and even, since weight sequence  $\{w_{1m}\}$  is real and even.

For a general lag weighting  $w_2(\tau)$ , the effective weighting is given by (78). The effective window  $W_e(f)$  is given by (51) as the Fourier transformation of (78):

$$W_e(f) = \Delta_t \sum_k \phi_{1k} w_2(k\Delta_t) \exp(-i2\pi f k \Delta_t) \quad , \quad (87)$$

which also has period  $1/\Delta_t$  in  $f$ , and is real and even, since lag weighting  $w_2(\tau)$  is real and even. This result holds for *any* lag weighting  $w_2(\tau)$  and is a very useful form for computing  $W_e(f)$  for any value of frequency  $f$ . The convolutional form of (51) is not very useful for computing  $W_e(f)$  for general  $W_2(f)$ .

As a special case, we can evaluate (87) at particular frequencies  $f_n = n\Delta_f = n/(N\Delta_t)^{-1}$ , as in (33) and (34):

$$W_e\left(\frac{n}{N\Delta_t}\right) = \Delta_t \sum_k \phi_{1k} w_2(k\Delta_t) \exp(-i2\pi nk/N) \quad , \quad (88)$$

which can be accomplished as an  $N$ -point FFT. We should choose  $N$  large in order that (88) be capable of tracing the fine detail of  $W_e(f)$ . This is an attractive and efficient way to evaluate the effective window.

### A Special Lag Window for Discrete-Time Processing

The result in (87) applies for discrete time sampling and arbitrary lag weighting. We now specialize to the lag window given in (38):

$$W_2(f) = \Delta_f \sum_n W_{2n} \delta(f - n\Delta_f) \quad , \quad (89)$$

where sequence  $\{W_{2n}\}$  is real and even, and frequency spacing  $\Delta_f$  need not be related to time spacing  $\Delta_t$  in (24). Then, via inverse Fourier transformation (20), the corresponding lag weighting is

$$w_2(\tau) = \Delta_f \sum_n W_{2n} \exp(i2\pi n \Delta_f \tau) \quad , \quad (90)$$

and, in particular, sample values

$$w_2(k\Delta_t) = \Delta_f \sum_n W_{2n} \exp(i2\pi nk \Delta_f \Delta_t) \quad , \quad (91)$$

which can be used in (87) to evaluate  $W_e(f)$  for any frequency  $f$  whatsoever.

An alternative form to (87) for calculation of  $W_e(f)$  for this special lag window (89) is afforded by substitution of (89) in the convolutional form of (51):

$$W_e(f) = \Delta_f \sum_n W_{2n} W_1^2(f - n\Delta_f) \quad (92)$$

The temporal window  $W_1(f)$  is given here by (86). Equation (92) is an attractive form when the number,  $N_2$ , of nonzero coefficients  $\{W_{2n}\}$  is small and  $W_1(f)$  can be evaluated in closed form. In fact, (92) actually holds for *any* temporal weighting  $w_1(t)$ ; it is not limited to the discrete-time forms (24) and (86). Equations (87) and (92) are duals in the sense that (87) applies to any  $w_2(\tau)$  and an impulsive  $w_1(t)$ , whereas (92) applies to any  $W_1(f)$  and an impulsive  $W_2(f)$ . Either equation can be evaluated at any  $f$  of interest.

Our first example is rectangular temporal weighting; from figure 2, (24), and (73),  $w_{1m} = L_1^{-1/2}$ , where  $L_1 = N_1 \Delta_t$ . Then, from (86),

$$W_1^2(f) = L_1 \left[ \frac{\sin(\pi L_1 f)}{N_1 \sin(\pi L_1 f / N_1)} \right]^2 \equiv L_1 Q_{N_1}(L_1 f) \quad (93)$$

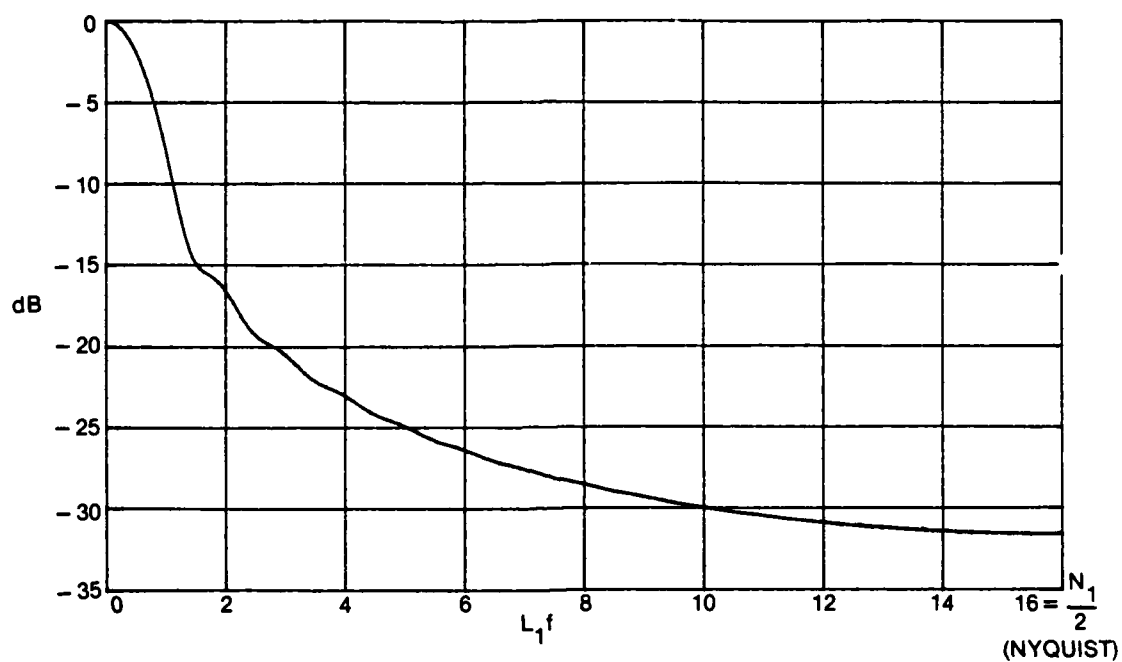
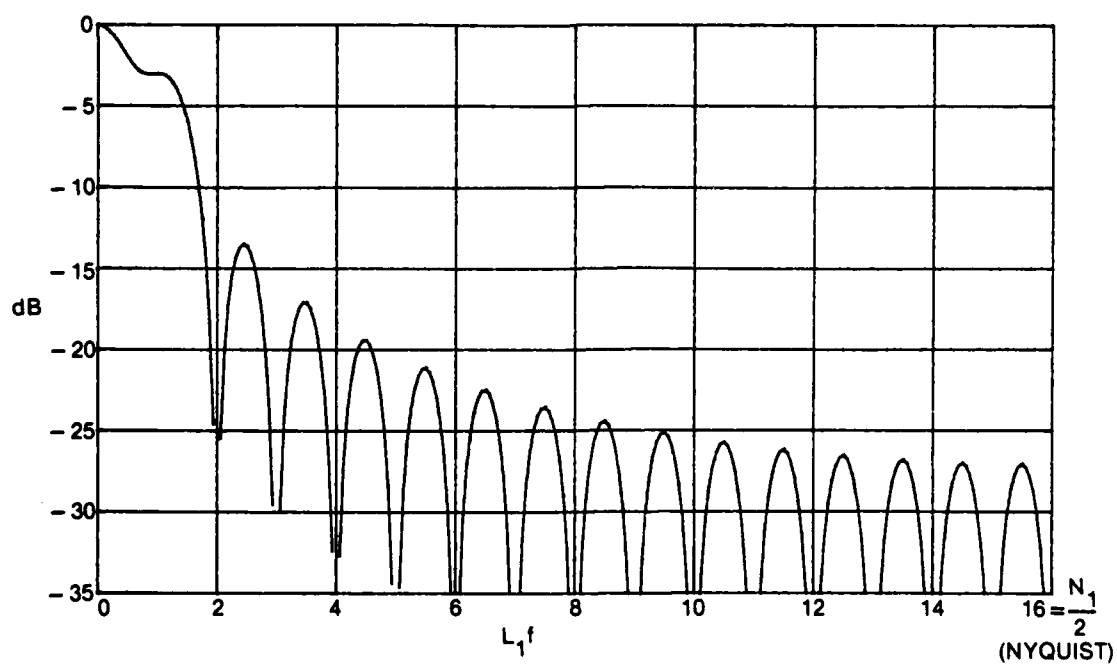
For the lag window, we take impulsive form (89); then (92) and (93) give

$$W_e(f) = L_1 \Delta_f \sum_n W_{2n} Q_{N_1}(L_1 f - nL_1 \Delta_f) \quad (94)$$

Two important choices yet to be made are  $L_1 \Delta_f$ , the relative frequency spacing used in frequency smoothing, and the set of coefficients  $\{W_{2n}\}$ . For Hanning frequency smoothing, the latter is

$$W_{2n} = \frac{1}{\Delta_f} \begin{cases} 1/2 & \text{for } n = 0 \\ 1/4 & \text{for } n = \pm 1 \\ 0 & \text{otherwise} \end{cases}, \quad N_2 = 3 \quad (95)$$

The effective windows for  $L_1 \Delta_f = 1/2$  and 1 are given in figure 9 for  $N_1 = 32$ . Window (94) is even about  $f=0$  and has period  $1/\Delta_f$  in  $f$ ; hence only the region  $0, (2\Delta_f)^{-1}$  is plotted in  $f$ . The window in figure 9A has no deep notches since the frequency displacement (spacing)  $\Delta_f = (2L_1)^{-1}$  causes the notches to be filled in; the window for  $\Delta_f = L_1^{-1}$  in figure 9B reinforces the notches and has a significant shoulder near  $f = 1/L_1$ . Both windows have slow decay with frequency and do not have significant rejection, even near Nyquist frequency. Closer spacings than  $(2L_1)^{-1}$  do not improve the decay or rejection capabilities; wider spacings than  $L_1^{-1}$  generate humps in the effective window. The bad features of rectangular temporal weighting are not undone by Hanning frequency smoothing; see also figure 7A.

9A.  $L_1 \Delta_f = 1/2, N_1 = 32$ 9B.  $L_1 \Delta_f = 1, N_1 = 32$ 

**Figure 9. Effective Window for Discrete-Time Rectangular Temporal Weighting and Hanning Frequency-Smoothing**



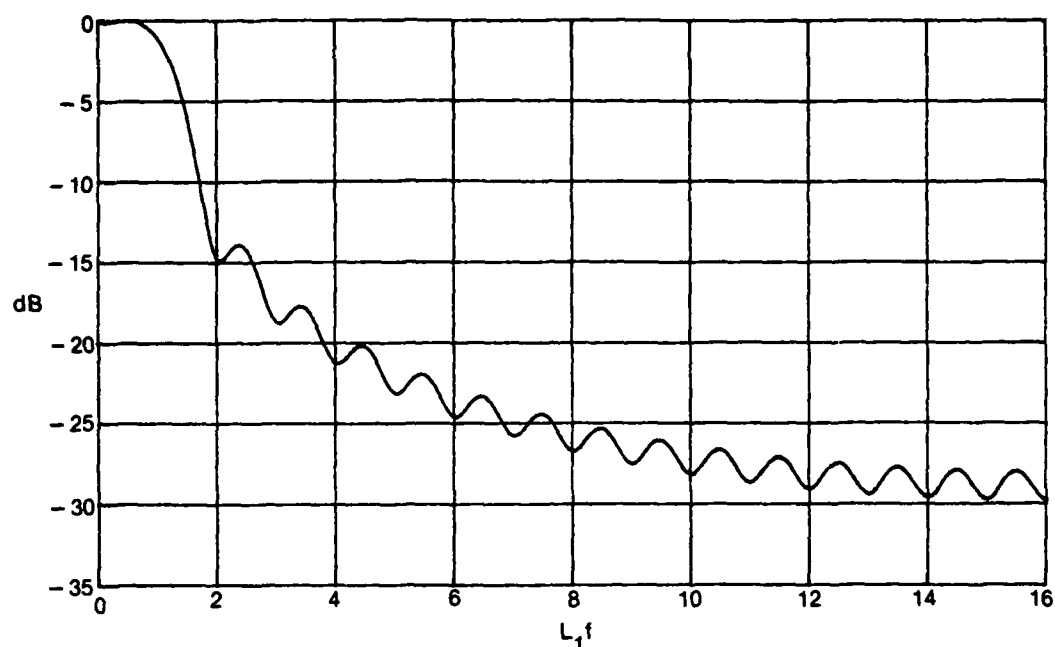
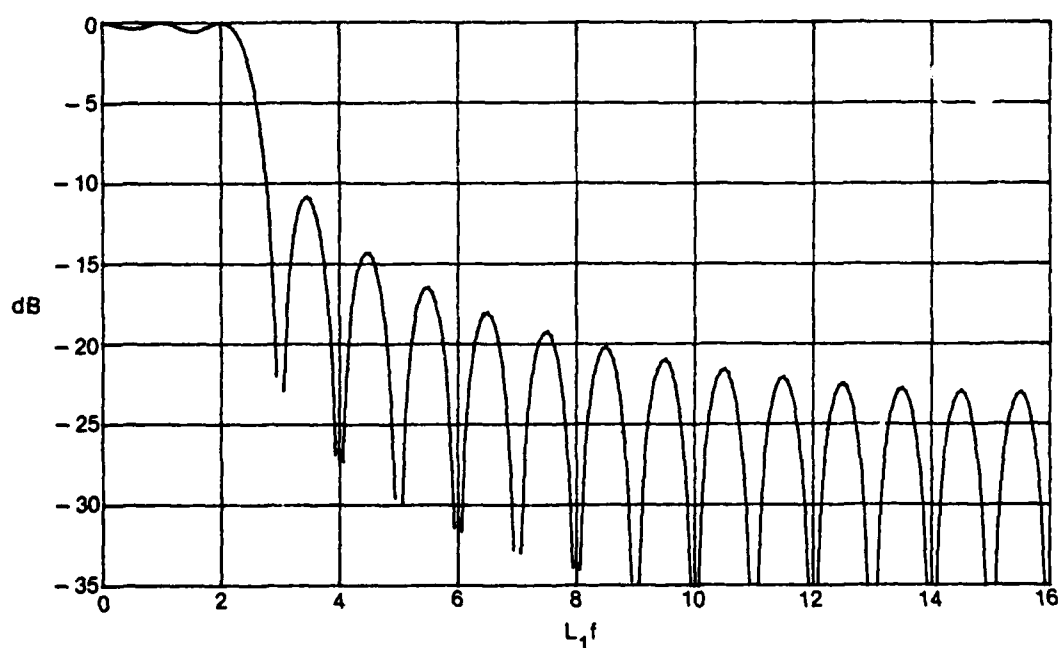
The second example is rectangular temporal weighting with  $N_1 = 32$  and rectangular frequency smoothing over five frequency samples; i.e.,

$$w_{2n} = \frac{1}{\Delta_f} \begin{cases} 1/5 & \text{for } |n| \leq 2 \\ 0 & \text{otherwise} \end{cases}, \quad N_2 = 5. \quad (96)$$

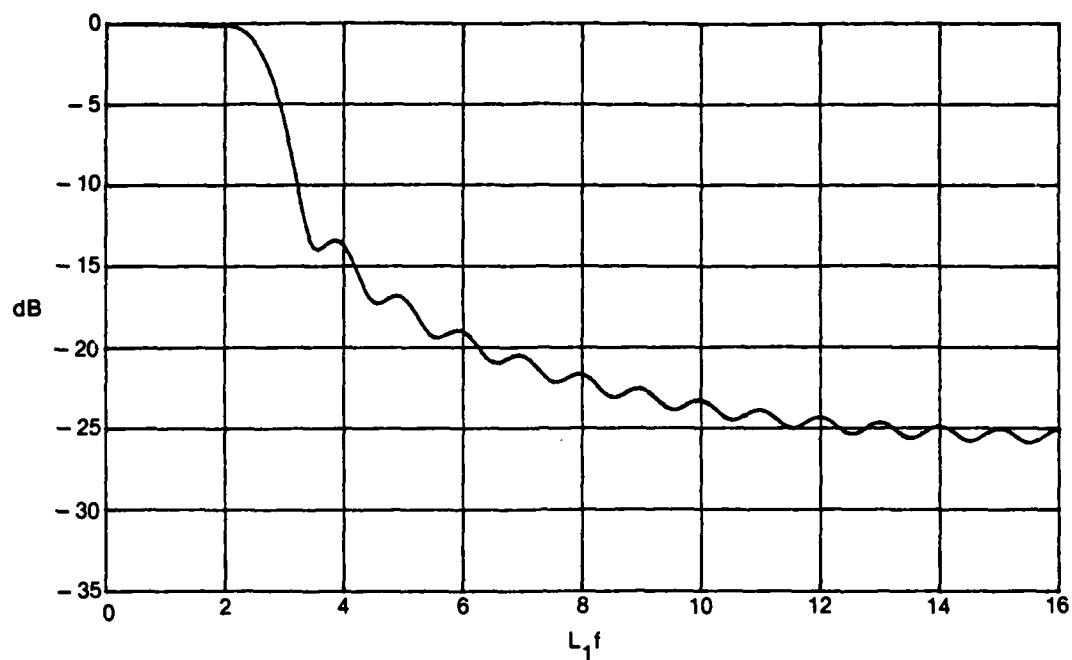
The effective windows for  $L_1 \Delta_f = 1/2$  and 1 are given in figure 10. The main lobe humps in figure 10B are caused by the displacements of  $W_1^2(f)$  according to (92). Both windows again have poor decay and poor rejection; however, the main lobe is more box-like in shape than previously.

The third example is identical to the previous one except that  $N_2 = 11$ . The plots in figure 11 reveal that the main lobe is quite box-like, but the decay and rejection are no better than previous cases. According to (92), we are merely taking the poor side lobes and decay of  $W_1^2(f)$  and moving them about, but not improving them in any way.

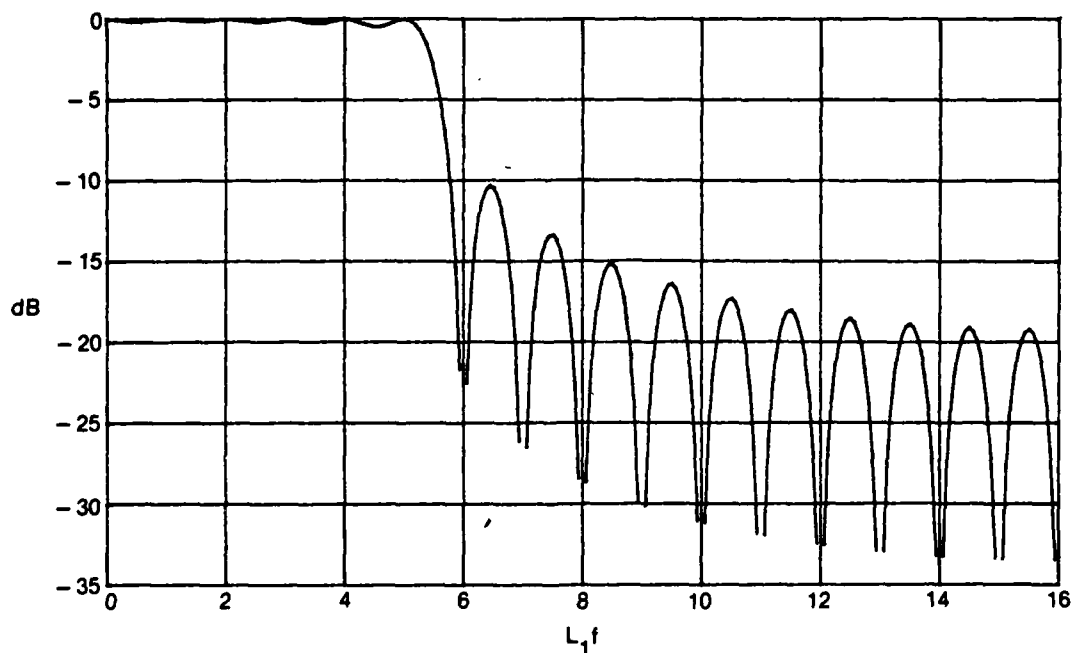
The last example in this subsection is Hanning temporal weighting with no frequency smoothing at all. The effective window for  $N_1 = 32$  is simply  $W_1^2(f)$  and is plotted in figure 12. It has the familiar -31.5 dB peak side lobe, a rapid decay, and significant rejection capability.

10A.  $L_1 \Delta_f = 1/2, N_1 = 32$ 10B.  $L_1 \Delta_f = 1, N_1 = 32$ 

**Figure 10. Effective Window for Discrete-Time Rectangular Temporal Weighting and Rectangular Frequency-Smoothing with  $N_2 = 5$**



11A.  $L_1 \Delta_f = 1/2, N_1 = 32$



11B.  $L_1 \Delta_f = 1, N_1 = 32$

Figure 11. Effective Window for Discrete-Time Rectangular Temporal Weighting and Rectangular Frequency-Smoothing with  $N_2 = 11$

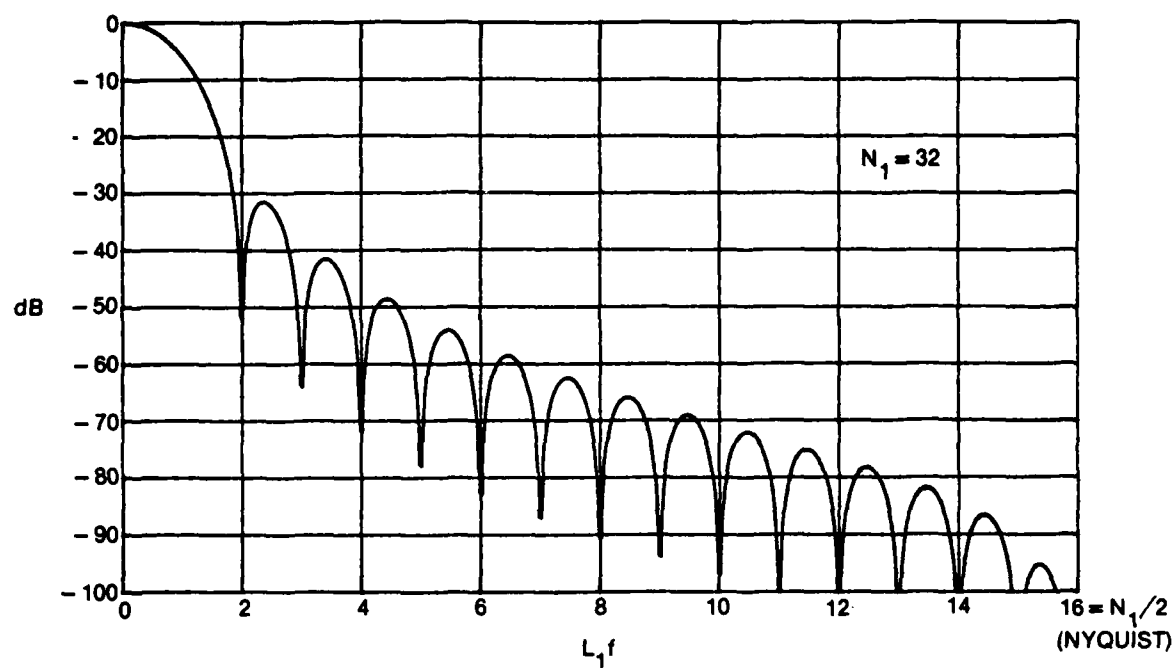


Figure 12. Effective Window for Discrete-Time Hanning Temporal Weighting

### Lag Reshaping for Desired Effective Windows

From (48), the effective weighting of the generalized spectral analysis technique is given by

$$w_e(\tau) = \phi_1(\tau) w_2(\tau) \quad , \quad (97)$$

where  $\phi_1(\tau)$  is the correlation of temporal weighting  $w_1(t)$ ; see (44). Now suppose that for a given temporal weighting  $w_1(t)$ , with associated correlation  $\phi_1(\tau)$ , we choose lag weighting

$$w_2(\tau) = \frac{w_d(\tau)}{\phi_1(\tau)} \quad \text{for } |\tau| \leq L_2 \leq L_1 \quad , \quad (98)$$

where  $w_d(\tau)$  is a desirable weighting with  $w_d(0) = 1$  (in keeping with (67) and (70)) and

$$w_d(\tau) = 0 \quad \text{for } |\tau| > L_2 \quad . \quad (99)$$

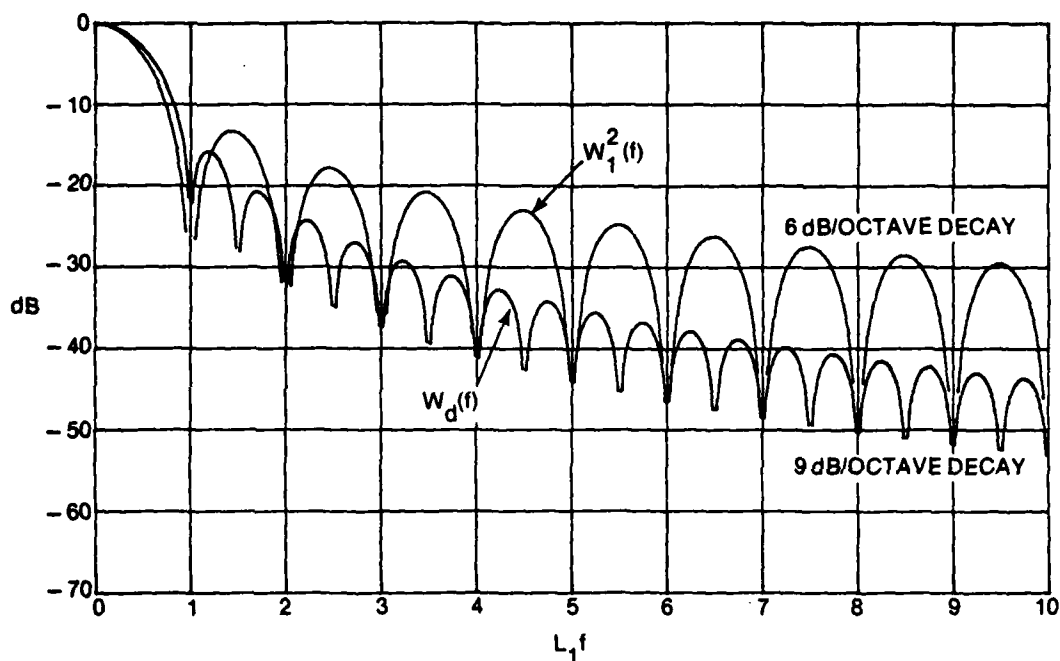
Notice that  $L_2 > L_1$  is disallowed in (98) since  $\phi_1(\tau) = 0$  for  $|\tau| > L_1$ . Then substitution of (98) in (97) yields

$$w_e(\tau) = w_d(\tau) \quad , \quad W_e(f) = W_d(f) \quad . \quad (100)$$

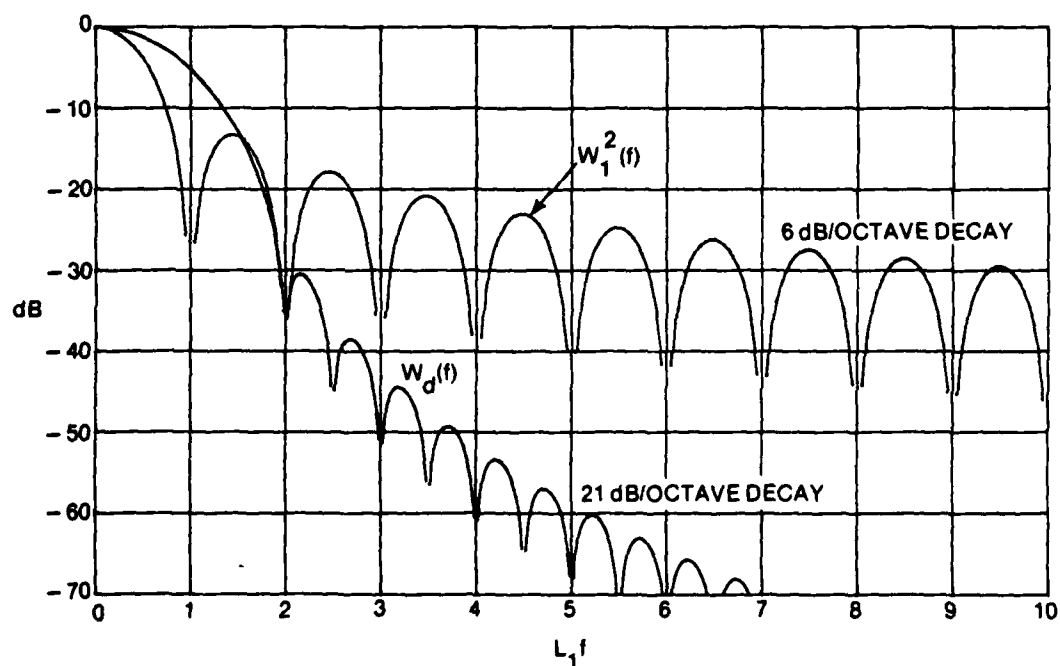
That is, the effective weighting and window are equal to the desired behavior. We have "undone" the effects of bad side lobes in temporal window  $W_1(f)$  by reshaping according to lag weighting  $w_2(\tau)$  in (98). (The effect on the variance of the second-stage spectral estimate  $\hat{G}_2(f)$  will be considered later.)

To see how much can be accomplished by this approach, some attainable effective windows that can be realized via lag reshaping, for continuous rectangular temporal weighting, are given in figure 13 for the largest possible value of  $L_2$ , namely,  $L_2 = L_1$ . Superposed on the window  $W_1(f)$  for rectangular temporal weighting are the effective windows for four candidate lag reshaping, for  $L_2 = L_1$ . These are the narrowest possible effective windows for a given  $L_1$ . The first one in figure 13A corresponds to an effective Hanning weighting. The peak side lobe is only reduced from -13.3 dB to -15.7 dB, and the asymptotic decay is improved to 9 dB/octave from 6 dB/octave. The main lobe width is only slightly broadened.

Much greater improvements in side lobe behavior are possible with other lag weightings, and are illustrated in parts (B)-(D) of figure 13. They illustrate, respectively, peak side lobe levels and decays of: -30.5 dB, 21 dB/octave; -41.3 dB, 15 dB/octave; and -46.7 dB, 9 dB/octave. The deeper peak side lobe is realized at the expense of a slower asymptotic decay. They all have about the same main lobe width. The C5, C3, C1 weightings were introduced and explained in (60).

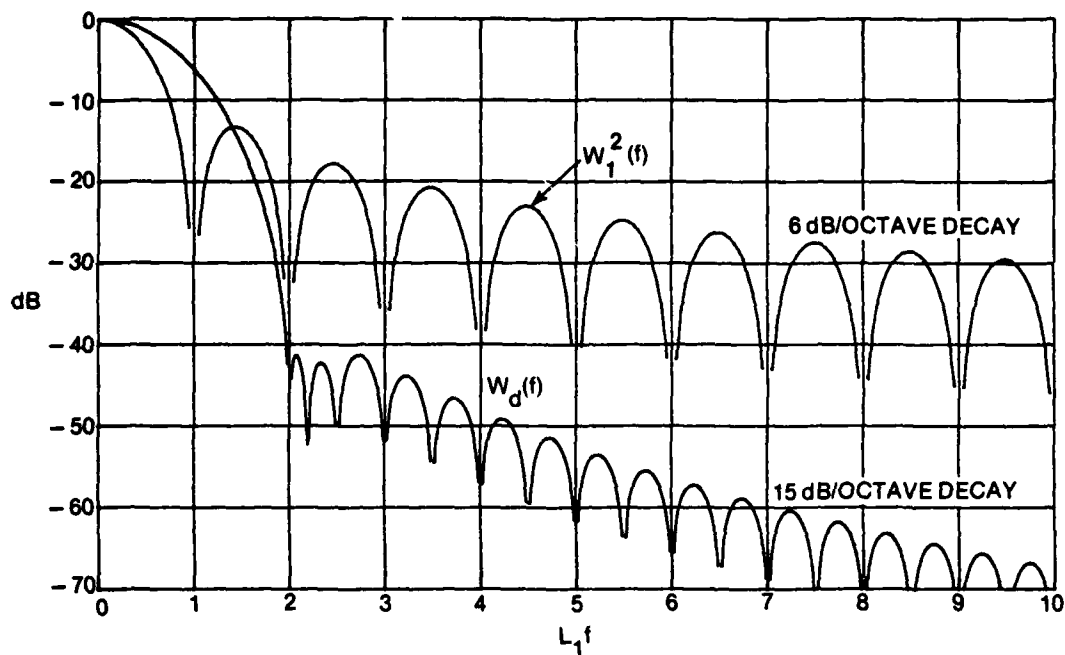


13A. Reshaping to Achieve Hanning Weighting

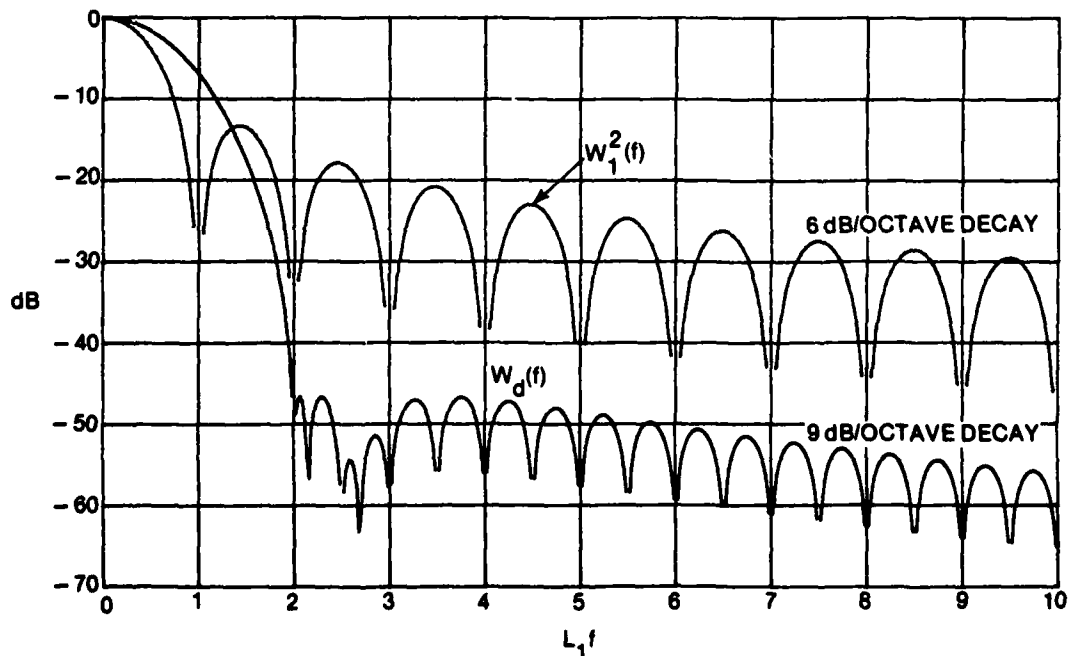


13B. Reshaping to Achieve C5 Weighting

Figure 13. Some Attainable Effective Windows via Lag Reshaping  
for Rectangular Temporal Weighting and  $L_2 = L_1$



13C. Reshaping to Achieve C3 Weighting



13D. Reshaping to Achieve C1 Weighting

Figure 13. Some Attainable Effective Windows via Lag Reshaping for Rectangular Temporal Weighting and  $L_2 = L_1$  (Cont'd)

Figure 13 illustrates how advantageous the reshaping technique can be in terms of peak side lobe and asymptotic decay, although the main lobe width is significantly increased. In fact, the peak side lobe at  $f \cong 1.5/L_1$  for the rectangular window is really not suppressed, so much as it is smeared out; however, the other peaks of  $W_f^2(f)$  for  $|f| > 2/L_1$  are indeed significantly reduced. Thus reduction of leakage via lag reshaping is a very effective method, *provided* that we accept the nearest side lobe of the temporal window; this conclusion is in contrast to reference 20, page 57. These general conclusions on lag reshaping hold also for temporal weightings other than rectangular, although the exact degree of improvement will be different.

If  $L_2$  is chosen less than  $L_1$ , the effective windows in figure 13 are simply broadened according to the ratio  $L_1/L_2$ . The peak side lobe levels and asymptotic decay are unchanged, but the main lobe width is increased. Here we are presuming  $L_1$  fixed and decreasing  $L_2$ .

If we insist that the combination of temporal weighting  $w_1(t)$  and lag reshaping  $w_2(\tau)$  in (98) have effective bandwidth  $B_e$ , then use of (52), (99)-(100), and (57)-(58) yields

$$B_e = \frac{w_e^2(0)}{\int d\tau w_e^2(\tau)} = \frac{w_d^2(0)}{\int d\tau w_d^2(\tau)} = \frac{1}{2L_2 c\{w_d\}}, \quad (101)$$

where  $c\{w_d\}$  is the shape factor of  $w_d(\tau)$  (see table 1). Thus

$$B_e L_2 = \frac{1}{2 c\{w_d\}} \quad \text{for } L_2 \leq L_1 \leq T; \quad (102A)$$

the limits on  $L_1$  in (102A) follow from (98) and (15).

A plot of the interrelationship between  $L_1$  and  $L_2$  (introduced in figure 5) is shown in figure 14 for the case of lag reshaping. The reason that the plot is flat, in contrast to figures 5 and 6, is that the *shape* of  $w_2(\tau)$  now changes as  $L_1$  changes. This behavior is discernible from (98), since the denominator varies while the numerator remains fixed according to the selection of  $w_d(\tau)$  and its associated bandwidth-length factor (102A).

If the maximum segment length,  $L_1$ , is specified (as for example when the maximum FFT size and the time-sampling spacing  $\Delta_t$  are fixed), the condition under which a desired effective frequency resolution,  $B_d$ , can be met is given by figure 14. Namely, we see that

$$B_e \geq \frac{1}{2 c\{w_d\} L_1}. \quad (102B)$$

Thus if desired resolution  $B_d$  is greater than or equal to the right-side of (102B), there exists a choice for segment length  $L_1$  that will yield the desired frequency resolution. The shape factor in (102B) depends only on the desired weighting  $w_d(\tau)$ . (See (65) and the accompanying discussion for the case where lag reshaping is not employed.)



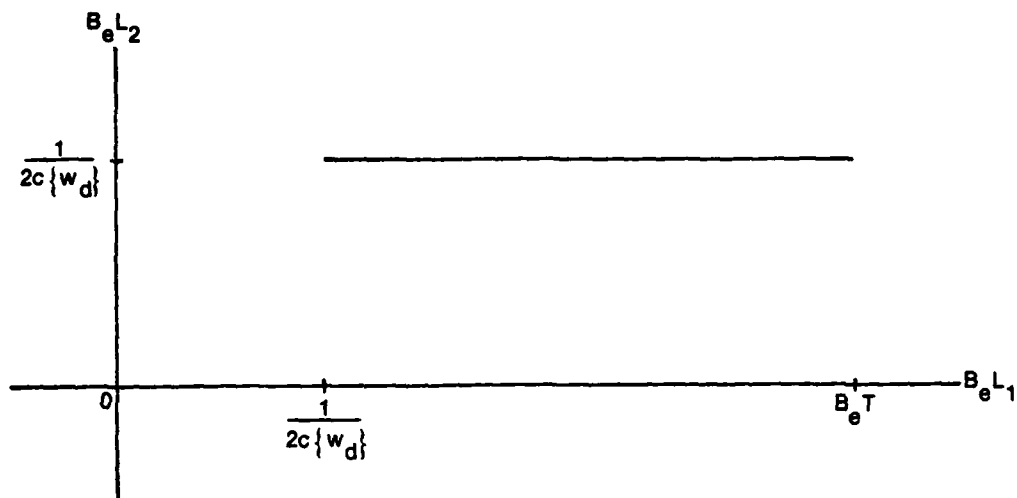


Figure 14.  $B_e L_2$  vs  $B_e L_1$  Plot for Lag Reshaping to Desired Weighting  $w_d(\tau)$

### Variance of Spectral Estimate

Up to this point, we have presumed nothing about the process  $x(t)$  except that it be (second-order) stationary during the observation interval  $T$ . Now we make a couple of assumptions about the process in order to obtain manageable expressions for the variance of the second-stage spectral estimate  $\hat{G}_2(f)$ , at frequency  $f$ . Our first assumption is that the true spectrum  $G$  of  $x(t)$  varies slowly in the neighborhood of the frequency of interest,  $f$ . More precisely, from (50) and (70), we obtain, for the mean spectral estimate,

$$\text{Av}\{\hat{G}_2(f)\} = \int du G(f - u) W_e(u) = G(f) \int du W_e(u) = G(f) , \quad (103)$$

where we assume that spectrum  $G$  is relatively constant in the frequency band  $(f - B_e/2, f + B_e/2)$ ; i.e., the only region where effective window  $W_e$  in (103) is substantially nonzero is in the range  $(-B_e/2, B_e/2)$ .

Our second assumption is that  $x(t)$  is a complex Gaussian process. The variance of  $\hat{G}_2(f)$  is developed under this assumption in appendix D, culminating in the exact result in (D-13):

$$\text{Var}\{\hat{G}_2(f)\} = \iint d\alpha d\beta G(\alpha) G(\beta) |\gamma(f - \alpha, f - \beta)|^2 Q_p(S(\alpha - \beta)) , \quad (104)$$

where window convolution function

$$\gamma(x, y) \equiv \int du W_2(u) W_1(x - u) W_1^*(y - u) \quad (105)$$

and periodic function

$$Q_p(u) \equiv \left[ \frac{\sin(\pi Pu)}{P \sin(\pi u)} \right]^2 . \quad (106)$$

The variance result in (104) does not require that spectrum  $G$  vary slowly in the neighbor of  $f$ ; the result utilizes only the Gaussian assumption on the process  $x(t)$ . The temporal and lag windows contribute through the window convolution function  $\gamma$ , while the shift  $S$  and number of pieces  $P$  appear through the periodic function  $Q_p$ .

When the assumption regarding a slowly varying spectrum  $G$  in the neighborhood of frequency  $f$  of interest is also invoked, (104) simplifies to forms given in (D-20) and (D-24); the latter is a "weighting domain" version of the variance:

$$\text{Var}\{\hat{G}_2(f)\} = G^2(f) \frac{1}{P} \sum_{p=1-P}^{P-1} \left( 1 - \frac{|p|}{P} \right) \int d\tau w_2^2(\tau) \phi_3(\tau, pS) , \quad (107)$$

where

$$\begin{aligned}\phi_3(\tau, \mu) &\equiv \int dt \, w_1\left(t + \frac{\mu - \tau}{2}\right) w_1\left(t + \frac{-\mu - \tau}{2}\right) w_1\left(t + \frac{\mu + \tau}{2}\right) w_1\left(t + \frac{-\mu + \tau}{2}\right) \\ &= \phi_3(\underline{+\tau}, \underline{+\mu})\end{aligned}\tag{108}$$

is a third-order correlation of temporal weighting  $w_1(t)$ . The form (107) is very useful if  $\phi_3$  can be evaluated in closed form. An "ambiguity domain" version of the variance is given by (D-20).

### Quality Ratio

The quality ratio for spectral estimation was defined in (4). With the aid of (103) and (107), it is given by

$$Q = \frac{\text{Var}\{\hat{G}_2(f)\}}{\text{Av}^2\{\hat{G}_2(f)\}} = \frac{1}{P} \sum_{p=1-P}^{P-1} \left(1 - \frac{|p|}{P}\right) \int d\tau w_2^2(\tau) \phi_3(\tau, pS) \quad (109)$$

Since the smallest possible value of  $Q$  is  $(TB_e)^{-1}$  (see (11) et seq.), the normalized quality ratio is

$$NQR \equiv Q \cdot TB_e = \frac{TB_e}{P} \sum_{p=1-P}^{P-1} \left(1 - \frac{|p|}{P}\right) \int d\tau w_2^2(\tau) \phi_3(\tau, pS) \quad (110)$$

This quantity can never be smaller than unity.

If we employ (52) and the normalizations (67) and (69), the convenient form

$$NQR = T \frac{\frac{1}{P} \sum_{p=1-P}^{P-1} \left(1 - \frac{|p|}{P}\right) \int d\tau w_2^2(\tau) \phi_3(\tau, pS)}{\int d\tau w_2^2(\tau) \phi_1^2(\tau)} \quad (111)$$

for the normalized quality ratio is obtained. We are interested in the behavior of the normalized quality ratio for different choices of  $P$ ,  $S$ ,  $w_1(t)$ , and  $w_2(\tau)$ . The constraint of a fixed effective bandwidth  $B_e$  has been injected into the normalized quality ratio via the use of (52) in (111). The quantities  $\phi_1$  and  $\phi_3$  needed in (111) are given by (44) and (108) respectively.

Before we embark on particular cases, some general observations on overlap (shift  $S$ ) are in order. For a minimum normalized quality ratio (minimum variance) with each temporal weighting  $w_1(t)$ , we should use approximately the optimum overlap as derived in reference 9. For example, Hanning temporal weighting should be employed with approximately 62 percent overlap, although there is only an 8 percent loss in stability if 50 percent overlap is used for convenience (reference 9, tables 5 and 6). There is no point in considering excessive or inadequate overlap, since this leads to excessive computational effort or more variance, respectively. Inadequate temporal overlap cannot be made up, in terms of variance reduction, by any amount of quadratic smoothing. This can be seen by observing that poor first-stage correlation estimates  $\hat{R}_1(\tau)$  are merely multiplied by lag weighting  $w_2(\tau)$ , and are not improved statistically in any way for  $|\tau| < L_2$ ; those estimates for  $|\tau| > L_2$  are discarded by the lag weighting.

Some related work on the effects of windowing on stability is given in references 21 and 22. However, the present report is more thorough and detailed in its treatment of the problem and the inclusion of a bandwidth constraint.

### Special Cases of Generalized Spectral Analysis Technique

This section will consider several special cases of the normalized quality ratio and show how some earlier results are obtained as limiting cases. The next section will treat the generalized spectral analysis results.

#### One Piece, $P = 1$

When only one piece is used in the first-stage spectral estimate  $\hat{G}_1(f)$  in (14), we have a generalized version of the Blackman-Tukey approach, in that the data  $x(t)$  are weighted by  $w_1(t)$  prior to computing the sample correlation; see (16) and (13). Also, we allow length  $L_1 < T$  (although we soon show that the best  $L_1$  is equal to  $T$ , the available record length). From (111),

$$NQR_1 = T \frac{\int d\tau w_2^2(\tau) \phi_2(\tau)}{\int d\tau w_2^2(\tau) \phi_1^2(\tau)}, \quad (112)$$

where (using (108))

$$\phi_2(\tau) \equiv \phi_3(\tau, 0) = \int dt w_1^2\left(t + \frac{\tau}{2}\right) w_1^2\left(t - \frac{\tau}{2}\right) = \int dt w_1^2(t) w_1^2(t - \tau) \quad (113)$$

is the correlation of the squared temporal weight function  $w_1^2(t)$ .

Now if  $L_1 \gg L_2$ ,  $w_2$  is much narrower than  $\phi_1$  or  $\phi_2$ . In that case, the exact shape of  $w_2$  is irrelevant, and (112), (113), (44), figure 2, and Schwarz's inequality yield

$$NQR_1 = T \frac{\phi_2(0)}{\phi_1^2(0)} = T \frac{\int dt w_1^4(t)}{\left[\int dt w_1^2(t)\right]^2} \geq \frac{T}{L_1} \quad \text{for } L_1 \gg L_2. \quad (114)$$

Equality in (114) results if and only if  $w_1^2(t)$  is constant for  $|t| < L_1/2$ ; furthermore, the best value for  $L_1$  is then its largest allowed value  $T$  (see (15)), in which case we have Blackman-Tukey processing and

$$NQR_1(\text{rectangular } w_1) = 1 \quad \text{for } T = L_1 \gg L_2. \quad (115)$$

This result agrees with reference 2, section B.8. It should be noted that  $L_1 \gg L_2$  implies  $B_e L_1 \gg B_e L_2 \geq .5/c\{w_2\} \sim 1$ , according to figure 5 and table 1; thus stable estimates result in this case.

Instead of rectangular temporal weighting, consider Hanning weighting:

$$w_1(t) = \left(\frac{8}{3L_1}\right)^{1/2} \cos^2\left(\frac{\pi t}{L_1}\right) \quad \text{for } |t| < L_1/2. \quad (116)$$

Then

$$\phi_1(0) = \int dt w_1^2(t) = 1, \quad \phi_2(0) = \int dt w_1^4(t) = \frac{35}{18L_1}, \quad (117)$$

and (114) yields

$$\text{NQR}_1(\text{Hanning } w_1) \approx \frac{35}{18} \frac{T}{L_1} \quad \text{for } L_1 \gg L_2. \quad (118)$$

The best  $L_1$  is again  $T$ ; however, the minimum value of the normalized quality ratio is then  $35/18$ , which is twice the value in (115) for rectangular temporal weighting. This is due to the squandering of the edges of the available data record by the small values there of Hanning temporal weighting.

Now instead of assuming  $L_1 \gg L_2$ , let us reconsider, for general  $w_1$ ,  $L_1$ ,  $L_2$ , the normalized quality ratio (112). Since  $w_1(t)$  is zero for  $|t| > L_1/2$ , we have from (44),

$$\phi_1(\tau) = \int_{a(\tau)}^{b(\tau)} dt w_1(t) w_1(t - \tau) \quad \text{for } |\tau| < L_1, \quad (119)$$

where

$$\left. \begin{aligned} a(\tau) &= \max(-L_1/2, -L_1/2 + \tau) \\ b(\tau) &= \min(L_1/2, L_1/2 + \tau) \end{aligned} \right\} \quad \text{for } |\tau| < L_1. \quad (120)$$

Then by Schwarz's inequality, (113), and (120),

$$\begin{aligned} \phi_1^2(\tau) &\leq \int_{a(\tau)}^{b(\tau)} dt w_1^2(t) w_1^2(t - \tau) \int_{a(\tau)}^{b(\tau)} dt 1 \\ &= \phi_2(\tau) (L_1 - |\tau|) \quad \text{for } |\tau| < L_1. \end{aligned} \quad (121)$$

Equality is realized in (121) if and only if  $w_1(t)$  is constant for  $|t| < L_1/2$ ; that is, the best temporal weighting for maximum stability is rectangular when  $P=1$ . This conclusion holds regardless of the form of lag weighting  $w_2(\tau)$  or the relative sizes of  $L_1$  and  $L_2$ .

As an example, for rectangular temporal weighting,

$$\begin{aligned} w_1(t) &= L_1^{-1/2} \quad \text{for } |t| < L_1/2, \\ \phi_1(\tau) &= 1 - |\tau|/L_1 \quad \text{for } |\tau| < L_1, \\ \phi_2(\tau) &= \frac{1}{L_1}(1 - |\tau|/L_1) \quad \text{for } |\tau| < L_2, \end{aligned} \quad (122)$$

and (112) yields for general  $w_2(\tau)$ ,

$$\text{NQR}_1(\text{rect. } w_1) = \frac{T}{L_1} \frac{\int_{-L_1}^{L_1} d\tau w_2^2(\tau) \left(1 - \frac{|\tau|}{L_1}\right)}{\int_{-L_1}^{L_1} d\tau w_2^2(\tau) \left(1 - \frac{|\tau|}{L_1}\right)^2} \quad (123)$$

The ratio of integrals is obviously greater than 1. For a monotonically decreasing lag weighting  $w_2(\tau)$  of fixed shape, the ratio of integrals is minimized by choosing  $L_1$  as large as possible. Since the leading factor also has the same behavior, the best value for the normalized quality ratio is

$$\text{NQR}_1(\text{rect. } w_1) = \frac{\int_{-T}^T d\tau w_2^2(\tau) \left(1 - \frac{|\tau|}{T}\right)}{\int_{-T}^T d\tau w_2^2(\tau) \left(1 - \frac{|\tau|}{T}\right)^2} \quad \text{for } L_1 = T \quad (124)$$

We cannot give numerical values to this ratio of integrals until we select a lag weighting  $w_2(\tau)$  and determine the specific value of  $L_2(T)$ ; see figures 5 and 6. But if  $TB_e \gg 1$ , which is the usual case for reasonably good spectral estimates, then  $L_2 \ll L_1 = T$  and

$$\text{NQR}_1(\text{rect. } w_1) \approx 1 \quad \text{for } L_1 = T, \quad TB_e \gg 1 \quad (125)$$

This result holds independently of the exact shape of the lag weighting  $w_2(\tau)$ ; thus we could choose  $w_2(\tau)$  such that the effective weighting  $w_e(\tau)$  in (48) has good side lobe behavior, as discussed in an earlier section.

### No Quadratic Frequency-Smoothing

No quadratic smoothing corresponds to

$$\begin{aligned} w_2(f) &= \delta(f), \\ w_2(\tau) &= 1 \quad \text{for all } \tau \end{aligned} \quad (126)$$

Thus  $L_2 = \infty$ , and (109) becomes

$$\begin{aligned} Q &= \frac{1}{P} \sum_{p=1-P}^{P-1} \left(1 - \frac{|p|}{P}\right) \int d\tau \phi_3(\tau, pS) \\ &= \frac{1}{P} \sum_{p=1-P}^{P-1} \left(1 - \frac{|p|}{P}\right) \phi_1^2(pS) \end{aligned} \quad (127)$$

since

$$\begin{aligned} \int d\tau \phi_3(\tau, \mu) &= \int d\tau \int du w_1(u) w_1(u - \mu) w_1(u + \tau) w_1(u + \tau - \mu) \\ &= \int du w_1(u) w_1(u - \mu) \phi_1(\mu) = \phi_1^2(\mu) \end{aligned} \quad (128)$$

by use of (108). The result in (127) is identical to reference 9, equation 8, when we recall definition (109) and normalization (67).

### Non-Overlapping Segments

Let us choose time shift  $S$  in (13) equal to the segment length  $L_1$ ; this leads to abutting time segments. From (15), we have

$$PL_1 = T, \quad (129)$$

where we have chosen to use up all of the available data length. (This is different from the earlier subsection for  $P=1$  where we allowed  $L_1 < T$ .) The general normalized quality ratio in (111) reduces to

$$NQR_P = L_1 \frac{\int d\tau w_2^2(\tau) \phi_2(\tau)}{\int d\tau w_2^2(\tau) \phi_1^2(\tau)}, \quad (130)$$

where we used (129), the fact that  $w_1(t)$  is of length  $L_1$ , and (113).

Once again, we refer to bound (121) and the fact that equality is realized only for a flat weighting  $w_1(t)$ . Thus, from (130) and (122),

$$NQR_P(\text{rect. } w_1) = \frac{\int_0^{L_1} d\tau w_2^2(\tau) \left(1 - \frac{\tau}{L_1}\right)}{\int_0^{L_1} d\tau w_2^2(\tau) \left(1 - \frac{\tau}{L_1}\right)^2} \quad (131)$$

for any (real symmetric) lag weighting  $w_2(\tau)$ . The ratio of integrals is obviously always greater than unity; therefore, for a monotonically decreasing lag weighting  $w_2(\tau)$  of fixed shape, values of  $L_1$  large in comparison with  $L_2$  are preferred. However,  $L_1 \gg L_2$  means that

$$TB_e = PL_1 B_e \gg PL_2 B_e \geq \frac{P}{2c\{w_2\}} \sim P, \quad (132)$$

according to (129) and figure 5. Thus large time-bandwidth products,  $TB_e$ , are required; also  $P$  must be kept small enough to realize  $L_1 \gg L_2$ . In this case, we have

$$NQR_P(\text{rect. } w_1) \approx 1 \text{ for } TB_e \gg 1, \quad L_1 \gg L_2, \quad (133)$$



regardless of lag weighting  $w_2(\tau)$ . Qualitatively, when  $L_1 \gg L_2$ , the edge effects of segmenting the data  $x(t)$  are negligible, since only a small fraction of the utilized correlation values that can be calculated from a record of length  $T$  are neglected when using segments of length  $L_1$ . Stated alternatively, all the first-stage correlation estimates that are used, namely  $\hat{R}_1(\tau)$  for  $|\tau| < L_2$ , have the same quality (stability) when  $L_2 \ll L_1$ .

An example of the exact normalized quality ratio for Hanning lag weighting and rectangular temporal weighting is afforded by substituting the equation

$$w_2(\tau) = \cos^2 \left( \frac{\pi}{2} \frac{\tau}{L_2} \right) \quad \text{for } |\tau| < L_2 \quad (134)$$

into (131) (see figure 7A for the effective window):

$$NQR_p(\text{rect. } w_1, \text{Hann. } w_2) = \frac{\int_0^y dx \cos^4 x \left( 1 - \frac{2}{\pi} \frac{L_2}{L_1} x \right)}{\int_0^y dx \cos^4 x \left( 1 - \frac{2}{\pi} \frac{L_2}{L_1} x \right)^2}, \quad (135)$$

where

$$y = \frac{\pi}{2} \min \left( 1, \frac{L_1}{L_2} \right). \quad (136)$$

Equation (135) is plotted\* as the top curve in figure 15A. As expected, the normalized quality ratio tends to 1 as  $L_2/L_1$  tends to zero. But even for as large a value as  $L_2/L_1 = .5$ , the normalized quality ratio has increased only by 12 percent. Thus the penalty in increased variance, for not realizing a small ratio for  $L_2/L_1$ , is not severe.

Also plotted in figure 15A is the normalized quality ratio for the three lag weightings introduced in (60) et seq. They all lead to smaller values of the normalized quality ratio, for the same value of  $L_2/L_1$ ; in fact, lag weighting  $C_5$  incurs only a 7 percent increase in variance when  $L_2/L_1 = .5$ , in relation to the ideal value 1. The reason that the normalized quality ratio is lower is due to the fact that the lag weightings drop to zero faster within their length  $L_2$ .

#### Non-Overlapping Segments; Lag Reshaping

The possibilities of lag reshaping have been discussed earlier with regard to the mean of the spectral estimate and the effective window. We now want to see what effect lag reshaping has on the normalized quality ratio in (130). Substitution of (98) in (130) yields

$$NQR_p(\text{lag reshaping}) = L_1 \frac{\int d\tau w_d^2(\tau) \frac{\phi_2(\tau)}{\phi_1^2(\tau)}}{\int d\tau w_d^2(\tau)} \quad \text{for } L_2 \leq L_1. \quad (137)$$

\*The quantity  $TB_e$  is not involved in figure 15; some related computational considerations are discussed in appendix E.

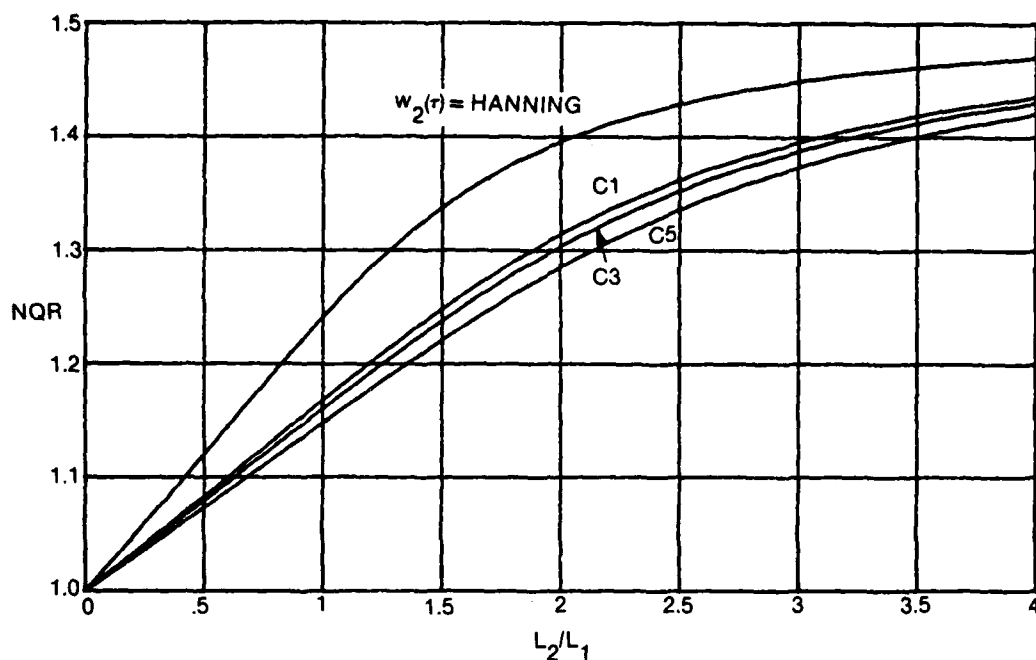
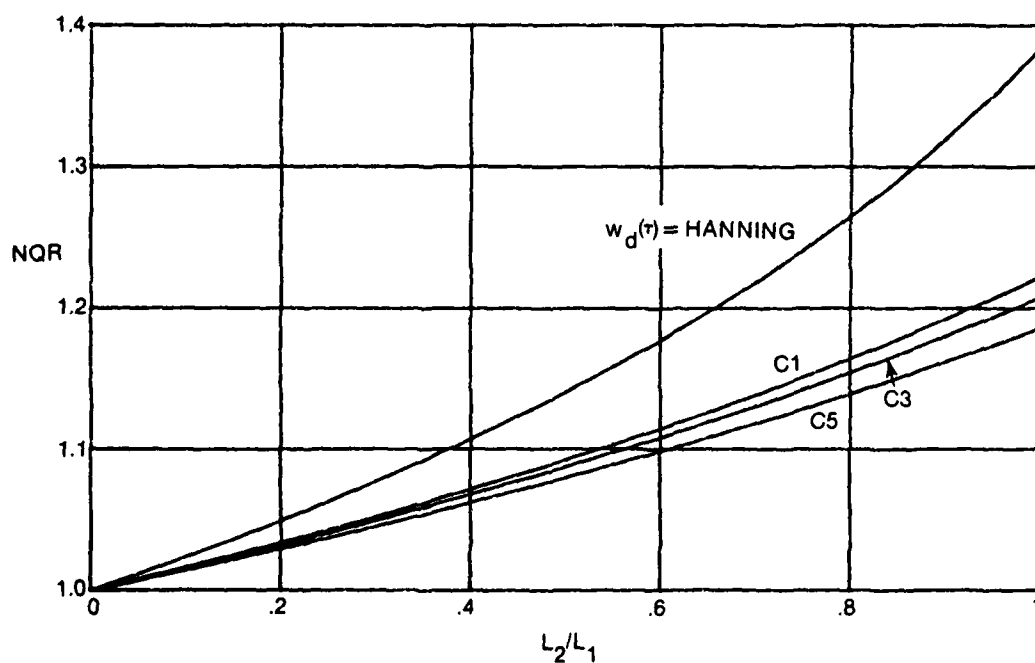
15A. Various Lag Weightings  $w_2(\tau)$ 15B. Reshaping to Desired Lag Weighting  $w_d(\tau)$ 

Figure 15. Normalized Quality-Ratio for Rectangular Temporal Weighting and No Overlap

The special case of rectangular temporal weighting is obtained by employing (122) in (137):

$$\text{NQR}_p(\text{rect. } w_1, \text{ lag reshaping}) = \frac{\int_0^{L_2} d\tau w_d^2(\tau) \left(1 - \frac{\tau}{L_1}\right)^{-1}}{\int_0^{L_2} d\tau w_d^2(\tau)} \quad \text{for } L_2 \leq L_1 \quad (138)$$

The division by  $\phi_1(\tau)$  in reshaping (98) increases the variance (for a *specified*  $L_2/L_1$  and for  $w_d(\tau) = w_2(\tau)$ ) above that in (131), because we are more heavily weighting regions where the denominator in (138) is smaller.

Equation (138) is plotted in figure 15B for desired effective weightings of Hanning, C1, C3, and C5. Notice that the abscissa is now limited to  $L_2/L_1 \leq 1$ . As expected, the normalized quality ratio tends to 1 as  $L_2/L_1$  tends to zero; that is, we can do lag reshaping for good side lobe behavior and lose little in terms of stability, provided that  $L_1$  is chosen sufficiently larger than  $L_2$ . Of course, the normalized quality ratio values in figure 15B are larger than those in figure 15A, for the same value of  $L_2/L_1$ . As an example, for desired effective weighting C1, if we take  $L_1 = 2L_2$ , the increase in variance over the ideal value is only 9 percent. Thus lag reshaping is an attractive procedure for spectral estimation; recall from figure 14 that  $L_2$  is set by the specified  $B_e$  and the shape of  $w_d(\tau)$ .

### General Results on Stability

We now return to the general normalized quality ratio in (111) and recall constraint (15). We will select time shift  $S$  according to

$$S = qL_1 \quad (139)$$

where  $q = q\{w_1\}$  is a fraction specified to be in the range  $(0, 1]$  and is dependent on the particular temporal weighting  $w_1(t)$  employed. The observations made in the paragraph following (111) are relevant in this regard. For example, with no quadratic frequency smoothing and with Hanning temporal weighting,  $q = .39$  (61 percent overlap) is virtually optimum, although  $q = 1/2$  loses only 8 percent in variance-reduction capability (reference 9, tables 4-7). We also select equality in (15) so as to make maximum use of the available record length, i.e., minimum variance of the spectral estimate. Then we have

$$L_1 = \frac{T}{1 + (P - 1)q} \quad (P \geq 1) \quad (140)$$

Thus for a given  $T$  and specified shift fraction  $q$ ,  $L_1$  can take on only a discrete set of values.

Arbitrarily large values of  $P$  are not allowed in (140), because this would result in such small values of  $L_1$  that the bandwidth constraint,  $B_c$ , could not be met. From figure 5, the lower bound on  $B_c L_1$  limits

$$P_{\max} = 1 + \frac{2c\{\phi_1\} B_e T - 1}{q} \quad (141)$$

(Actually,  $P_{\max}$  must be the integer part of the right-hand side.) Thus  $P_{\max}$  depends on the temporal weighting  $w_1(t)$  directly through its shape factor  $c\{\phi_1\}$  and indirectly via the selected shift fraction  $q = q\{w_1\}$ . For  $q = 1$ , no overlap, (141) reduces to (E-1).

When  $P = P_{\max}$ ,  $L_1$  is at its minimum value, and  $L_2$  must be greater than  $T$ ; it can be  $\infty$  (see figures 5 and 6A). In this case, there is no quadratic frequency smoothing, and we have the situation studied in detail in references 9 and 12, and mentioned earlier in (126)-(128). At the other extreme, when  $P = 1$ , we have Blackman-Tukey processing with the generalization that the temporal weighting need not be rectangular; this case was considered in the previous section. The range of values of  $L_2/L_1$  is shown in (E-2) and (E-3) to be very wide when  $B_c T \gg 1$ , which is a usual practical case.

More generally, for  $P$  in the range  $[1, P_{\max}]$ , we can investigate the tradeoff between the amounts of temporal- and lag-weighting, for specified resolution  $B_c$  and for specified weighting shapes of interest. Below, we consider the two cases of rectangular temporal weighting and Hanning temporal weighting.

### Rectangular Temporal Weighting

It was shown earlier in figure 15 that rectangular temporal weighting with no overlap results in small values for the normalized quality ratio, whether the lag weighting is reshaped or not, provided that  $L_2$  is chosen somewhat smaller than  $L_1$ . Now the question arises as to whether one should use any overlap, such as 50 percent, with rectangular temporal weighting.

We presume  $B_c T \gg 1$ . For no overlap, the estimate of first-stage correlation  $R_1(\tau)$  at  $\tau \approx L_1/2$  has only half the degrees of freedom as the estimate at  $\tau = 0$ . But with 50 percent overlap, the degrees of freedom for estimation at  $\tau \approx L_1/2$  are about the same as at  $\tau = 0$ . This is why 50 percent overlap for rectangular temporal weighting appears attractive.

However, for estimation of  $R_1(\tau)$  at  $\tau > L_1/2$ , we still do not get as many degrees of freedom as for Blackman-Tukey processing, because some data points never interact. For example, although at  $\tau = 3L_1/4$  we have doubled the degrees of freedom by using 50 percent overlap, we still have only about half of the number that are available at this  $\tau$  value via Blackman-Tukey processing.

In order to ascertain quantitatively the merit of overlapping for rectangular temporal weighting, we have evaluated the normalized quality ratio (111) for lag reshaping to realize a desired effective weighting equal to  $C1$  as given in (60) and (61) (reference 19, figure 12). That is, in (111), we use

$$w_2(\tau) = \frac{w_d(\tau)}{\phi_1(\tau)} \quad \text{for} \quad |\tau| < L_2 \leq L_1, \quad (142)$$

where  $\phi_1(\tau)$  is given by (122). In addition, we need the third-order correlation (108), which is

$$\phi_3(\tau, \mu) = \frac{1}{L_1} \left( 1 - \frac{|\tau| + |\mu|}{L_1} \right) \quad \text{for} \quad |\tau| + |\mu| < L_1 \quad (143)$$

for rectangular temporal weighting.

For the two cases of  $B_c T = 100$  and  $B_c T = 1000$ , the normalized quality ratio has been evaluated for  $q = 1, .75$ , and  $.5$ , and plotted in figure 16. The explanation of the behavior of the curves is as follows:

#### $q = 1$ No Overlap

If  $P = 1$ , then  $L_2 \ll L_1$  and it follows that for all  $|\tau| < L_2$ ,  $R_1(\tau)$  is estimated with virtually the same degrees of freedom as at  $\tau = 0$ , where we have the maximum degrees of freedom possible to estimate  $R_1(0)$ . As  $P$  increases toward  $P_{\max}$ , then  $L_1$  tends to  $L_2$ . Now  $R_1(0)$  is still estimated with the full degrees of freedom, but  $R_1(\tau)$  for  $\tau \neq 0$  is estimated with fewer degrees of freedom. For  $\tau$  near  $L_2$ , the loss in degrees of freedom in estimation of  $R_1(\tau)$  is significant, and the variance increases.

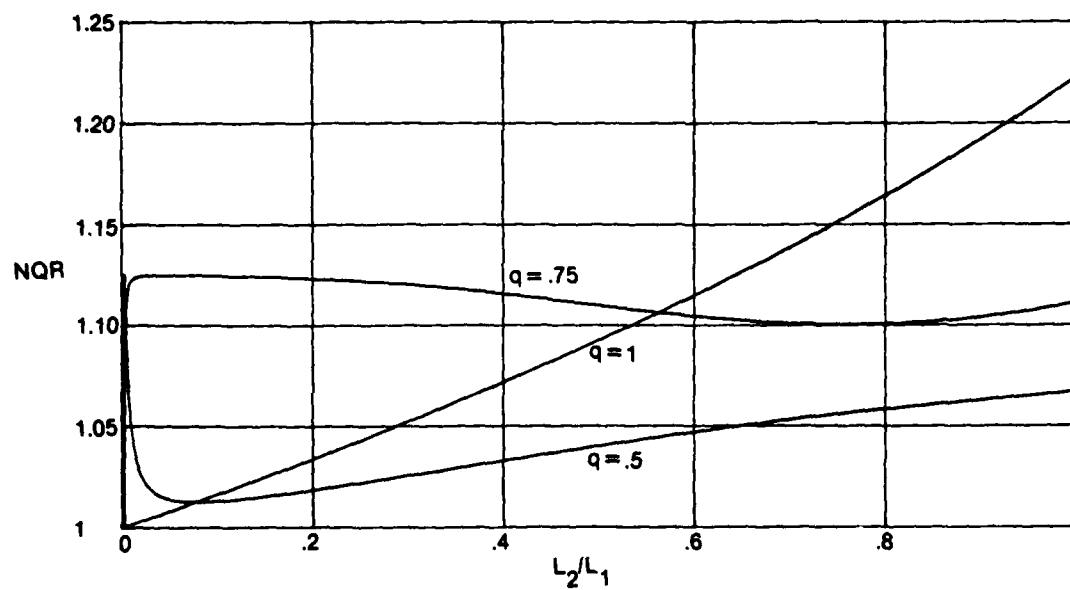
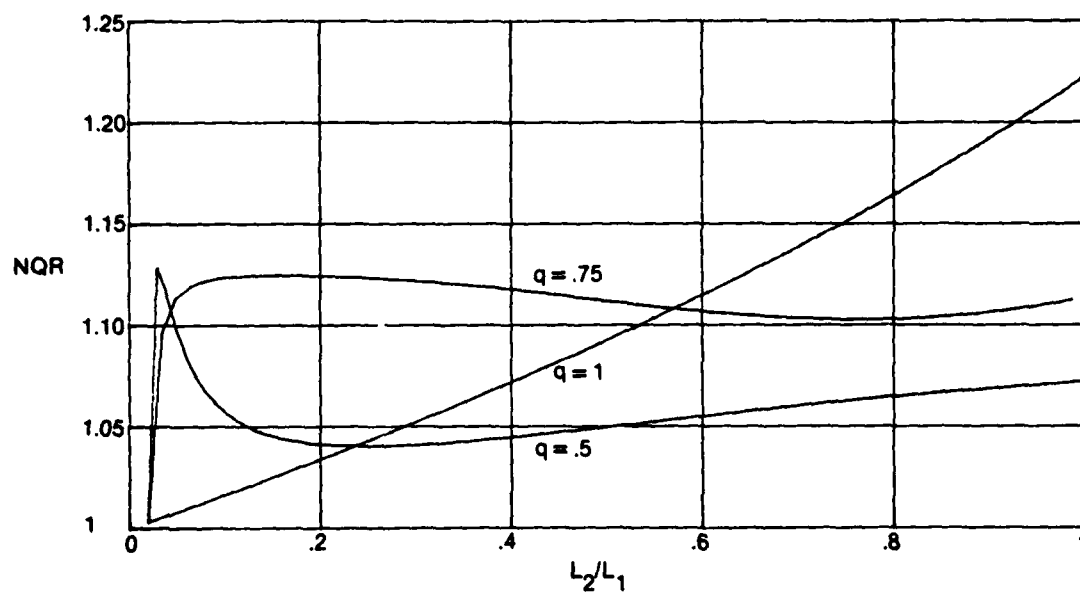


Figure 16. Normalized Quality-Ratio for Overlapped Rectangular Temporal Weighting and Lag Reshaping to C1

**q = .5 50 Percent Overlap**

For  $P=1$ , there is no overlap and conditions are identical to those described above. For  $P=2$ , the sudden increase in variance can be explained as follows: from (16), the first-stage estimate is

$$\hat{R}_1(\tau) = \frac{1}{2} \left[ \int dt y_0(t) y_0^*(t - \tau) + \int dt y_1(t) y_1^*(t - \tau) \right] \quad (144)$$

In particular,

$$\begin{aligned} \hat{R}_1(0) &= \frac{1}{2} \left[ \int dt |y_0(t)|^2 + \int dt |y_1(t)|^2 \right] \\ &= \frac{1}{T} \int_0^T dt x^2(t) O(t) \quad (145) \end{aligned}$$

where the overall weighting  $O(t)$  of  $x^2(t)$  is depicted in figure 17. As shown, the overall weighting is very uneven, causing loss in stability. As  $P$  increases above 2, the unevenness of the overall weighting (for  $q = .5$ ) occurs only towards the edges of the  $(0, T)$  interval, yielding a decrease of variance, since more data points tend to get the same overall weighting, insofar as their effect upon the estimation of  $R_1(\tau)$  is concerned. However, at the same time, the effect of fewer degrees of freedom in estimation of  $R_1(\tau)$ , for  $\tau$  values near  $L_2$ , becomes more pronounced as  $P$  increases and  $L_1$  decreases; this is true even for the 50 percent overlap case being considered here. Eventually, this effect dominates, and the variance increases with  $P$ .

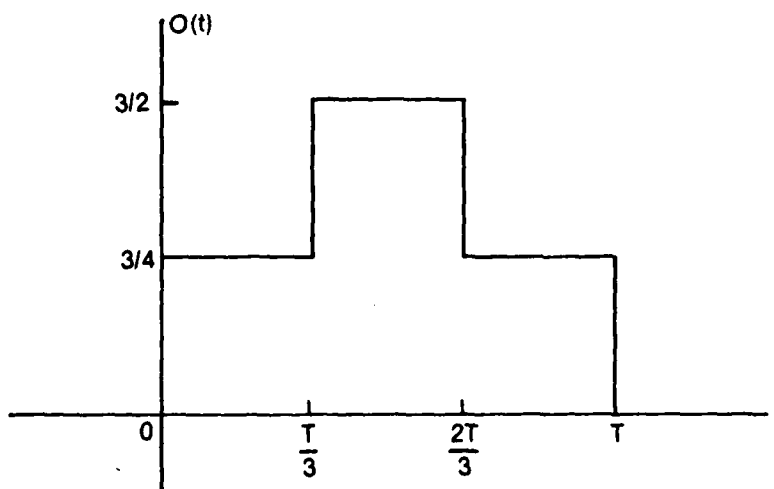


Figure 17. Overall Weighting of  $x^2(t)$  for  $q = .5$ ,  $P = 2$ , Rectangular  $w_1(t)$

### $q = .75$ 25 Percent Overlap

For *any* value of  $P > 1$ , the overall weighting  $O(t)$  is very jagged (as above), and the jaggedness does *not* decrease or concentrate near the edges as  $P$  increases. This is true for any overlap greater than 0 and less than 50 percent.

In summary, for rectangular temporal weighting, the smallest values for the normalized quality ratio are realized by choosing  $q = 1$ , no overlap, and making  $L_1$  several times larger than  $L_2$ . This conclusion about the ratio  $L_2/L_1$  is consistent with those reached earlier.

### Hanning Temporal Weighting

The temporal weighting and associated correlation for this case are given by (116), (C-9), and (C-10):

$$w_1(t) = \left(\frac{8}{3L_1}\right)^{1/2} \cos^2\left(\frac{\pi t}{L_1}\right) \quad \text{for } |t| < \frac{L_1}{2} ,$$

$$\phi_1(\tau) = \left(1 - \frac{|\tau|}{L_1}\right) \left[ \frac{2}{3} + \frac{1}{3} \cos\left(\frac{2\pi\tau}{L_1}\right) \right] + \frac{1}{2\pi} \sin\left(\frac{2\pi|\tau|}{L_1}\right) \quad \text{for } |\tau| < L_1 .$$

(146)

Evaluation of third-order correlation  $\phi_3(\tau, \mu)$  in (108) is rather tedious; the end result is given in (F-1) and (F-2). The procedure and program for the evaluation of the normalized quality ratio is given in appendix F.

The normalized quality ratio for Hanning lag weighting and  $B_c T = 100$  is plotted in figure 18 for several values of the shift fraction  $q$ . When  $q = 1$ , no overlap, the small values of the Hanning temporal weighting at its edges cannot be compensated for, by any choice of  $L_2/L_1$ , and the variance remains at approximately twice the ideal value. For 50 percent overlap of the Hanning temporal weighting,  $q = 1/2$ , the situation is markedly improved, there being a value,  $L_2/L_1 = .4$ , at which the excess variance is only 8 percent above ideal; this is reminiscent of the variance ratio for the case of no quadratic smoothing in reference 9, tables 5-7. When  $q$  is decreased to  $3/8$  or  $1/4$  (62.5 and 75 percent overlap, respectively), virtually the ideal variance reduction can be achieved by choosing  $L_2 \approx L_1$ .

In figure 19, the shift fraction  $q$  is kept at  $3/8$ , while  $B_c T$  is taken at both 100 and 32. The smaller value of  $B_c T$  leads to a slightly larger loss in performance because of more significant edge effects. However, even so, the normalized quality ratio does reach a very desirable level only 4 percent above ideal when  $L_2 \sim 2L_1$ .



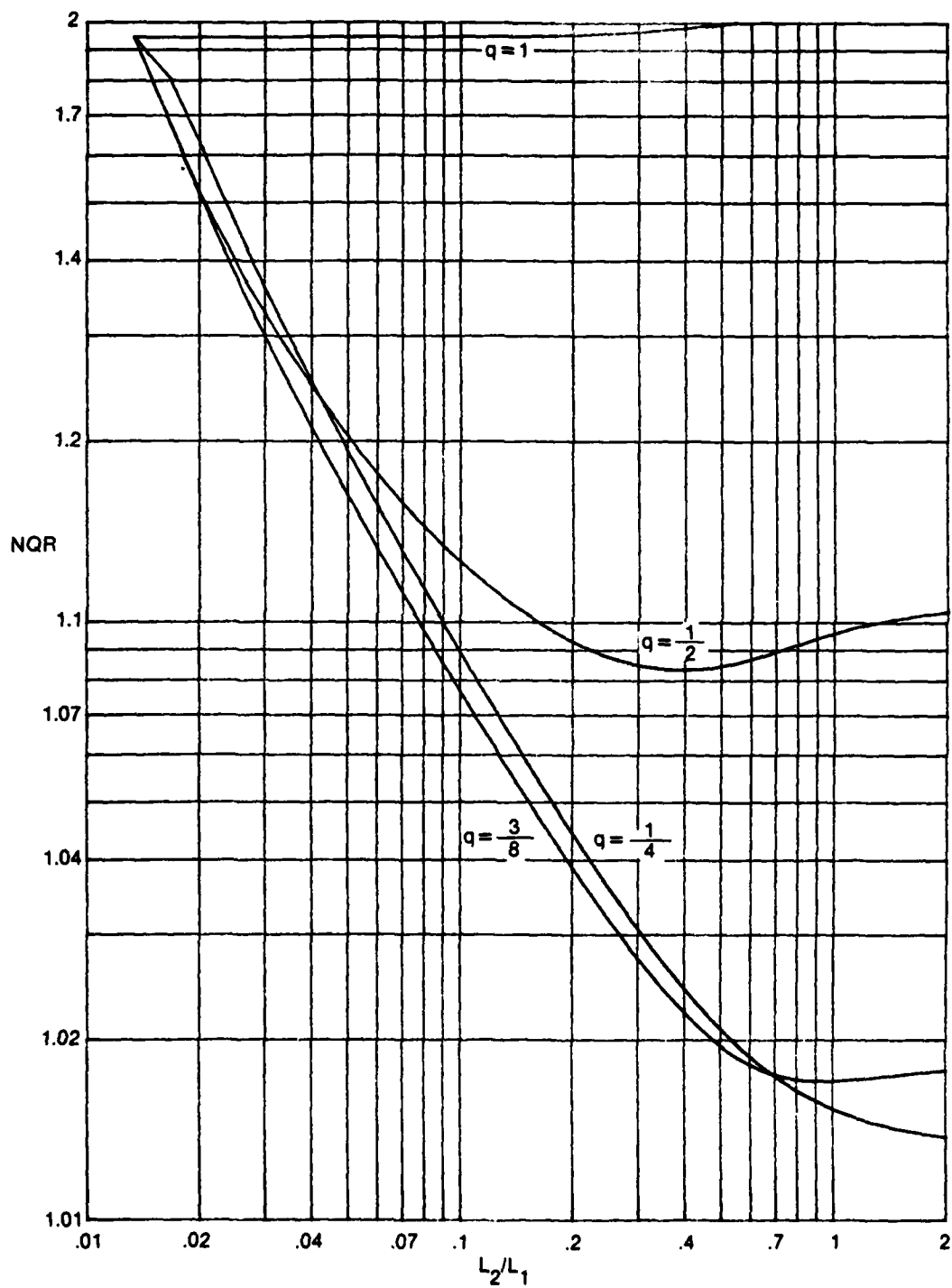


Figure 18. Normalized Quality-Ratio for Hanning Temporal Weighting and Hanning Lag Weighting;  $B_e T = 100$

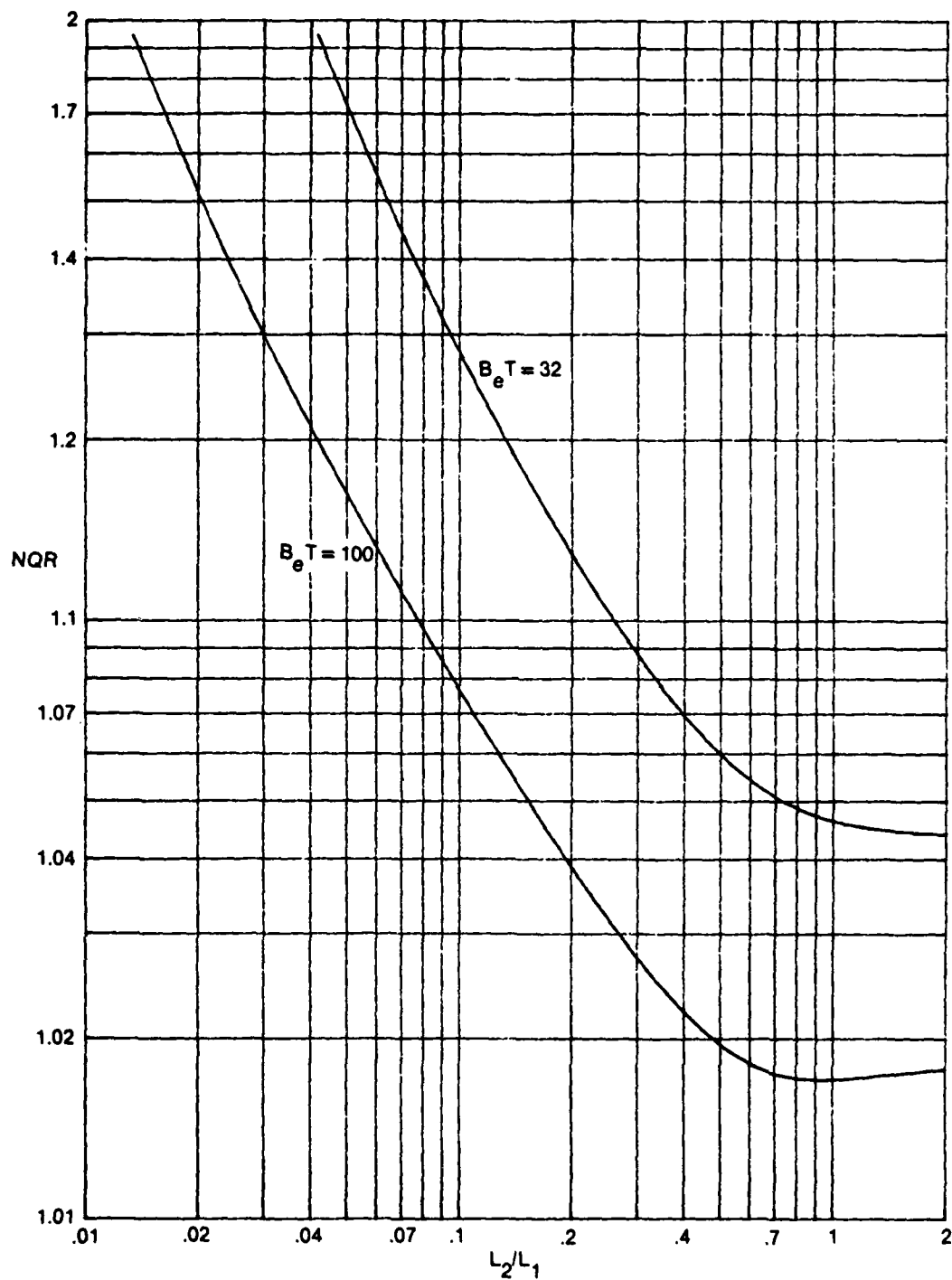


Figure 19. Normalized Quality-Ratio for Hanning Temporal Weighting and Hanning Lag Weighting;  $q = 3/8$

### Summary

The possibilities and performance of a generalized spectral analysis technique employing temporal and lag weighting have been investigated in terms of the mean and variance of the spectral estimate. The only assumption required about the process under analysis, in so far as the mean is concerned, is that it be second-order stationary over the observation interval. We then were able to extract a simple expression for the effective window involving the temporal and lag windows.

The possibility of doing lag reshaping to achieve desirable effective windows was considered in detail and found to be reasonable for a wide variety of windows with good side lobe behavior and decay rates. In particular, if rectangular temporal weighting is employed, its inherent poor side lobe structure can be corrected via proper lag weighting, in so far as the effective window is concerned. Strictly speaking, the closest side lobe cannot be eliminated; however, all the other side lobes can be suppressed.

The effect of temporal and lag weighting on the variance of the spectral estimate was evaluated and compared with the ideal value for large  $B_e T$ . For rectangular temporal weighting, it was found that small values of  $L_2/L_1$  and no overlap led to values of the normalized quality ratio virtually equal to the best attainable by any spectral analysis technique. The comparison is made under the constraint that the effective frequency resolution  $B_e$  is maintained the same for all techniques under consideration. On the other hand, if Hanning temporal weighting is employed, overlapping must be used for maximum variance reduction and the length ratio  $L_2/L_1$  ought to be of the order of unity.

Since Hanning temporal weighting requires multiplication of each and every data segment ( $P$  pieces) and significant overlap ( $\sim 50$  percent), whereas rectangular temporal weighting requires no multiplication and no overlap, the latter approach is a strong candidate for spectral analysis, particularly since excellent effective windows (low side lobes and rapid decay) and virtually ideal variance reduction can be achieved by proper lag weighting and choice of ratio  $L_2/L_1$ . Investigation of other cases than those evaluated here can be achieved by appropriate modification of the program in appendix F. A major analytical task will be the evaluation of the third-order correlation (108), if temporal weighting  $w_1(t)$  is taken other than rectangular or Hanning.

## Appendix A

### Comparison of Two Bandwidth Measures

The effective bandwidth of narrowband window  $W_o(f)$  was defined in (1) as

$$B_e = \frac{\left[ \int df W_o(f) \right]^2}{\int df W_o^2(f)} \quad (A-1)$$

The half-power bandwidth,  $B_h$ , is defined as the solution of

$$\frac{W_o\left(f_o \pm \frac{1}{2} B_h\right)}{W_o(f_o)} = \frac{1}{2} \quad (A-2)$$

where it is assumed that window  $W_o(f)$  is real, even about  $f_o$ , and peaked at  $f_o$ . We let  $W_e(f) = W_o(f + f_o)$ ; thus  $W_e(f)$  is even about  $f = 0$ .

The inverse Fourier transform of lowpass window  $W_e(f)$  is called the weighting

$$w_e(\tau) = \int df \exp(i2\pi f\tau) W_e(f) \quad (A-3)$$

We consider here the class of weightings given by

$$w_e(\tau) = \sum_{k \geq 0} a_k \cos(\pi k \tau / L_e) \quad \text{for } |\tau| < L_e, \quad (A-4)$$

and zero otherwise, where  $\{a_k\}$  are real and non-negative. This class includes rectangular, Hanning, Hamming, Blackman, and the optimal windows of Nuttall, reference 19. The Fourier transform of (A-4) yields lowpass window

$$W_e(f) = \frac{2L_e}{\pi} \sin(2\pi L_e f) \sum_{k \geq 0} \frac{(-1)^k a_k}{(2L_e f)^2 - k^2};$$

$$W_e\left(\frac{n}{2L_e}\right) = L_e \begin{cases} 2a_0 & \text{for } n = 0 \\ a_{|n|} & \text{for } n \neq 0 \end{cases} \quad (A-5)$$

A table of bandwidths  $B_e$  and  $B_h$  and their ratio is given below for the window in (A-5). Although these bandwidths vary significantly for the different weightings, their ratio is much more stable. In fact, for the last four weightings listed, the ratio is constant within  $\pm 1$  percent. The weightings listed under C5, C3, C1 are those given in reference 19, figures 10, 11, 12; the notation means

C5: continuous fifth derivative of weighting  
 C3: continuous third derivative of weighting  
 C1: continuous first derivative of weighting (A-6)

**Table A-1. Bandwidths for Various Weightings**

Weighting	$B_e L_e$	$B_h L_e$	$B_e/B_h$
Rectangular	0.5000	0.6034	0.8287
Hanning	1.3333	1.0000	1.3333
Hamming	1.2614	0.9109	1.3848
Blackman	1.6415	1.1494	1.4281
C5	2.2165	1.5371	1.4420
C3	2.0478	1.4139	1.4483
C1	1.9544	1.3444	1.4537

## Appendix B

### Some Lag Weighting and Lag Windowing Considerations For Discrete-Time Processing

It is convenient here to define an equispaced unit-impulse train by the notation

$$\delta_a(b) = \sum_n \delta(b - na) \quad , \quad (B-1)$$

where the summation on  $n$  extends over  $\pm \infty$ .

For discrete time sampling at spacing  $\Delta_t$ , it has been observed in (30) that  $\hat{G}_1(f)$  has period  $1/\Delta_t$  in  $f$ . Therefore lag window  $W_2(f)$  could be confined to  $|f| < (2\Delta_t)^{-1}$  with no loss in generality, in so far as its effects on  $\hat{G}_2(f)$  by means of (18) are concerned. In fact, for a general lag window  $W_2(f)$  specified arbitrarily, the equivalent band limited lag window is

$$\tilde{W}_2(f) = \text{rect}(\Delta_t f) \left[ W_2(f) \otimes \delta_{\frac{1}{\Delta_t}}(f) \right] \quad , \quad (B-2)$$

where we will utilize definitions

$$\text{rect}(x) = \begin{cases} 1 & \text{for } |x| < 1/2 \\ 0 & \text{otherwise} \end{cases} \quad , \quad \text{sinc}(x) = \frac{\sin(\pi x)}{\pi x} \quad , \quad (B-3)$$

and where  $\otimes$  denotes convolution. That is,  $W_2(f)$  is aliased into the band  $|f| < (2\Delta_t)^{-1}$ , and only this band-limited portion is retained for  $\tilde{W}_2(f)$ .

A way to demonstrate this mathematically is to note that the only values of lag weighting  $w_2(\tau)$  that can affect  $\hat{R}_2(\tau)$  are the samples

$$w_2(q\Delta_t) = \int df \exp(i2\pi f q\Delta_t) W_2(f) \quad . \quad (B-4)$$

The band-limited lag weighting function that passes through all these specified values, for all  $q$ , is

$$\tilde{w}_2(\tau) = \sum_q w_2(q\Delta_t) \text{sinc}\left(\frac{\tau}{\Delta_t} - q\right) \quad , \quad (B-5)$$

with corresponding Fourier transform

$$\bar{W}_2(f) = \Delta_t \text{rect}(\Delta_t f) \sum_q w_2(q\Delta_t) \exp(-i2\pi f q \Delta_t) \quad (\text{B-6})$$

$$= \Delta_t \text{rect}(\Delta_t f) \sum_q \exp(-i2\pi f q \Delta_t) \int du \exp(i2\pi u q \Delta_t) W_2(u)$$

$$= \text{rect}(\Delta_t f) \int du W_2(u) \Delta_t \sum_q \exp[-i2\pi(f - u)q\Delta_t]$$

$$= \text{rect}(\Delta_t f) \int du W_2(u) \delta_{\frac{1}{\Delta_t}}(f - u)$$

$$= \text{rect}(\Delta_t f) \left[ W_2(f) \odot \delta_{\frac{1}{\Delta_t}}(f) \right] \quad (\text{B-7})$$

Relation (B-4) indicates how an arbitrarily specified  $W_2(f)$  fixes the lag weights at the sample points. For the reverse problem, where sampled lag weights  $\{w_2(q\Delta_t)\}$  are specified for all  $q$ , relation (B-6) gives an equivalent lag window, in particular the band-limited spectral window, which results in the same estimates  $\hat{R}_2(\tau)$  and  $\hat{G}_2(f)$ . Notice that  $W_2(f)$  is not uniquely specified by samples  $\{w_2(q\Delta_t)\}$ ; however, the band-limited  $W_2(f)$ , which realizes weights  $\{w_2(q\Delta_t)\}$  for all  $q$ , is unique and is given by (B-6).

As a special case of the above, consider discrete frequency smoothing with frequency spacing  $\Delta_f = (M\Delta_t)^{-1}$ , where  $M\Delta_t$  is of the order of  $2L_1$ ; i.e., from (38),

$$W_2(f) = \frac{1}{M\Delta_t} \sum_n W_{2n} \delta\left(f - \frac{n}{M\Delta_t}\right) \quad (\text{B-8})$$

where we set  $W_{2n} = 0$  for  $|n| > M/2$  without loss of generality, in accordance with the observation above (B-2). Then lag weights (B-4), given now by

$$w_2(q\Delta_t) = \frac{1}{M\Delta_t} \sum_{|n| \leq M/2} W_{2n} \exp(i2\pi n q / M) \quad (\text{B-9})$$

will equivalently accomplish the same purpose. This last relation can be accomplished by an  $M$ -point FFT, where  $W_{2, \pm M/2}$  receive the same complex exponential weighting in (B-9).

It should be noted that the discrete function  $w_2(q\Delta_t)$  in (B-9) has period  $M$  in  $q$ ; this means that  $w_2(q\Delta_t)$  in (B-9) will increase in magnitude for  $M/2 < q < M$ . If  $\hat{R}_{1q}$  is nonzero for  $|q| > M/2$ , this lag weighting may cause a problem. One guaranteed way to avoid the problem is to choose  $M/2$  larger than the nonzero extent,  $N_1$ , of  $\hat{R}_{1q}$ . Physically, this means that the frequency spacing  $\Delta_f = (M\Delta_t)^{-1}$ , used in frequency smoothing (B-8), must be small enough so as not to miss any information in  $\hat{G}_1(f)$ . Coarse frequency spacing gives spurious results for  $\hat{G}_2(f)$ . (It will also yield poor effective windows.)

Since from (24),  $\hat{R}_{1q} = 0$  for  $q \geq N_1$ , where  $N_1$  is the number of time samples per segment, only a finite number of the general weights  $\{w_2(q\Delta_t)\}$  in (B-4) affect  $\hat{R}_{2q}$ . Thus in example (B-8), although (B-9) has period  $M$  in  $q$ , only the values for  $|q| < N_1$  are relevant to the effect on  $\hat{R}_{2q}$ ; more generally, the values yielded by (B-4) for a general  $W_2(f)$  are relevant only for  $|q| < N_1$ , and only these need be evaluated and retained if we choose to process via the lag domain.

Now let us consider the reverse problem, where lag weights  $\{w_2(q\Delta_t)\}$  are specified for all  $q$ , and we wish to determine some allowable lag windows  $W_2(f)$  that will realize the same estimates  $\hat{R}_2(\tau)$  and  $\hat{G}_2(f)$ , but which take advantage of the fact that only  $w_2(q\Delta_t)$  for  $|q| < N_1$  must be realized. One obvious candidate is the band-limited lag weighting version

$$\hat{w}_2(\tau) = \sum_{|q| < N_1} w_2(q\Delta_t) \operatorname{sinc}\left(\frac{\tau}{\Delta_t} - q\right) ; \quad (\text{B-10})$$

notice the limitation on  $q$  employed. The corresponding lag window is

$$\hat{W}_2(f) = \Delta_t \operatorname{rect}(\Delta_t f) \sum_{|q| < N_1} w_2(q\Delta_t) e^{-i2\pi f q \Delta_t} . \quad (\text{B-11})$$

A second candidate is

$$\hat{w}_2(\tau) = \hat{w}_2(\tau) \odot \delta_{M\Delta_t}(\tau) , \quad (\text{B-12})$$

provided that  $M \geq 2N_1 - 1$ ; this provision guarantees non-overlap of the displacements of  $\hat{w}_2(\tau)$ . Then

$$\hat{W}_2(f) = \hat{w}_2(f) \frac{1}{M\Delta_t} \delta_{\frac{1}{M\Delta_t}}(f) = \sum_n w_{2n} \delta\left(f - \frac{n}{M\Delta_t}\right) \quad (\text{B-13})$$

where

$$w_{2n} \equiv \frac{1}{M\Delta_t} \hat{w}_2\left(\frac{n}{M\Delta_t}\right) = \frac{1}{M} \operatorname{rect}\left(\frac{n}{M}\right) \sum_{|q| < N_1} w_2(q\Delta_t) \exp(-i2\pi nq/M) \quad (\text{B-14})$$

from (B-11). Notice that (B-13) has the form of discrete frequency smoothing in (B-8); (B-14) gives the area of each impulse needed in (B-13). Also notice from (B-14) that all these areas are zero for  $|n| > M/2$ ; thus we have a finite sequence to apply in the frequency domain, which is equivalent to a specified finite set of lag weights.

Equations (B-14) and (B-9) are complementary to each other. In fact, we can derive (B-9) from (B-14) as follows: from (B-14),

$$w_{2n} = \frac{1}{M} \operatorname{rect}\left(\frac{n}{M}\right) \sum_q \bar{w}_q \exp(-i2\pi nq/M) , \quad (\text{B-15})$$



where

$$\bar{w}_q \equiv \begin{cases} w_2(q\Delta_t) & \text{for } |q| < N_1 \\ 0 & \text{otherwise} \end{cases} \quad (B-16)$$

Then

$$\begin{aligned} \sum_{|n| \leq M/2} w_{2n} \exp(i2\pi np/M) &= \sum_{|n| \leq M/2} \exp(i2\pi np/M) \frac{1}{M} \text{rect}\left(\frac{n}{M}\right) \sum_q \bar{w}_q \exp(-i2\pi nq/M) \\ &= \sum_q \bar{w}_q \frac{1}{M} \sum_{|n| \leq M/2} \text{rect}\left(\frac{n}{M}\right) \exp(i2\pi n(p - q)/M) \\ &= \sum_q \bar{w}_q I_{p-q}^{(M)} = \bar{w}_p \otimes I_p^{(M)}, \end{aligned} \quad (B-17)$$

where

$$I_p^{(M)} \equiv \begin{cases} 1 & \text{for } p = 0, \pm M, \pm 2M, \dots \\ 0 & \text{otherwise} \end{cases} \quad (B-18)$$

Now if  $M \geq 2N_1 - 1$  (as assumed above (B-13)), then

$$\sum_{|n| \leq M/2} w_{2n} \exp(i2\pi np/M) = w_2(q\Delta_t) \quad \text{for } |q| < N_1 \quad (B-19)$$

This is (B-9) for  $|q| < N_1$ , which is the only range that affects  $\hat{R}_{2q}$ .

## Appendix C

### Correlation $\phi_1(\tau)$ of a General Class of Temporal Weightings

The class of temporal weightings of interest here is given by a sum of complex exponentials:

$$w_1(t) = \sum_k \alpha_k \exp(i2\pi kt/L_1) \quad \text{for } |t| < L_1/2, \quad (C-1)$$

and zero otherwise. We assume that the coefficient sequence has conjugate symmetry

$$\alpha_{-k} = \alpha_k^* \quad \text{for all } k; \quad (C-2)$$

then  $w_1(t)$  is real, and it follows that the (aperiodic) correlation

$$\phi_1(\tau) = \int dt w_1(t) w_1(t - \tau) \quad (C-3)$$

is also real, in addition to being even about  $\tau = 0$ .

Substitution of (C-1) in (C-3) yields

$$\phi_1(\tau) = \sum_{km} \alpha_k \alpha_m^* \int_{\tau-L_1/2}^{L_1/2} dt \exp[i2\pi kt/L_1 - i2\pi m(t - \tau)/L_1] \quad \text{for } 0 \leq \tau \leq L_1. \quad (C-4)$$

This can be evaluated and then extended to  $\tau < 0$  by the use of the even character of  $\phi_1(\tau)$ ; there follows

$$\begin{aligned} \phi_1(\tau) = (L_1 - |\tau|) & \left[ \alpha_0^2 + 2 \sum_{k>0} |\alpha_k|^2 \cos(2\pi k\tau/L_1) \right] \\ & - \frac{2L_1}{\pi} \sum_{m>k} \frac{(-1)^{m-k}}{m-k} \operatorname{Re}(\alpha_k \alpha_m^*) \sin(2\pi m|\tau|/L_1) \\ & \quad \text{for } |\tau| < L_1, \end{aligned} \quad (C-5)$$

and zero otherwise. This is the general result for the correlation of weighting (C-1).

We now specialize (C-5) to the case of real symmetric coefficients in (C-1):

$$\alpha_k \text{ real}, \quad \alpha_{-k} = \alpha_k. \quad (C-6)$$

For all coefficients zero except for  $\alpha_0$ , we have

$$w_1(t) = \alpha_0 \quad \text{for } |t| < L_1/2, \quad (C-7)$$

$$\phi_1(\tau) = (L_1 - |\tau|) \alpha_0^2 \quad \text{for } |\tau| < L_1. \quad (C-8)$$

For all coefficients zero except for  $\alpha_0, \alpha_1$ , we have

$$w_1(t) = \alpha_0 + 2\alpha_1 \cos(2\pi t/L_1) \quad \text{for } |t| < L_1/2, \quad (C-9)$$

$$\begin{aligned} \phi_1(\tau) = (L_1 - |\tau|) \left[ \alpha_0^2 + 2\alpha_1^2 \cos(2\pi\tau/L_1) \right] \\ + \frac{L_1}{\pi} \alpha_1(2\alpha_0 - \alpha_1) \sin(2\pi|\tau|/L_1) \quad \text{for } |\tau| < L_1. \end{aligned} \quad (C-10)$$

For all coefficients zero except for  $\alpha_0, \alpha_1, \alpha_2$ , we have

$$w_1(t) = \alpha_0 + 2\alpha_1 \cos(2\pi t/L_1) + 2\alpha_2 \cos(4\pi t/L_1) \quad \text{for } |t| < L_1/2, \quad (C-11)$$

$$\begin{aligned} \phi_1(\tau) = (L_1 - |\tau|) \left[ \alpha_0^2 + 2\alpha_1^2 \cos(2\pi\tau/L_1) + 2\alpha_2^2 \cos(4\pi\tau/L_1) \right] \\ + \frac{L_1}{6\pi} \left[ 2\alpha_1(6\alpha_0 - 3\alpha_1 - 4\alpha_2) \sin(2\pi|\tau|/L_1) \right. \\ \left. - \alpha_2(6\alpha_0 - 16\alpha_1 + 3\alpha_2) \sin(4\pi|\tau|/L_1) \right] \\ \text{for } |\tau| < L_1. \end{aligned} \quad (C-12)$$

For all coefficients zero except for  $\alpha_0, \alpha_1, \alpha_2, \alpha_3$ , we have

$$\begin{aligned} w_1(t) = \alpha_0 + 2\alpha_1 \cos(2\pi t/L_1) + 2\alpha_2 \cos(4\pi t/L_1) + 2\alpha_3 \cos(6\pi t/L_1) \\ \text{for } |t| < L_1/2, \end{aligned} \quad (C-13)$$

$$\phi_1(\tau) = (L_1 - |\tau|)$$

$$\begin{aligned} & \cdot \left[ \alpha_0^2 + 2\alpha_1^2 \cos(2\pi\tau/L_1) + 2\alpha_2^2 \cos(4\pi\tau/L_1) + 2\alpha_3^2 \cos(6\pi\tau/L_1) \right] \\ & + \frac{L_1}{30\pi} \left[ 5\alpha_1(12\alpha_0 - 6\alpha_1 - 8\alpha_2 + 3\alpha_3) \sin(2\pi|\tau|/L_1) \right. \\ & - \alpha_2(30\alpha_0 - 80\alpha_1 + 15\alpha_2 + 48\alpha_3) \sin(4\pi|\tau|/L_1) \\ & \left. + \alpha_3(20\alpha_0 - 45\alpha_1 + 72\alpha_2 - 10\alpha_3) \sin(6\pi|\tau|/L_1) \right] \\ & \text{for } |\tau| < L_1 . \end{aligned} \quad (C-14)$$

This last case includes all the weightings considered in reference 19, with the identification of coefficients as

$$\alpha_0 = a_0 , \quad \alpha_k = \frac{1}{2}a_k \quad \text{for } k > 0 . \quad (C-15)$$

Then we can express the temporal weighting as

$$w_1(t) = \sum_{k \geq 0} a_k \cos(2\pi kt/L_1) \quad \text{for } |t| < L_1/2 . \quad (C-16)$$

## Appendix D

### Derivation of Variance of Spectral Estimate

Our starting point is (14). The integral on  $t$  is a Fourier transform of the product in (13), and can therefore be expressed as a convolution:

$$\begin{aligned} Y_p(f) &= X(f) \otimes \left[ W_1(f) \exp\left(-i2\pi f\left(\frac{L_1}{2} + pS\right)\right) \right] \\ &= \int du X(f - u) W_1(u) \exp\left(-i2\pi u\left(\frac{L_1}{2} + pS\right)\right), \end{aligned} \quad (D-1)$$

where we used (46) and defined

$$X(f) = \int dt x(t) \exp(-i2\pi ft). \quad (D-2)$$

Although the relations to follow could be derived in the time domain, it is more convenient to develop them in the frequency domain because of the frequent and useful occurrence of delta functions.

$X(f)$  is complex Gaussian for all  $f$ , since (D-2) is a linear transformation and we have assumed  $x(t)$  to be a complex Gaussian process, for the variance calculation to follow. Furthermore covariance

$$\begin{aligned} \text{Av}\{X(f_1) X^*(f_2)\} &= \iint dt_1 dt_2 \overline{x(t_1) x^*(t_2)} \exp(-i2\pi f_1 t_1 + i2\pi f_2 t_2) \\ &= \iint dt_1 dt_2 R(t_1 - t_2) \exp(-i2\pi f_1 t_1 + i2\pi f_2 t_2) \\ &= \iint du dt_2 R(u) \exp(-i2\pi f_1 (u + t_2) + i2\pi f_2 t_2) \\ &= G(f_1) \delta(f_1 - f_2), \end{aligned} \quad (D-3)$$

upon use of (43) and (45). When  $x(t)$  is a single-sided (analytic) complex process, there then follows for the fourth-order average, which will be needed later (reference 23),

$$\begin{aligned} &\text{Av}\{X(f_1) X^*(f_2) X(f_3) X^*(f_4)\} \\ &= G(f_1) G(f_3) \left[ \delta(f_1 - f_2) \delta(f_3 - f_4) + \delta(f_1 - f_4) \delta(f_2 - f_3) \right]. \end{aligned} \quad (D-4)$$

(When  $x(t)$  is a real process, there would be a third term in addition. However, even then, this term contributes only near  $f = 0$ ; see reference 9, equations (A-4) - (A-8).)

Upon use of (D-1), (14) becomes\*

$$\hat{G}_1(f) = \frac{1}{P} \sum_{p=0}^{P-1} \iint du dv X(f-u) X^*(f-v) \cdot W_1(u) W_1^*(v) \exp\left(-i2\pi(u-v)\left(\frac{L_1}{2} + pS\right)\right) \quad (D-5)$$

Then the average of the product of the first-stage spectral estimates is

$$\begin{aligned} \text{Av}\{\hat{G}_1(f_1) \hat{G}_1(f_2)\} &= \frac{1}{P^2} \sum_{p,q=0}^{P-1} \iiint du dv d\mu dv \\ &\cdot \overline{X(f_1-u) X^*(f_1-v) X(f_2-\mu) X^*(f_2-\nu) W_1(u) W_1^*(v) W_1(\mu) W_1^*(\nu)} \\ &\cdot \exp\left(-i2\pi(u-v)\left(\frac{L_1}{2} + pS\right)\right) \exp\left(-i2\pi(\mu-\nu)\left(\frac{L_1}{2} + qS\right)\right) \quad (D-6) \end{aligned}$$

Reference to (D-4) enables us to express the fourth-order average as

$$\begin{aligned} &G(f_1-u) G(f_2-\mu) \\ &\cdot \left[ \delta(u-v) \delta(\mu-\nu) + \delta(f_1-f_2+v-\mu) \delta(f_1-f_2+\mu-\nu) \right] \quad (D-7) \end{aligned}$$

Use of the first term of (D-7) in (D-6) yields

$$\begin{aligned} &\frac{1}{P^2} \sum_{p,q=0}^{P-1} \iint du d\mu G(f_1-u) G(f_2-\mu) |W_1(u)|^2 |W_1(\mu)|^2 \\ &= \int du G(f_1-u) |W_1(u)|^2 \cdot \int d\mu G(f_2-\mu) |W_1(\mu)|^2 \\ &= \text{Av}\{\hat{G}_1(f_1)\} \cdot \text{Av}\{\hat{G}_1(f_2)\} \quad (D-8) \end{aligned}$$

where we employed (45) in the last line. Moving this term to the left side of (D-6), and using the second term of (D-7), we obtain, for the covariance of the first-stage spectral estimates,

\*For more generality, we allow temporal weight  $w_1$  and window  $W_1$  to be complex in this appendix.

$$\begin{aligned}
\text{Cov}\{\hat{G}_1(f_1), \hat{G}_1(f_2)\} &= \frac{1}{P^2} \sum_{p,q=0}^{P-1} \iint du dv G(f_1 - u) G(f_1 - v) \\
&\cdot W_1(u) W_1^*(v) W_1(v + f_2 - f_1) W_1^*(u + f_2 - f_1) \exp(-i2\pi(u - v)(p - q)S) \\
&= \frac{1}{P^2} \sum_{p,q=0}^{P-1} \iint d\alpha d\beta G(\alpha) G(\beta) W_1(f_1 - \alpha) W_1^*(f_1 - \beta) \\
&\cdot W_1(f_2 - \beta) W_1^*(f_2 - \alpha) \exp(-i2\pi(\beta - \alpha)(p - q)S) \\
&= \frac{1}{P^2} \sum_{p,q=0}^{P-1} \left| \int d\alpha G(\alpha) W_1(f_1 - \alpha) W_1^*(f_2 - \alpha) \exp(i2\pi\alpha(p - q)S) \right|^2 \\
&= \frac{1}{P} \sum_{p=1-P}^{P-1} \left(1 - \frac{|p|}{P}\right) \left| \int d\alpha G(\alpha) W_1(f_1 - \alpha) W_1^*(f_2 - \alpha) \exp(i2\pi\alpha p S) \right|^2 \\
&= \iint d\alpha d\beta G(\alpha) G(\beta) W_1(f_1 - \alpha) W_1^*(f_1 - \beta) W_1(f_2 - \beta) W_1^*(f_2 - \alpha) \\
&\cdot \left[ \frac{\sin(\pi P S(\alpha - \beta))}{P \sin(\pi S(\alpha - \beta))} \right]^2. \tag{D-9}
\end{aligned}$$

Here we have used the identities

$$\begin{aligned}
\frac{1}{P^2} \sum_{p,q=0}^{P-1} \exp(i2\pi(p - q)u) &= \frac{1}{P} \sum_{p=1-P}^{P-1} \left(1 - \frac{|p|}{P}\right) \exp(i2\pi pu) \\
&= \left[ \frac{\sin(\pi Pu)}{P \sin(\pi u)} \right]^2 \equiv Q_p(u). \tag{D-10}
\end{aligned}$$

For  $f_1 = f_2$ , (D-9) checks with reference 9, equation (A-9); more generally, it is equation D-2 of reference 9. We observe that if  $|f_2 - f_1|$  is greater than the effective bandwidth of temporal window  $W_1$ , (D-9) will be small since  $W_1(f_1 - \alpha)$  and  $W_1^*(f_2 - \alpha)$  will then not overlap significantly on the  $\alpha$ -scale. Also notice that spectrum  $G$  is still left under the integral sign; i.e., there are no assumptions yet on the character of the spectrum.

We are now prepared to consider the second-stage spectral estimate  $\hat{G}_2(f)$  as given by (18):

$$\hat{G}_2(f) = \int df_1 \hat{G}_1(f_1) W_2(f - f_1). \tag{D-11}$$

Then

$$\hat{G}_2(f) - \text{Av}\{\hat{G}_2(f)\} = \int df_1 \left[ \hat{G}_1(f_1) - \text{Av}\{\hat{G}_1(f_1)\} \right] W_2(f - f_1) \quad , \quad (\text{D-12})$$

and therefore (recall that  $W_2$  is real) the variance of the second-stage spectral estimate is

$$\begin{aligned} \text{Var}\{\hat{G}_2(f)\} &= \iint df_1 df_2 \text{Cov}\{\hat{G}_1(f_1), \hat{G}_1(f_2)\} W_2(f - f_1) W_2(f - f_2) \\ &= \frac{1}{P} \sum_{p=1}^{P-1} \left( 1 - \frac{|p|}{P} \right) \iint d\alpha d\beta G(\alpha) G(\beta) \exp(i2\pi(\alpha - \beta)pS) |\gamma(f - \alpha, f - \beta)|^2 \\ &= \iint d\alpha d\beta G(\alpha) G(\beta) |\gamma(f - \alpha, f - \beta)|^2 Q_p(S(\alpha - \beta)) \quad , \quad (\text{D-13}) \end{aligned}$$

where we used (D-9) and (D-10), interchanged integrals, and defined window convolution function

$$\gamma(x, y) \equiv \int du W_2(u) W_1(x - u) W_1^*(y - u) \quad . \quad (\text{D-14})$$

Relation (D-13) is exact; it makes no presumption about the relative widths of the spectrum  $G$  and the windows  $W_1, W_2$ . The compact expression (D-13) involves the windows  $W_1, W_2$  through the convolution function  $\gamma$ , and involves the shift  $S$  and number of pieces  $P$  through the periodic function  $Q_p$  defined in (D-10).

The window convolution function  $\gamma$  in (D-14) realizes its peak value at  $x=0, y=0$ , and is rather small everywhere else, since the windows are virtually unimodal and rather narrow. In fact, a special case is the diagonal slice

$$\gamma(x, x) = \int du W_2(u) |W_1(x - u)|^2 = |W_1(x)|^2 \otimes W_2(x) = W_e(x) \quad , \quad (\text{D-15})$$

by reference to (51). Generally,  $\gamma(x, y)$  is substantially nonzero only in the region  $B_e, B_e$  at the origin of  $x, y$  space.

We now employ the assumption discussed in connection with approximation (103), namely, that spectrum  $G$  is relatively constant in the band of width  $B_e$  about the frequency  $f$  of interest. Then the major contribution to the variance, (D-13), comes from the region near  $\alpha = \beta = f$  in  $\alpha, \beta$  space. There follows the approximation for the variance of the second-stage spectral estimate,



$$\begin{aligned}
\text{Var}\{\hat{G}_2(f)\} &= G^2(f) \frac{1}{P} \sum_{p=1-P}^{P-1} \left(1 - \frac{|p|}{P}\right) \\
&\quad \cdot \iint d\alpha d\beta \exp(i2\pi(\alpha - \beta)pS) |\gamma(f - \alpha, f - \beta)|^2 \\
&= G^2(f) \frac{1}{P} \sum_{p=1-P}^{P-1} \left(1 - \frac{|p|}{P}\right) \iint dx dy \exp(i2\pi(y - x)pS) |\gamma(x, y)|^2 \\
&= G^2(f) \iint dx dy |\gamma(x, y)|^2 Q_p(S(y - x)) \quad , \quad (D-16)
\end{aligned}$$

where we used (D-10) again.

We now simplify the double integral in (D-16); from the second line of (D-16) and from (D-14),

$$\begin{aligned}
D &\equiv \iint dx dy \exp(i2\pi(y - x)pS) \left| \int du W_2(u) W_1(x - u) W_1^*(y - u) \right|^2 \\
&= \iint du dv W_2(u) W_2(v) \left| \int dx \exp(-i2\pi xpS) W_1(x - u) W_1^*(x - v) \right|^2 \\
&= \iint du dv W_2(u) W_2(v) |\chi_1(pS, u - v)|^2 \quad , \quad (D-17)
\end{aligned}$$

where the complex ambiguity function of the temporal weight and window is defined as

$$\begin{aligned}
\chi_1(\tau, \nu) &= \int df \exp(i2\pi f\tau) W_1\left(f + \frac{\nu}{2}\right) W_1^*\left(f - \frac{\nu}{2}\right) \\
&= \int dt \exp(-i2\pi \nu t) W_1\left(t + \frac{\tau}{2}\right) W_1^*\left(t - \frac{\tau}{2}\right) \quad . \quad (D-18)
\end{aligned}$$

Now let  $\nu = u - v$  in (D-17), and obtain a single integral for D:

$$\begin{aligned}
D &= \int d\nu |\chi_1(pS, \nu)|^2 \int du W_2(u) W_2(u - \nu) \\
&= \int d\nu |\chi_1(pS, \nu)|^2 \chi_2(0, \nu) \quad , \quad (D-19)
\end{aligned}$$

in terms of the ambiguity function  $\chi_2$  of the lag window and weight. Substitution of (D-19) in the second line of (D-16) yields for the variance,

$$\text{Var}\{\hat{G}_2(f)\} = G^2(f) \frac{1}{P} \sum_{p=1-P}^{P-1} \left(1 - \frac{|p|}{P}\right) \int d\nu |\chi_1(pS, \nu)|^2 \chi_2(0, \nu) \quad . \quad (D-20)$$

An alternative, and perhaps more useful form, to (D-20) is attained as follows; the integral in (D-20) is expressible (by use of the definition (D-18) of the ambiguity function) as

$$\begin{aligned}
& \int dv |\chi_1(pS, v)|^2 \int dt \exp(-i2\pi vt) w_2^2(t) \\
& = \int dt w_2^2(t) \int dv \exp(-i2\pi vt) |\chi_1(pS, v)|^2 .
\end{aligned} \tag{D-21}$$

Now we have the general result that

$$\begin{aligned}
& \int dv \exp(-i2\pi vt) |\chi_1(\tau, v)|^2 \\
& = \int dv \exp(-i2\pi vt) \iint dt_1 dt_2 \exp(-i2\pi v(t_1 - t_2)) \\
& \quad \cdot w_1\left(t_1 + \frac{\tau}{2}\right) w_1^*\left(t_1 - \frac{\tau}{2}\right) w_1^*\left(t_2 + \frac{\tau}{2}\right) w_1\left(t_2 - \frac{\tau}{2}\right) \\
& = \iint dt_1 dt_2 w_1\left(t_1 + \frac{\tau}{2}\right) w_1^*\left(t_1 - \frac{\tau}{2}\right) w_1^*\left(t_2 + \frac{\tau}{2}\right) w_1\left(t_2 - \frac{\tau}{2}\right) \delta(t + t_1 - t_2) \\
& = \int dt_1 w_1\left(t_1 + \frac{\tau}{2}\right) w_1^*\left(t_1 - \frac{\tau}{2}\right) w_1^*\left(t + t_1 + \frac{\tau}{2}\right) w_1\left(t + t_1 - \frac{\tau}{2}\right) \\
& = \int du w_1\left(u + \frac{\tau - t}{2}\right) w_1^*\left(u + \frac{-\tau - t}{2}\right) w_1^*\left(u + \frac{\tau + t}{2}\right) w_1\left(u + \frac{-\tau + t}{2}\right) \\
& \equiv \phi_3(t, \tau) .
\end{aligned} \tag{D-22}$$

This is a third-order correlation of temporal weighting  $w_1$ ; see the footnote to (9). Thus (D-21) becomes

$$\int dt w_2^2(t) \phi_3(t, pS) , \tag{D-23}$$

and the variance in (D-20) becomes

$$\text{Var}\{\hat{G}_2(f)\} = G^2(f) \frac{1}{P} \sum_{p=1-P}^{P-1} \left(1 - \frac{|p|}{P}\right) \int dt w_2^2(t) \phi_3(t, pS) \tag{D-24}$$

This "weighting-domain" version of the variance is very useful if third-order correlation  $\phi_3$  can be evaluated in closed form.

## Appendix E

### Computational Considerations for Non-Overlapping Segments

The curves in figure 15 for non-overlapping time segments are drawn over a continuum of values of  $L_2/L_1$ . However, if we were given a value of  $TB_e$ , all values of  $L_2/L_1$  may not be allowed. To develop this point, suppose that we pick an integer value for the number of pieces,  $P$ , and solve for  $L_1B_e = TB_e/P$  according to (129). From figures 5 and 6, this dictates the value for  $L_2B_e$ , and hence a discrete value for  $L_2/L_1$  is specified for each value of  $P$ . The number of pieces,  $P$ , can range from 1 to  $P_{\max}$ , where

$$B_e L_1 (\min) = \frac{B_e T}{P_{\max}} = \frac{1}{2c\{\phi_1\}} \quad , \quad P_{\max} = 2c\{\phi_1\} B_e T \quad , \quad (E-1)$$

from figure 5. For  $B_e T \gg 1$ , we have, for

$$P = 1, \quad B_e L_1 = B_e T, \quad B_e L_2 = \frac{1}{2c\{w_2\}}, \quad \frac{L_2}{L_1} = \frac{1}{2c\{w_2\}B_e T} \ll 1 \quad , \quad (E-2)$$

and for

$$P = P_{\max}, \quad B_e L_1 = \frac{1}{2c\{\phi_1\}}, \quad B_e L_2 \geq B_e T, \quad \frac{L_2}{L_1} \geq 2c\{\phi_1\}B_e T \gg 1 \quad . \quad (E-3)$$

Thus a very wide range of discrete values of  $L_2/L_1$  is allowed when  $B_e T \gg 1$ .

The problem with this approach is that when  $B_e L_1$  is calculated,  $B_e L_2$  must be solved for from the integral relation (52) (or approximately from figure 6). This tedious procedure can be circumvented by specifying  $L_2/L_1$  instead; if desired, we could then use (52) to determine  $B_e L_1$ , and solve for  $P = B_e T/(B_e L_1)$ . However,  $P$  will not necessarily turn out to be an integer for a given fixed  $T$ ; thus only a set of discrete values of  $L_2/L_1$  are strictly legal. But if  $NQR_p$  in (130) does not vary radically with  $L_2/L_1$ , this is not a significant limitation. And since it is simpler, we adopt it. In Appendix F, we cannot avoid the calculation of  $B_e L_2$  from a given  $B_e L_1$ .

## Appendix F

### Computational Considerations for Overlapping With Hanning Temporal Weighting

The temporal weighting is given by (146). Substitution in (108) and evaluation of the integral yields

$$\phi_3(\tau, \mu) = \frac{4}{9\pi L_1} \left\{ V_0(\pi - \alpha - \beta) + \sum_{k=1}^4 (-1)^{k-1} V_k \sin(k(\alpha + \beta)) \right\} \quad \text{for } \alpha + \beta \leq \pi, \quad (\text{F-1})$$

where

$$\begin{aligned} \alpha &= \frac{\pi}{L_1} |\tau|, \quad \beta = \frac{\pi}{L_1} |\mu|, \\ C_\alpha &= \cos(\alpha) = \cos\left(\frac{\pi\tau}{L_1}\right), \quad C_\beta = \cos(\beta) = \cos\left(\frac{\pi\mu}{L_1}\right), \\ V_0 &= \frac{3}{8} - C_\alpha^2 - C_\beta^2 + 4C_\alpha^2 C_\beta^2 + C_\alpha^4 + C_\beta^4, \\ V_1 &= C_\alpha C_\beta (4C_\alpha^2 + 4C_\beta^2 - 1), \\ V_2 &= -\frac{1}{4} + \frac{1}{2}(C_\alpha^2 + C_\beta^2) + C_\alpha^2 C_\beta^2, \\ V_3 &= \frac{1}{3} C_\alpha C_\beta, \quad V_4 = \frac{1}{32}. \end{aligned} \quad (\text{F-2})$$

The procedure for the evaluation of the normalized quality ratio follows. We specify a value for  $B_e T$  and select a temporal weighting  $w_1(t)$  and a lag weighting  $w_2(\tau)$ . We then evaluate shape factor  $c\{\phi_1\}$  from (64) or table 2, and select a shift fraction  $q = q\{w_1\}$  according to (139). We then solve (141) for  $P_{\max}$ , and allow  $P$  to take integer values in the range  $1 \leq P \leq P_{\max}$ .  $B_e L_1$  can then be evaluated from (140) as

$$B_e L_1 = \frac{B_e T}{1 + (P - 1)q} \quad (\text{F-3})$$

an integer value of  $P$ . We then solve (52) in the form

$$\int_0^1 dx \left[ w_2^2(L_1 x) - z_1^2(L_1 x) \right] = 0, \quad (\text{F-4})$$

where  $z_1(L_1 x)$  is independent of  $B_e L_1$ .

$$Q = \frac{1}{P} \sum_{p=1-P}^{P-1} \left(1 - \frac{|p|}{P}\right) \int dx w_2^2(L_1 x) L_1 \phi_3(L_1 x, pq L_1) \quad (F-5)$$

where we let  $\tau = L_1 x$  and used (139). The quantity  $w_2(L_1 x)$  is a function of only  $L_2/L_1$ , while the remaining quantity in the integrand of (F-5) is independent of  $L_1$  and  $L_2$ . Finally, we multiply (F-5) by  $B_e T$  according to (110) in order to determine the normalized quality ratio.

To reduce computation time, we take advantage of various properties of the functions involved. First, since  $\phi_3(\tau, \mu)$  is even in  $\tau$  and  $\mu$  (see (108)), and  $w_2$  is even, we express (F-5) as

$$Q = \frac{4}{P} \sum_{k=0}^{P-1} \epsilon_k \left(1 - \frac{k}{P}\right) \int_0^\infty dx w_2^2(L_1 x) L_1 \phi_3(L_1 x, qk L_1) \quad (F-6)$$

where

$$\epsilon_k \equiv \begin{cases} 1/2 & \text{for } k = 0 \\ 1 & \text{for } k \geq 1 \end{cases} \quad (F-7)$$

Also, from (F-1) and (F-2), we have normalized form

$$L_1 \phi_3(L_1 a, L_1 b) = \frac{4}{9\pi} \left\{ V_0 \pi(1 - a - b) + \sum_{k=1}^4 (-1)^{k-1} V_k \sin[k\pi(a + b)] \right\} \\ \text{for } 0 \leq a, \quad 0 \leq b, \quad a + b \leq 1 \quad (F-8)$$

where now

$$C_\alpha = \cos(\pi a), \quad C_\beta = \cos(\pi b) \quad (F-9)$$

and  $\{V_k\}_0^4$  are still as given in (F-2).

Since  $L_1 \phi_3(L_1 x, pq L_1)$  in (F-6) is zero if  $x + qk > 1$ , we can limit the sum on  $k$  in (F-6) to  $k_m = \min(P-1, 1/q)$ , and we need to evaluate the integral on  $x$  in (F-6) only up to  $X_m = \min(L_2/L_1, 1 - qk)$ . The number of  $x$  intervals needed in (F-6) is about 16 with the Trapezoidal rule for integration. These features are incorporated in the program listing below.

```

1 ! NUSC TECHNICAL REPORT 6459, 29 MAY 1991, A. H. TUTTALL
10  Bet=100 ! Be T
20  C1=1/6+35/(48*PI^2) ! HANNING TEMPORAL-WEIGHTING W1; TABLE 2
30  Q1=3/8 ! 62.5% OVERLAP FOR W1; 0<Q1<=1
40  Pm=1+(2*C1*Bet-1)/Q1 ! Pmax; EQ. 141
50  PRINT "Be T =";Bet,"q = q(w1) =";Q1
60  PRINT
70  COM T1,T2,T3,T4
80  T2=2*PI
90  T3=1/3
100 T4=1/T2
110 FOR P=1 TO Pm
120  Be11=Bet/(1+(P-1)*Q1) ! Be L1; EQ. 140
130  L211=FNL211(Be11,C1) ! L2/L1; SOLUTION OF EQ. 52
140  T5=.5*PI/L211
150  Km=MIN(P-1,1/Q1)
160  S=.5*FNInt(0,L211,T5)
170  FOR K=1 TO Km
180  S=S+(1-K/P)*FNInt(Q1*K,L211,T5)
190  NEXT K
200  Q=4/P*S
210  PRINT P,L211,Q*Bet
220  NEXT P
230  END
240  !
250  DEF FNL211(Be11,C1) ! SOLVE EQ. 52 FOR L2/L1
260  Eps=Be11-.5/C1
270  X1=4/(3*Be11)
280  IF Be11<10 THEN X1=.603246/SQR(Eps)-Eps/(6+12*Eps)
290  X2=X1*1.037
300  F1=FNf(X1,Be11)
310  F2=FNf(X2,Be11)
320  IF ABS(F2-F1)<1E-6 THEN 380
330  T=X2
340  X2=(F2*X1-F1*X2)/(F2-F1)
350  X1=T
360  F1=F2
370  GOTO 310
380  RETURN X2
390  FNEED
400  !

```

```

410 DEF FNF(L211,Bel1) ! RIGHT SIDE - LEFT SIDE OF E0. F-4
420 COM T1
430 Xm=MIN(1,L211)
440 T1=.5*PI/L211
450 N=16
460 Del=Xm/N
470 F=.5
480 FOR K=1 TO N-1
490 F=F+FNG(K*Del)
500 NEXT K
510 RETURN 2*Del*(F-1/Bel1)
520 FNEND
530 !
540 DEF FNG(X) ! (W2(L1*X)+Phi1(L1*X))^2
550 COM T1,T2,T3,T4
560 P=T2*X
570 G=(1-X)*(2+COS(P))*T3+T4*SIN(P)
580 W2=COS(T1*X)^2 ! HANNING LAG-WEIGHTING W2
590 RETURN (W2*G)^2
600 FNEND
610 !
620 DEF FNInt(Qk,L211,T5) ! INTEGRAL OF E0. F-5
630 Xm=MIN(L211,1-Qk)
640 Del=Xm/16
650 S=.5*FNPhi3(0,Qk)
660 FOR J=1 TO 15
670 X=Del*J
680 S=S+COS(T5*X)^4*FNPhi3(X,Qk)
690 NEXT J
700 RETURN Del*S
710 FNEND
720 !
730 DEF FNPhi3(A,B) ! L1*Phi3(L1*A,L1*B) for A>=0, B>=0; E0. F-8
740 IF A+B>=1 THEN RETURN 0
750 Ab=PI*(A+B)
760 Ca=COS(PI*A)
770 Cb=COS(PI*B)
780 Ca2=Ca^2
790 Cb2=Cb^2
800 S=Ca2+Cb2
810 V0=.375-S+4*Ca2*Cb2+Ca2^2+Cb2^2
820 V1=Ca+Cb*(4*S-1)
830 V2=-.25+.5*S+Ca2+Cb2
840 V3=Ca+Cb/3
850 S=V1*SIN(Ab)-V2*SIN(2*Ab)+V3*SIN(3*Ab)-.03125*SIN(4*Ab)
860 L1phi3=4/(9*PI)*(V0*(PI-Ab)+S)
870 RETURN L1phi3
880 FNEND

```

### References

1. M. S. Bartlett, *An Introduction to Stochastic Processes, with Special Reference to Methods and Applications*, Cambridge University Press, Cambridge, 1953.
2. R. B. Blackman and J. W. Tukey, *The Measurement of Power Spectra from the Point of View of Communications Engineering*, Dover Publications, Inc., New York, 1959.
3. E. Parzen, "Mathematical Considerations in the Estimation of Spectra," *Technometrics*, vol. 3, 1961.
4. R. B. Blackman, *Data Smoothing and Prediction*, Addison-Wesley Publishing Company, Inc., Reading, Mass., 1965.
5. J. S. Bendat and A. G. Piersol, *Measurement and Analysis of Random Data*, J. Wiley & Sons, Inc., New York, 1966.
6. G. M. Jenkins and D. G. Watts, *Spectral Analysis and Its Applications*, Holden-Day Company, San Francisco, 1968.
7. P. D. Welch, "The Use of FFT for the Estimation of Power Spectra: a Method Based on Time Averaging over Short Modified Periodograms," *IEEE Transactions on Audio and Electroacoustics*, vol AU-15, no. 2, June 1967, pp. 70-73.
8. C. Bingham, M. D. Godfrey, and J. W. Tukey, "Modern Techniques of Power Spectrum Estimation," *IEEE Transactions on Audio and Electroacoustics*, vol. AU-15, no. 2, June 1967.
9. A. H. Nuttall, "Spectral Estimation by Means of Overlapped Fast Fourier Transform Processing of Windowed Data," NUSC Report No. 4169, 13 October 1971.
10. A. H. Nuttall, "Estimation of Cross-Spectra via Overlapped Fast Fourier Transform Processing," NUSC Technical Report 4169-S, 11 July 1975.
11. A. H. Nuttall, "Minimum-Bias Windows for Spectral Estimation by Means of Overlapped Fast Fourier Transform Processing," NUSC Technical Report 4513, 11 April 1973.
12. A. H. Nuttall, "Probability Distribution of Spectral Estimates Obtained via Overlapped FFT Processing of Windowed Data," NUSC Technical Report 5529, 3 December 1976.
13. A. H. Nuttall and G. C. Carter, "A Generalized Framework for Power Spectral Estimation," *IEEE Transactions on Acoustics, Speech, and Signal Processing*, vol. ASSP-28, no. 3, pp. 334-335, June 1980.
14. G. C. Carter and A. H. Nuttall, "A Brief Summary of a Generalized Framework for Spectral Estimation," *Signal Processing*, vol. 2, no. 4, pp. 387-390, October 1980.
15. G. C. Carter and A. H. Nuttall, "On the Weighted Overlapped Segment-Averaging Method for Power Spectral Estimation," *Proceedings IEEE*, vol. 68, no. 10, pp. 1352-1354, October 1980.



### List of References (Cont'd)

16. J. S. Bendat and A. G. Piersol, *Random Data: Analysis and Measurement Procedures*, J. Wiley & Sons Inc., N.Y., 1971. See section 9.6, especially subsection 9.6.2.
17. R. K. Otnes and L. Enochson, *Applied Time Series Analysis*, J. Wiley and Sons Inc., N.Y., 1978. See section 8.8, esp. pp. 354-355.
18. A. H. Nuttall, "Reconstruction of Power Spectral Estimates," NUSC Technical Memorandum 781051, 6 March 1978.
19. A. H. Nuttall, "Some Windows with Very Good Sidelobe Behavior," *IEEE Trans. on Acoustics, Speech, and Signal Processing*, vol. ASSP-29, no. 1, pp. 84-91, February 1981.
20. C. Bingham, M.D. Godfrey, and J. W. Tukey, "Modern Techniques of Power Spectrum Estimation," *IEEE Trans. on Audio and Electroacoustics*, vol. AU-15, no. 2, pp. 56-66, June 1967.
21. E. A. Sloane, "Comparison of Linearly and Quadratically Modified Spectral Estimates of Gaussian Signals," *IEEE Trans. on Audio and Electroacoustics*, vol. AU-17, no. 2, pp. 133-137, June 1969.
22. G. H. Robertson, "Influence of Data Window Shape on Detectability of Small CW Signals in White Noise," *J. Acoust. Soc. Am.*, vol. 67, no. 4, pp. 1274-1276, April 1980.
23. A. H. Nuttall, "High-Order Covariance Functions for Complex Gaussian Processes," *IEEE Trans. on Information Theory*, vol. IT-8, no. 3, pp. 255-256, April 1962.

## Initial Distribution List

Addressee	No. of Copies
ASN (RE&S)	1
OUSDR&E (Research & Advanced Technology	2
Deputy USDR&E (Res & Adv Tech)	1
OASN	1
ONR, ONR-100, -200, -102, -222, 486	5
CNO, OP-098, -96	2
CNM, MAT-08T, -08T2, SP-20	3
DIA, DT-2C	1
NAV SURFACE WEAPONS CENTER, White Oak Laboratory	1
NRL	1
NRL, USRD	1
NORDA (Dr. R. Goodman, 100)	1
USOC, Code 241, 240	2
SUBASE LANT	1
NAVSUBSUPACNLON	1
OCEANAV	1
NAVOCEANO, Code 02	1
NAVELECSYSCOM, ELEX 03	1
NAVSEASYSCOM, SEA-003	1
NAVAL SEA SYSTEM DETACHMENT, Norfolk	1
NASC, AIR-610	1
NAVAIRDEVCEN	1
NOSC	1
NOSC, Code 6565 (Library)	1
NAVWPNSCEN	1
DTNSRDC	1
NAVCOASTSYSLAB	1
CIVENGRLAB	1
NAVSURFWPNCEN	1
NUWES, San Diego	1
NUWES, Hawaii	1
NISC	1
NAVSUBSCOL	1
NAVPGSCOL	1
NAVWARCOL	1
NAVTRAEQUIPCENT (Technical Library)	1
APL/UW, Seattle	1
ARL/Penn State, State College	1
Center for Naval Analyses (Acquisition Unit)	1
DTIC	12
DARPA	1
NOAA/ERL	1
National Research Council	1

**Initial Distribution (Cont'd)**

Weapon System Evaluation Group	1
Woods Hole Oceanographic Institute	1
ARL, Univ of Texas	1
Marine Physical Lab, Scripps	1
Dr. David Middleton, 127 East 91st St., New York, NY 10028	1
Bolt, Beranek, and Newman, Cambridge, MA (Herbert Gish)	1
Bolt, Beranek, and Newman, Canoga Park, CA (Dr. Allan G. Piersol)	1
Colorado State University (Prof. Louis Scharf)	1
University of Rhode Island (Prof. Donald Tufts)	1
Nat. Def. Res. Org. (C. van Schooneveld)	1
The Analytic Sciences Corp. (Dr. S. L. Marple)	1
Gould Inc. (T. E. Barnard, P. F. Lee)	2
Yale University (Prof. P. M. Schultheiss)	1
Royal Military College (Prof. Y. T. Chan)	1
University of Florida (Donald G. Childers)	1
Diagnostic Retrieval Systems (Jack Williams)	1

DATE  
FILMED  
- 8